8-2018

The Role of Developmental Timing Regulators in Progenitor Proliferation and Cell Fate Specification During Mammalian Neurogenesis

Jennifer S. Romer-Seibert
Rowan University

THE ROLE OF DEVELOPMENTAL TIMING REGULATORS IN PROGENITOR PROLIFERATION AND CELL FATE SPECIFICATION DURING MAMMALIAN NEUROGENESIS.

Jennifer S. Romer-Seibert, B.S., M.S.

A Dissertation submitted to the Graduate School of Biomedical Sciences, Rowan University in partial fulfillment of the requirements for the Ph.D. Degree.

Stratford, New Jersey 08084

August 2018

Table of Contents

Acknowledgements

I would like to thank my thesis advisor Dr. Eric Moss for the opportunity to earn my PhD in his lab. I am grateful for all the advice, training, and mentoring he has provided over the years. It has been a wonderful experience. I would like to thank Kevin Kemper for all his help with troubleshooting, general science discussion, and for being a great labmate. I would like to thank my committee, Dr. Jeremy Francis, Dr. Ronald Ellis, Dr. Hristo Houbaviy, and Dr. Nathaniel Hartman, for all the time they put in to reviewing my thesis work and the guidance and advice they have provided over the years. I would also like to thank Dr. Houbaviy for providing plasmids that were used in this thesis work. I would like to thank Dr. Hartman for allowing me to collaborate and train with him, as well, work in his lab and use his mice and materials. I would like to thank John Rokita and his staff in the animal lab at Stockton for their help caring for mice, and for notifying me when mouse pups were available. I would like to thank both Rowan and Stockton Universities for allowing me the opportunity to work on my thesis.

I would last like to acknowledge my family. I would like to thank my parents, Al and Debbie Romer, and my sister, Vanessa Romer, for all of their help and support, and for pushing me to achieve my best during my thesis and throughout my academic and professional career. I would like to thank my mother-in-law, Joanne Carlson for her support through my degree. I would last like to thank my husband, Timothy Seibert, for supporting me through these last seven years. We sacrificed and worked together, so that I could achieve this milestone.

Abstract

Developmental timing is a key aspect of tissue and organ formation in which distinct cell types are generated through a series of steps from common progenitors. These progenitors undergo specific changes in gene expression that signifies both a distinct progenitor type and developmental time point that thereby specifies a particular cell fate at that stage of development. The nervous system is an important setting for understanding developmental timing because different cell types are produced in a certain order and the switch from stem cells to progenitors requires precise timing and regulation. Notable examples of such regulatory molecules include the RNA-binding protein LIN28, and its downstream target, miRNA let-7. Although LIN28 is known to regulate both cell fate and tissue growth, and at times to promote an undifferentiated state, thus far a unified understanding of LIN28's biological role at the cellular level has not been attained. Here I address LIN28's activity in mammalian postnatal neurogenesis. Constitutive expression of LIN28 in cells derived from the subventricular zone of the mouse caused several distinct effects: (1) the number of differentiated neurons was dramatically reduced while the relative abundance of two neuronal subtypes was significantly altered; (2) the population of proliferating neural progenitors in the SVZ was reduced while the proportion of neuroblasts was increased, (3) neuroblast exit from the SVZ increased, and (4) the number of astrocytes was reduced while occasionally causing them to appear early. Thus, LIN28 acts at a post-stem cell/pre-differentiation step, and its continuous expression caused a precocious, not a reiterative phenotype, as is seen in other experimental systems. I made use of a circular RNA sponge that effectively inhibits let-7 activity to address the degree to which

LIN28's effects are due to its inhibition of let-7. Moreover, since LIN41 contributes to a subset of LIN28's function in *C. elegans*, I explored whether LIN41 played a role in mammalian neurogenesis. I found that although LIN28 has a multifaceted role in the number and types of cells produced during postnatal neurogenesis, it appears that its action through let-7 accounts for only a fraction of these effects.

Chapter 1: Introduction

The progression of diploid eukaroytes from embryos to adult organisms requires elaborate coordination of different factors, both external and internal, to generate the extensive diversity and quantity of cells. The assortment and diversity of cells found in each organism is extensive even in the smallest examples, such as *Caenorhabiditis elegans*. The cells that make up these organisms, and their distinct organs and tissues, are generated from a small pool of common stem cells. To understand how these organisms can develop from a few pluripotent cells, much work has gone into understanding the role of external signaling, environmental cues, niche environments, and signal transduction pathways and how they can regulate the progression of stem cells to ultimately terminally differentiated cell types. Although each of these play a role in proper development, researchers have questioned whether these factors tell the entire story, leading them to question how cells can determine when to proliferate and when to differentiate (Raff & Lillien, 1988). The exact reconstitution *in vitro* of specific cell types in the correct order at the correct time as seen *in vivo* suggested that some internal mechanism regulated the nature of these cells and their cell fate choices (Temple & Raff, 1986; Shen et al., 2006). This lead to the question how do progenitors choose between different fates (Cayoutte et al., 2003).

Developmental Timing and Cell Fate Specification

Developmental timing refers to a sequence of events that occur in a specific order for proper development. Cell divisions and commitment to terminal differentia-

tion are tightly controlled in a temporal manner (Euling & Ambros, 1996). Inappropriate alteration in the order or timing of these events can result in a range of mild to catastrophic phenotypes (Moss, 2007). Developmental timing is a key aspect of tissue and organ formation in which distinct cell types are generated through a series of steps from common progenitors. These progenitors undergo stage-specific changes that alter their competency to generate different lineages. Stage-specific cell fate decisions from stem cell self-renewal, progenitor proliferation, and ultimately the switch to terminal differentiation are highly regulated by an extensive network of proteins and microRNAs.

Research to better understand this intrinsic regulatory network and the role of developmental timing in specifying cell fate began years ago, and has continued to present day. Martin Raff and his laboratory investigated how cells determined the appropriate time for stem cells to generate daughter cells, when to cease proliferation, when to differentiate to terminal cell types, and which terminal cell type to become. To answer these questions, they studied cell fate decisions in the oligodendrocyte lineage of the nervous system (Raff, 2007). Raff and his team were able to culture neural precursor cells of the rat optic nerve that could generate all terminal cell types seen in the *in vivo* tissue (Raff & Lillien, 1988). Whether grown together or in separate dishes, daughter cells underwent division at the same time (Gao et al., 1997). Furthermore, they determined the number of divisions was variable between cultured clones, but ultimately, all clones ceased dividing and committed to differentiation at approximately the same time (Temple & Raff, 1986). Their work also demonstrated that lineage decisions occurred in the presence and absence of external factors (Raff,

2007). Taken together, this work suggested the precursor cells had some intrinsic mechanism controlling these decisions. The cells did not rely on the number of divisions to note the appropriate point for cell cycle exit and terminal differentiation, instead they relied on time (Temple & Raff, 1986; Gao et al., 1997). How does a cell "read" this internal clock and "know" it's time to make cell fate choices? Cell types at each developmental time point exhibit stage-specific gene expression that specifies cell fate at that particular stage of development. This idea that gene expression regulated the timing of developmental changes was slightly touched on by Raff and his group, but was extensively explored in *C. elegans* (Raff, 2007).

In the nematode worm, *C. elegans*, scientists of several labs identified clear phenotypic features of developmental timing regulators (Ambros & Horvitz, 1987). When these genes were mutated, ultimately, developmental stages would be completely skipped or continually reiterated. Developmental timing has been explored in many model systems, including Drosophila, *C. elegans*, mammalian retina development, and neural development from several vertebrates. In each of these systems, the genes responsible for specifying cell fate and timing of different developmental stages vary, but each does display characteristics of developmental timing genes such as precocious or retarded development.

In the developing nervous system of Drosophila, different subtypes of neurons and some glia cells are generated from the same precursor neuroblasts (Qian et al., 1998; Homem & Knoblich, 2012; Kohwi & Doe, 2013; Moss & Romer-Seibert, 2014). These precursors exhibit timing specific expression of unique transcription

factors, Hunchback, Kruppel, POU domain protein, and Castor, that alters their competency and results in the production of specific neurons at different times (Isshiki et al., 2001; Maurange et al., 2008; Moss & Romer-Seibert, 2014). The intrinsic change in gene expression of the neuroblasts is crucial for the end result of a highly diverse collection of neurons. Kruppel, for example, displays the hallmark characteristics of a developmental timing gene, gain- and loss-of function mutations result in opposite phenotypes. Where the loss of Kruppel causes a precocious skipping of the second stage, its constitutive expression causes a reiteration of the second stage (Isshiki et al., 2001).

In the mammalian retina as well, common progenitors produce a diverse set of functionally distinct cell types. The length of time into the differentiation process dictates the competency of these progenitors. Early in the timeline, the progenitors will produce retinal ganglion cells, cone receptors, amacrine cells, and horizontal cells. Later in the timeline, the progenitors switch competency and produce bipolar cells, rod photoreceptor cells, and Müller glia cells (Kohwi & Doe, 2013; Moss & Romer-Seibert, 2014). Ikaros is an on-early-off-late protein that when lost, moves the production of later born cell types earlier in the process, and skips the production of horizontal and amacrine cells (Elliott et al., 2008). In both of these model systems, we get a glimpse into the role of developmental timing genes and how their particular expression helps progenitor cells identify “when” they are in the differentiation process.

C. elegans and the Heterochronic Pathway

In *C. elegans*, seam cells of the hypodermis (similar to stem cells) undergo a specific division pattern at each of the four larval stage molts and the final transition to adulthood (Ambros & Horvitz, 1987). These seam cells will terminally differentiate, join the syncytia, and secrete the adult cuticle structure, alae. In the first, third, and fourth larval stages (L1, L3, L4), these seam cells undergo asymmetric division maintaining their progenitor nature but also producing a specific daughter cell. In the second larval stage (L2) only, the seam cells undergo a symmetric division which increases the total number of cells, before eventually completing an asymmetric division. At each stage of development, these seam cells have characteristic gene expression that distinguishes from the cells of the previous stage. The heterochronic pathway of *C. elegans* revealed distinct regulators of timing independent of other processes (Moss, 2007).

Decades of research into developmental timing in this system has revealed an extensive network of proteins and miRNAs that work in a highly complex and intricate pathway to tightly regulate each larval stage of development. Mutations in each of the genes can result in either precocious or retarded phenotypes. Precocious phenotypes have early terminal differentiation and progression to adulthood as a result of skipping an earlier stage of development, whereas retarded phenotypes never reach adulthood and continually reiterate an early stage.

Genes of the Heterochronic Pathway

Studies of the *C. elegans* heterochronic pathway have revealed many important regulators. Key proteins of this pathway include: LIN-14, LIN-28, HBL-1, LIN-41, and LIN-29 (Fig 1). These proteins collectively regulate the four larval stages and the transition to adulthood (Ambros & Horvitz, 1987; Ambros, 1989; Euling & Ambros, 1996; Moss et al., 1997; Slack et al., 2000; Pepper et al., 2004; Abbott et al., 2005; Vadla et al., 2012; Tsialikas et al., 2017). Two miRNA families also contribute significantly to the larval molts and adult transition processes: let-7 and lin-4 (Fig 1; Moss et al., 1997; Reinhart et al., 2000; Slack et al., 2000; Abbott et al., 2005; Vadla et al., 2012; Tsialikas et al., 2017).

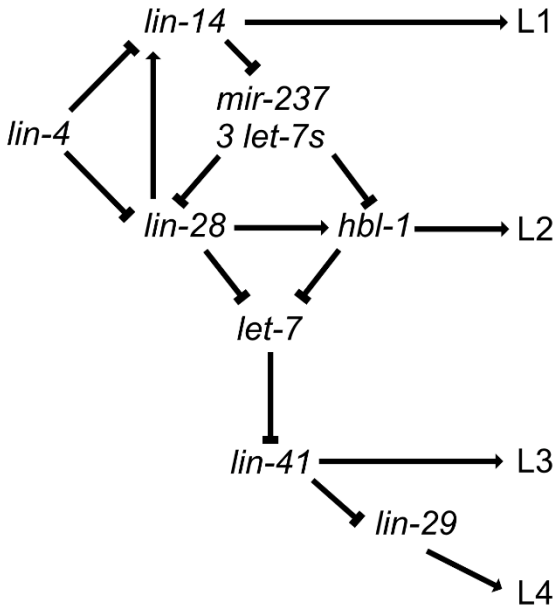

Figure 1. A model depicting the heterochronic pathway in *C. elegans*. Illustration depicting the genetic relationships of the various developmental timing regulators and the specific stage(s) they regulate.

LIN-14 regulates cell fates of the L1 and L2 stages (Ambros, 1989; Euling & Ambros, 1996). It regulates the L1 on its own; for instance, it specifies the asymmetric seam cell division of L1 (Ambros & Horvitz, 1987; Euling & Ambros, 1996; Harandi & Ambros, 2015). LIN-14 positively regulates the expression of LIN-28 by negatively regulating mir-237 (lin-4 family member) and mir-48, mir-241, and mir-84 (the let-7 sisters) (Tsialikas et al., 2017). Both LIN-14 and LIN-28 are negatively regulated by lin-4 (Lee et al., 1992; Moss et al., 1997).

LIN-28 regulates cell fates of the L2 and L3 stages by two distinct mechanisms (Vadla et al., 2012). LIN-28 first promotes L2 fates, including the symmetric division of seam cells (Harandi & Ambros, 2015). Then it promotes the L3 stage patterns over L4 patterns (Vadla et al., 2012). The second of these steps occurs through LIN28's direct inhibition of the microRNA let-7, thereby positively regulating LIN-41 expression. LIN-28 promotes L2 fates by positively regulating HBL-1 expression by an unknown mechanism. Both LIN-28 and HBL-1 are negatively regulated by the lin-4 and let-7 families (Abbott et al., 2005; Tsialikas et al., 2017). We can take a general concept away from this complex regulatory system. The sequential action and repression of key regulators drives the succession of cell fates. My question is whether, where homologs of these regulators exist in mammals, such as mouse and humans, do they also act as regulators of developmental transitions, and if so, do they act in a similar manner?

LIN28[1]

LIN28 is an RNA-binding protein that consists of a unique combination of two types of RNA binding domains: Cold Shock Domain (CSD) and CCHC zinc finger motifs (Moss et al., 1997). The CSD resembles that of bacteria CSDs and the Y-box family in eukaryotes. The zinc fingers are similar to those found in retroviral nucleocapsid proteins that interact with RNA in the virion packaging process. LIN28 is generally cytoplasmic, but can be detected in the nucleus and the nucleolus; as well, it localizes in these locations as a result of shuttling (Moss et al., 1997; Balzer & Moss, 2007; Kawahara et al., 2011; Vogt et al., 2012).

LIN28 has homologs in a variety of organisms including *C. elegans*, Drosophila, Xenopus, humans, and mice (Moss et al., 1997; Moss & Tang, 2003; Faunes et al., 2017). In *C. elegans*, LIN28 exhibits an on-early-off-late expression pattern, with high expression early in development that is downregulated over time (Moss et al., 1997). LIN28 regulates the L2/L3 molt directly and the L4/Adult transition indirectly (Moss et al., 1997; Slack et al., 2000; Vadla et al., 2012; Tsialikas et al., 2017). When LIN28 is null, the L2 is completely skipped and developmental stages are moved up in time; this results in a precocious phenotype, including a reduced number of some cells, and early terminal differentiation (Ambros & Horvitz, 1984). Gain-of-function LIN28 causes a retarded phenotype with constant reiteration of the L2 stage patterns

[1] Although there are two isoforms of LIN28 in mammals, A and B, all mention of LIN28 in this thesis refers to LIN28A except for the description of the let-7 regulation, where the role and contribution of both isoforms are discussed in general.

resulting in an increased number of some cells, and premature development and terminal differentiation (Moss et al., 1997).

The on-early-off-late expression pattern of LIN28 is conserved in other organisms. In Drosophila, it is expressed during embryogenesis through the first instar larval stage, downregulated, and then upregulated again in the pupal stage (Moss & Tang, 2003). Xenopus, as well, has expression during embryogenesis and metamorphosis, but no expression in differentiated tissues (Moss & Tang, 2003; Faas et al., 2013; Faunes et al., 2017). LIN28 is widely expressed in developing tissues of the mouse and chick embryos; this expression becomes increasingly restricted over time, and ultimately is downregulated with the exception of a few specific regions (Yang & Moss, 2003; Yokoyama et al., 2008). In the mouse, the transit-amplifying cells of the small intestine, epithelial cells of the Henle loop in the kidney, and cells of cardiac and skeletal tissue all exhibit adult LIN28 expression (Yang & Moss, 2003). LIN28 is expressed in cancer cells, embryonic stem cells, pluripotent cells, and neural progenitor cells, essentially undifferentiated cell types or cells with proliferative capacity (Moss & Tang, 2003; Darr & Benvenisty, 2009; Zheng et al., 2009; Balzer et al., 2010; Bhuiyan et al., 2013; Copley et al., 2013; Yang et al., 2015; Meares et al., 2018). As these cells commit to specific lineages and terminally differentiate, LIN28 is downregulated. Exceptions to this rule exist including the expression of LIN28 in erythroblasts and skeletal muscle cells, both committed cell types (Polesskaya et al., 2007; de Vasconcellos et al., 2014). Although LIN28 is often thought of as a pluripotency marker and a promoter of proliferation, at this time, a unified understanding of LIN28's role at the cellular level has not yet been achieved.

On the whole organismal scale, gain- and loss-of-function LIN28 results in increased or reduced size, respectively, of the whole mouse, brain, and other organs (Zhu et al., 2010; Shinoda et al., 2013; Yang et al., 2015; Corre et al., 2016). Constitutive LIN28 displays other retarded phenotypes including delays in puberty and estrus of mice, consistent with vulva defects in *C. elegans* (Moss et al., 1997; Zhu et al., 2010). Constitutive expression of LIN28 can contribute significantly to regeneration of tissue (Shyh-Chang et al., 2013; Faunes et al., 2017). Additionally, several studies have identified a role for LIN28 in glucose metabolism and insulin sensitivity (Zhu et al., 2010; Zhu et al., 2011; Perez et al., 2013; Shinoda et al., 2013; Docherty et al., 2016). Though the previous phenotypes are clearly the result of altered developmental timing and show a conservation of LIN28's function in mammals, glucose metabolism and insulin sensitivity show no clear connection with development or developmental timing.

In many cases, LIN28 plays a part in maintaining undifferentiated states, promoting proliferation while deferring differentiation, and supporting self-renewal (Xu & Huang, 2009; Xu et al., 2009; Peng et al., 2011; Bhuiyan et al., 2013; Copley et al., 2013; Ouchi et al., 2014; Yang et al., 2015; Meares et al., 2018). LIN28, in conjunction with Nanog, Oct4, and Sox2, induced somatic cells back into pluripotent stem cells (Yu et al., 2007; Hanna et al., 2009). In combination with the other work, this has led to the understanding and acceptance that LIN28 is a proliferation and pluripotency marker and regulator. During *in vitro* neural differentiation of cells expressing constitutive LIN28, it was discovered that LIN28 promotes neurogenesis at the expense of gliogenesis, but has no effect on proliferation suggesting LIN28 could play a

part in cell fate choices beyond just proliferation (Balzer et al., 2010). This was further supported when LIN28 knock down prevented myogenic differentiation (Wu & Belasco, 2005; Polesskaya et al., 2007). Additionally, LIN28 plays a crucial role in progression to terminal differentiation of the mesoderm fate in Xenopus (Faas et al., 2013). These rare examples of non-canonical expression and function of LIN28 strongly suggest there is more to its purpose in development besides playing a part in proliferation.

LIN28 was identified as a member of an elaborate regulatory pathway in *C. elegans*, where other developmental timing genes are located upstream and downstream in the pathway. LIN28's most notable and well-studied downstream target is the miRNA let-7. LIN28 negatively regulates the expression of mature let-7. These two molecules exhibit a reciprocal relationship, where when LIN28 is high, let-7 is low, and vice-versa (Balzer et al., 2010; Vadla et al., 2012). Extensive work has gone into understanding the molecular mechanism of LIN28's regulation of let-7 (Fig 2; Newman et al., 2008; Rybak et al., 2008; Viswanathan et al., 2008). LIN28 binds the terminal loop region of let-7 through the consensus site GGAG in both the primary and precursor forms (pri-miRNA, pre-miRNA) (Heo et al., 2008; Newman et al., 2008; Lightfoot et al., 2011; Loughlin et al., 2011; Nam et al., 2011; Piskonouva et al., 2011; Mayr et al., 2012). Binding of the pri-miRNA in the nucleus blocks processing by Drosha (Piskonouva et al., 2011; Van Wynsberghe et al., 2011). LIN28 localization to the nucleus may be enhanced by Mushashi1 (MSI1) binding (Kawahara et al., 2011). Additionally, LIN28 binds pre-let-7 in the cytoplasm and facilitates interaction and uridylation activity by TUT4 and 7 (Hagan et al., 2009; Heo et al.,

2009; Wang et al., 2017). The uridylation blocks Dicer processing to a mature miRNA. LIN28's binding may also induce a conformational change of the Dicer cleavage site further preventing Dicer activity (Lightfoot et al., 2011). Both mechanisms contribute to block the processing to a functional mature miRNA.

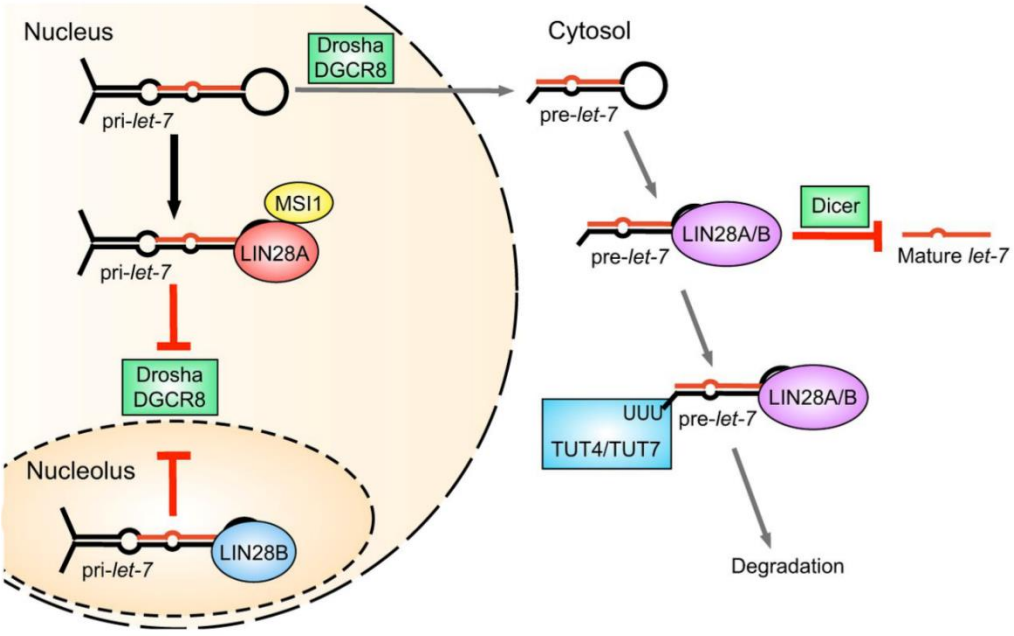

Figure 2. LIN28 blocks let-7 maturation through a combination of processes. Illustration depicting the many processes that LIN28 is involved in, either directly or indirectly, to block the processing of both the pri- and pre-let-7 molecules to mature let-7. MSI1, Mushashi1. (Figure from Tsialikas & Romer-Seibert, 2015)

LIN28's ability to bind and regulate the expression of let-7 remains true from *C. elegans* into mice and in some cases, genetic experiments demonstrated let-7 was the downstream effector for LIN28 (Rybak et al., 2008; Zhu et al., 2011; Vadla et al., 2012; Cimadamore et al., 2013; Copley et al, 2013; Perez et al., 2013; Ouchi et al.,

2014; Corre et al., 2016; Faunes et al., 2017; Wang et al., 2017). Although let-7 is considered LIN28's primary target, genetic experiments in both *in vitro* neurogenesis and in the hypodermis of *C. elegans* revealed LIN28 phenotypes that occurred seemingly independent of let-7 (Balzer et al., 2010; Vadla et al., 2012). First, during neurogenesis, LIN28 clearly altered the expression pattern of several genes long before mature let-7 had accumulated (Balzer et al., 2010). Second, the phenotypes of let-7 and LIN28 were genetically separated in *C. elegans*, and it was observed that let-7 only exhibited a subset of LIN28's phenotype (regulation of the L4/adult transition) suggesting its earliest effects are an independent activity (Vadla et al., 2012).

Several examples have either demonstrated that LIN28's phenotypes are either only partially due to let-7 or completely independent of it (Xu & Hang, 2009; Xu et al., 2009; Qui et al., 2010; Feng et al., 2012; Li et al., 2012; Shyh-Chang et al., 2013; Faas et al., 2013; Corre et al., 2016). The potential mammalian non-let-7 targets vary but in most cases, LIN28 appears to bind the mRNA of these targets directly and promote translational stimulation (Xu & Hang, 2009; Xu et al., 2009; Qui et al., 2010; Feng et al., 2012; Lei et al., 2012; Li et al., 2012; Hafner et al., 2013). Only one case has suggested LIN28 repressed translation through mRNA binding; as so many others have shown translational stimulation, this could suggest this is an outlier (Cho et al., 2012). It is possible LIN28 could 1) stabilize the mRNA, 2) block miRNA interactions with the 3'UTR, or 3) some other unidentified possibility. At this time, how this "translational stimulation" works is still unclear. It is likely, however the mechanism works, that LIN28 effects different processes in development through a combination of its two distinct activities.

let-7

let-7 is a miRNA first discovered in *C. elegans* and widely conserved (Reinhart et al., 2000; Pasquinelli et al., 2000). MicroRNAs are noncoding RNAs that are first transcribed as large primary transcripts, pri-miRNA, that are processed in the nucleus by Drosha to form an intermediate precursor, pre-miRNA (Bartel, 2004). The pre-miRNA is exported to the cytoplasm where it undergoes cleavage by Dicer resulting in the mature ~22 nucleotide double stranded miRNA (Bartel, 2004). The single strand is loaded into the RISC complex where it is able to assert its regulatory effects on mRNA either through perfect binding and mRNA degradation or imperfect binding and translational repression (Bartel, 2004).

Extensive search of the genomes by several groups revealed let-7's conservation in a variety of different species including worms, humans, mice, fruit flies, zebrafish, and frogs (Pasquinelli et al., 2000; Aravin et al., 2003; Lagos-Quintana et al., 2003; Lai et al., 2003; Lim et al, 2003; Lee et al., 2016). The number of let-7 family members varies greatly from species to species; frog, zebrafish, human, and mouse have many family members several of which are encoded by more than one gene. (Lagos-Quintana et al., 2003; Lim et al., 2003; Roush & Slack, 2008; Lee et al., 2016). Additionally, mir-98 is a related family member in humans and mice (Lee et al., 2016). Drosophila, on the other hand, has only one copy (Aravin et al., 2003; Lai et al., 2003). *C. elegans* has one let-7 copy, but has three highly related family members mir-48, mir-84, and mir-241, collectively known as "the let-7 sisters" (Roush & Slack, 2008; Tsialikas et al., 2017).

let-7 was first identified as a temporal regulator in the heterochronic pathway (Reinhart et al., 2000). It is upregulated late in the molting process demonstrating a reciprocal relationship with its upstream regulator, LIN-28; let-7 displays an off-early-on-late expression pattern (Pasquinelli et al., 2000; Reinhart et al., 2000; Slack et al., 2000; Lim et al., 2003). It specifically regulates the L4-to-adult transition in the hypodermis (Reinhart et al., 2000; Slack et al., 2000; Johnson et al., 2003). When let-7 is absent, the worm exhibits a retarded phenotype, additional molting cycles, no terminal differentiation of the hypodermis seam cells, and ultimately death as a result of a bursting vulva (Reinhart et al., 2000; Ecsedi et al., 2015). On the other hand, constitutive let-7 results in precocious development: early cell cycle exit and terminal differentiation to alae (Reinhart et al., 2000). Therefore, let-7 promotes later fates over earlier fates. let-7's family members, also developmental timing regulators, are expressed earlier in development and regulate the L2 stage distinct from let-7 (Vadla et al., 2012; Tsialikas et al., 2017). However, when the let-7 sisters are null, they also generate a retarded phenotype (Tsialikas et al., 2017). Whereas let-7 is downstream of LIN-28, the let-7 sisters are upstream (Tsialikas et al., 2017).

let-7's off-early-on-late expression pattern remains true in other species as well (Caygill & Johnston, 2008; Zhao et al., 2009; Wu et al., 2012; Xia & Ahmad, 2016). In Drosophila, it regulates the L3-pupal transition (a later stage in development) (Caygill & Johnston, 2008; Wu et al., 2012). In mammals, let-7 appears to be expressed in differentiated cells or its upregulation coincides with induction of differentiation (Zhao et al., 2009; Tong et al., 2011). In neural stem cells, meiotic germ cells, chondrocytes, and cardiac muscle cells, let-7 promotes differentiation and plays

some role in suppressing or reducing proliferation (Zhao et al., 2009; Tong et al., 2011; Papaioannou et al., 2013; Coppola et al., 2014). In the mammalian retina, for example, let-7 is upregulated at the progenitor shift from "early progenitor type" to "later progenitor type" and promotes the later cell fates: rod photoreceptors, bipolar cells, and müller glia (Xia & Ahmad, 2016). let-7 null reduces these late born cell types, whereas constitutive let-7 promotes an increase in these cells (Xia & Ahmad, 2016). More recently, it was demonstrated that let-7 regulates radial migration of neuroblasts (progeny of subventricular zone (SVZ) NSCs) in the OB and morphology of microglia found in the SVZ, both later stages of development and differentiated cell types (Petri et al., 2017; Morton et al., 2018).

let-7 exerts its effects in development through regulation of downstream targets. Its best studied target is the developmental timing gene LIN41. This regulatory relationship was first explored in *C. elegans,* but it remains true in a number of other species (Reinhart et al., 2000; Slack et al., 2000; Kloosterman et al., 2004; Vella et al., 2004; Kanamoto et al., 2006, Lin et al., 2007; O'Farrell et al., 2008; Rybak et al., 2009). Though many putative targets have been suggested based on bioinformatics exploration of let-7 target sites in the 3'UTR of different genes, very few have proven valid downstream targets at this time. As well, several legitimate let-7 targets have been identified but they seem to be species or tissue specific (Caygill & Johnston, 2008; Zhao et al., 2009; Wu et al., 2012; Pappouinnaou et al., 2013; Coppola et al., 2014; Xia & Ahmad, 2016; Petri et al., 2017).

LIN41

LIN41 (TRIM71) is an E3 ubiquitin ligase that contains the tripartite motif consisting of a ring finger, two B-box domains, and a coiled coil near the N-terminus; a filamin domain; and six NHL domains in the C-terminus (Slack & Ruvkun, 1998). The ring finger and B-box domains are zinc binding regions (Jackson et al., 2000). The ring finger is often involved in protein-protein interactions; B-box domains are also involved in protein-protein interactions both directly and indirectly (Torok & Etkin, 2000). LIN41 was first discovered in *C. elegans* as a member of the hetero-chronic pathway (Slack et al., 2000). LIN41 displays the on-early-off-late expression pattern similar to LIN28, but slightly delayed; this remains true for its chicken and mouse orthologs (Slack et al., 2000; Lancman et al., 2005; Schulman et al., 2005; Maller Schulman et al., 2008; Yu et al., 2010; Vadla et al., 2012). LIN41 expression is generally in pluripotent and embryonic cells and tissues. It is expressed in the developing chick and mouse embryos, pluripotent embryonic stem cells, neuroepithelial cells of the mouse nervous system, embryonic ectoderm, interfollicular stem cells of the epidermis, and male germ cells (Lancman et al., 2005; Schulman et al., 2005; Rybak et al., 2009; Yu et al., 2010; Chang et al., 2012; Chen et al., 2012; Kwon et al., 2013). One exception, LIN41 appears to be expressed in the terminally differentiated ependymal cells of the mouse lateral ventricle (Cuevas et al., 2015).

LIN41's initial identification as a developmental timing regulator in *C. elegans* revealed that it regulated the transition from the L4 molt to adulthood (Slack et al., 2000). Loss- and gain-of function mutants displayed opposing phenotypes, where

constitutive expression resulted in retarded development, a reduction in overall terminal differentiation of seam cells, and an increase in the number of seam cells; null LIN41 caused a precocious phenotype, early terminal differentiation, and a reduction in seam cells (Slack et al., 2000). LIN41 regulates other developmental processes in *C. elegans*, including male tip morphogenesis and proper oocyte development (Del Rio-Albrechtsen et al., 2006; Tocchini et al., 2014). In mammals, the expression of LIN41 is essential for proper development; its loss ranges from faulty neural tube closure to embryonic lethality (Maller Schulman et al., 2008; Chen et al., 2012; Cuevas et al., 2015; Mitschka et al., 2015). Loss of LIN41 during zebrafish development results in catastrophic defects as well (Lin et al., 2007). LIN41 activity seems to coincide with its functions in *C. elegans*. Loss of LIN41 results in a precocious phenotype: early neural differentiation and reduced proliferation of neural progenitor cells (Chen et al., 2012). The contribution to proliferation seems to vary from system to system, where it enhances proliferation in ESCs but plays no part in it in iPSCs (Chang et al., 2012; Worringer et al., 2014).

Some work has suggested LIN41 regulates developmental timing through RNA interaction. This can be direct mRNA binding of a repressive nature that causes either translational repression or mRNA decay, or association with miRNAs (Chang et al., 2012; Kwon et al., 2013; Loedige et al., 2013; Aeschimann et al., 2017; Tsukamoto et al., 2017). LIN41 may regulate RNA expression based on the location of its binding site, which can result in two different mechanisms of regulation (Aeschimann et al., 2017). It was suggested that LIN41 interacts with Ago2 through its ring finger

to regulate miRNA expression, however, more recent work has been unable to corroborate this result (Rybak et al., 2009; Chang et al., 2012; Chen et al., 2012). Overall, the NHL domain seems to have the most essential role in LIN41's function, however, the other domains do contribute in specific situations (Chang et al., 2012; Loedige et al., 2013; Nguyen et al., 2017).

LIN41 is downstream of the miRNA and developmental timing regulator let-7. LIN41 contains let-7 target sites in the 3'UTR. let-7 can bind these sites, and effectively downregulate LIN41 as a result. This is true in worms, zebrafish, fruit flies, and mice (Reinhart et al., 2000; Slack et al., 2000; Kloosterman et al., 2004; Vella et al., 2004; Kanamoto et al., 2006; Lin et al., 2007; Cevec et al., 2008; O'Farrell et al., 2008; Cevec et al., 2010;). These two molecules exhibit a reciprocal relationship (Slack et al., 2000; Schulman et al., 2005).

A variety of targets have been suggested in mammals, but they are inconsistent and seem to vary from system to system (Rybak et al., 2009; Chang et al., 2012; Chen et al., 2012; Loedige et al., 2013). However, in *C. elegans*, LIN41 is known to regulate the expression of LIN-29 (Slack et al., 2000). Like LIN41 and let-7, LIN41 and LIN-29 have reciprocal relationships, where LIN-29 expression is blocked in the presence of LIN41 (Slack et al., 2000). Although LIN41 regulates the L4-to-adult-transition through LIN-29 in seam cells and the hypodermis, LIN41's functions in other worm tissues are independent of this downstream molecule (Del Rio-Albrechtsen et al., 2006; Tocchini et al., 2014). This is interesting because it could suggest LIN41 has two unique functional pathways, similar to its developmental counterpart LIN28 (Balzer et al., 2010; Vadla et al., 2012).

The SVZ and postnatal neurogenesis

The nervous system is an important setting for understanding developmental timing. The ordered generation of different cell types and the critical switch from stem cells to progenitors requires precise timing and regulation to ensure the proper number and types of differentiated neural cells (McConnell, 1985). Postnatal neurogenesis occurs in only two special niches of the mouse brain following birth, the SVZ of the lateral ventricles and in the dentate gyrus of the hippocampus (Temple, 2001).

The SVZ is characterized and populated by four distinct cell populations: neural stem cells (NSCs-Type B), transit-amplifying or progenitor cells (TACs-Type C), neuroblasts (NBs-Type A), and ependymal cells (Type E). NSCs exhibit radial glia properties and are derived from embryonic precursors (Doetsch et al., 1999; Kriegstein & Alvarez-Buylla, 2009; Fuentealba et al., 2015). They can ultimately produce neurons, astrocytes, and oligodendrocytes (Menn et al., 2006; Merkle et al., 2007). The oligodendrocyte fate is specified and separated from the neural/astrocytic lineages very early on (Grebbin et al., 2016). NSCs asymmetrically divide maintaining their own population and generating TACs (Doetsch et al., 1999; Costa et al., 2011). NSCs produce their progeny in short bursts and in waves, then following a short life span, they become either quiescent or exhausted (Calzolari et al., 2015). As active individual NSCs become either quiescent or exhausted, other quiescent NSCs are activated to continue producing TACs (Calzolari et al., 2015). Following three to four rounds of division, TACs will further differentiate to the immature migratory neurons known as NBs (Doetsch et al., 1999; Ponti et al., 2013a; Ponti et al., 2013b). NBs migrate along the rostral migratory stream (RMS) in chains ensheathed by astrocytes

(Lois & Alvarez-Buylla, 1994; Lois et al., 1996; Alvarez-Buylla & Garcia-Verdugo, 2002). The NBs will end their migration in the olfactory bulb (OB); here they undergo radial migration throughout the OB and terminally differentiate into interneurons (Doetsch et al., 1999). The interneurons mainly integrate into the granule cell layer (GCL) or the glomerular layer (GL) with nearly 95% of these neurons embedding in the GCL (Hack et al., 2005; Lledo & Saghatelyan, 2005).

The glomerular layer of the OB contains distinct structures known as glomeruli, which contain the olfactory nerves (Kosaka & Kosaka, 2007). Each individual glomerulus contains two compartments, the ON (olfactory nerve) zone and the non-ON zone. These zones are defined by the structures contained in each region. The ON zone is characterized by 1) olfactory nerve terminals, 2) dendritic processes of interneurons, and 3) the presence of olfactory receptor cell synapses on their targets (Kosaka & Kosaka, 2007). The non-ON zone contains dendritic processes of interneurons and the dendrodendritic interactions between these interneurons (Kosaka & Kosaka, 2007). The interneurons of the GL, periglomerular cells (PGCs), can be divided into two populations, type I and II (Nagayama et al., 2014). Type I PGCs can be identified by their expression of tyrosine hydroxalase (TH) and comprise approximately 12.6-20% of the PGCs. These cells can be found in both the ON and non-ON zone (Kosaka & Kosaka 2007; Nagayama et al., 2014). Type II PGCs can be identified by Calbindin (calb) and comprise 9.8-15% of the PGCs, but are found only in the non-ON zone (Kosaka & Kosaka, 2007; Nagayama et al., 2014). The localization of TH+ cells to both zones and the Calb+ cells to the non-ON zone only could suggest

distinct physiological roles for these cell types. The two populations of PGCs are generated in a timing specific manner during embryonic development, with TH+ neurons generated first and Calb+ neurons second (Batista-Brito et al., 2008).

There has been limited research discerning the genes necessary for proper cell fate specification and developmental timing in the SVZ. Genes such as mTOR, Pax6, Meis2, Pbx1, and Olig2 are just a few that could potentially regulate cell fate in the SVZ (Hack et al., 2005; Kohwi et al., 2005; Jang & Goldman, 2011; Hartman et al., 2013; Agoston et al., 2014; Grebbin et al., 2016). Much of this work specifies the decision to embark on the oligodendrocyte lineage versus the neural lineage, but we know nothing at this time about the switch from neural to astrocytic lineages (Kohwi et al., 2005; Jang & Goldman, 2011; Agoston et al., 2014; Grebbin et al., 2016). We get a glimpse into the choice between self-renewal and differentiation and the role that mTOR plays in the mechanism, but still very little is known about this switch (Hartman et al., 2013). Pax6 and Meis2 play a role in cell fate choices of the PGCs of the GL but little else is known about the decision to become either type I or type II PGCs (Kohwi et al., 2005; Agoston et al., 2014).

What genes regulate the switch from proliferation to differentiation? What genes regulate the switch from neural to astroglial? Very little is known about the molecules that regulate these decisions, and so these questions remain unanswered. LIN28 is expressed in the developing nervous system and it plays a role in cell fate choices (Balzer et al., 2010). Could LIN28 and its developmental timing counterparts play a role in the cell fate choices of postnatal neurogenesis in the SVZ?

To study postnatal neurogenesis, I used postnatal electroporation to directly target the NSCs of the SVZ ((Lacar et al., 2010; Platel et al., 2010; Feliciano et al., 2012; Feliciano et al., 2013; Hartman et al., 2013). This system provides a unique opportunity to study self-renewal, proliferation, differentiation, and cell fate choices in one model and therefore is the perfect model to study LIN28 in postnatal neurogenesis, development, and cell fate specification. Though model systems such as Drosophila and *C. elegans* have provided us an essential understanding of developmental timing regulators such as LIN28, these systems are still limited in complexity and to have a full understanding of these genes as they function in mammals we need to use mammalian systems. Similarly, while *in vitro* culture systems can provide solid understanding of specific processes, ultimately, the goal is to understand these molecules *in vivo*. There are a couple obstacles to understanding LIN28's role in neural development *in vivo,* in particular at a postnatal time point. First, LIN28 is downregulated in the whole embryo during the embryonic days of development, making it difficult to study its role in neural development, in particular gliogenesis, since this stage of development does not start until after LIN28 is downregulated (Balzer et al., 2010; Sauvageot & Stiles, 2002). Second, when LIN28 is constitutively expressed, it can have catastrophic effects on several organs of the developing mouse embryo including the lungs and the nervous system making it extremely difficult to study its postnatal role (Yang et al., 2015). Postnatal electroporation allows me to bypass the above mentioned issues. This technique targets only a fraction of the total NSCs of the SVZ, after birth, leaving the rest of the brain and mouse wildtype.

Although it is known to regulate both cell fate and tissue growth, and at times to promote an undifferentiated state, thus far a unified understanding of LIN28's biological role at the cellular level has not been elucidated. We can also further our understanding of LIN28 by asking and answering the question, "does LIN28 regulate postnatal neurogenesis through let-7?" I will attempt to answer these questions in this thesis.

Chapter 2: Materials and Methods

Animals

Wild-type CD1 mice were purchased from Charles River Laboratories. All of the animals used in this study were maintained on a 12-h light/dark cycle with ad libitum access to food and water. All of the experiments involving live animals were performed in accordance with the guidelines and regulations of the Institutional Animal Care and Use Committee at Stockton University.

Postnatal Electroporation

Electroporation was performed as previously described (Hartman et al., 2013; Mahoney et al., 2016). CD1 pups were injected with 1μL plasmid DNA (1-2μg/μL) with 0.1% Fast Green as a tracer dye directly into the lateral ventricle using a pulled borosilicate glass pipette. Five square pulses of 50ms duration with 950ms intervals at 100V were applied using a pulse ECM830 BTX generator and platinum tweezer-type electrodes (model 520; BTX). Pups were then allowed to recover. Experiments were terminated at 1, 3, 7, and 21 days post electroporation (DPE). All experiments used littermate controls with a minimum of 6 mice (3+ for control and 3+ for the experimental condition).

Tissue Preparation

Mice were deeply anesthetized with isoflurane. The brains were quickly removed, and incubated in 4% paraformaldehyde in 1xPBS at 4ºC overnight. They were then transferred to 30% Sucrose in 1xPBS and incubated at 4ºC overnight with rocking.

Brains were embedded in O.C.T. compound and stored at -80ºC. Preserved brains were sliced into 50 or 100µM coronal sections or 40µM sagittal sections at -20ºC on a cryostat (Microm HM 550, Thermo Scientific). Slices were stored in antifreeze at -20ºC.

Primary Neural Progenitor Cell Culture

Primary neural progenitor cultures were prepared from SVZ regions of CD1 mouse pups. The brain was removed and placed into cold Hank's balanced salt solution (HBSS) supplemented with 5x Penicillin/Streptomycin. The brain was cut coronally and the SVZ was microdissected and the tissue minced. The tissue was incubated for 15 minutes in Accutase and the enzymatic digestion was stopped by an equal amount of inhibition solution (STEMCELL Technologies). The resulting cell suspension was washed by adding and resuspending in 10mL DMEM/F12 (Sigma-Aldrich). The cells were resuspended in Neural Proliferation Media (1:1 mixture of DMEM/F12 and Neurobasal medias supplemented with 1xB27, 1xN2, 1xPenicillin/Streptomycin, 1xGlutamax, 25µg/mL BSA, 20ng/mL FGF_2 and 20 ng/mL EGF) and strained with a 70µM pore cell filter. Primary neural stem cells of the SVZ were plated at $5x10^4$ and cultured in Neural Proliferation Media and grown on laminin-treated chamber slides. Growth factors were removed and $1.6x10^4$ NSCs were plated and differentiated for 5 days.

Immunostaining and Antibodies

Undifferentiated and differentiated NSCs were fixed in 4% paraformaldehyde for 15 minutes. Fixed cells were washed and blocked in Block solution for 1 hour at room temperature. Antibodies were diluted in 5% normal goat serum and 2% BSA in 1x PBS Block and incubated for 1 hour at room temperature: rat GFAP (1:500, Invitrogen); rabbit Ki67 (1:250, Neomarkers); rabbit DCX (1:400, Cell Signaling); rat LIN28 (1:500); rabbit Nestin (1:1000, Abcam). Goat anti-rat Alexa fluor 568, anti-chicken 633 (1:1000, Life Technology), and goat anti-rabbit dye light 550 and 633 (1:1000, Thermo Fisher) were used as secondary antibodies. Cells were then stained with DAPI (1:1000, Thermo Fisher Scientific), washed, and preserved with Prolong Gold Antifade Reagent (Invitrogen). Cells were coverslipped and examined by confocal microscopy. For *in vivo* experiments, each staining was replicated in slices from at least 3 mice in a region of interest (SVZ, OB, or RMS). Slices were washed 3x in 1xPBS. Slices were incubated in 100% methanol for 20 minutes at 4ºC, washed, and then blocked for 1 hour at room temperature in Block solution. Slices were then incubated for 48 hours at 4ºC in primary antibodies diluted in the block. Primary antibodies: rat GFAP (1:500, Invitrogen); rabbit Ki67 (1:250, Neomarkers); rabbit Sox2 (1:100, Abcam); rabbit DCX (1:400, Cell Signaling Technology); rabbit Calbindin (1:500, Abcam); chicken Tyrosine Hydroxalase (1:1000, Abcam); cleaved Caspase 3 (1:400; Cell Signaling Technology. Slices were washed as above, then incubated for 1.5 hours at room temperature in secondary antibodies diluted in the block. Secondary antibodies: Goat anti-rat Alexa fluor 568, anti-chicken 633 (1:1000, Life Technologies), and goat anti-rabbit dye light 550 and 633 (1:1000, Thermo Fisher Scientific).

Slices were washed and incubated in DAPI (1:1000, Thermo Fisher Scientific) for 15 minutes at room temperature. Slices were washed once again and placed on slides and covered in Prolong Gold Antifade Reagent (Invitrogen), then coverslipped.

Image Acquisition and Analysis

Images were acquired on a confocal microscope (Leica TCS SPE). Each staining was replicated in slices from at least three mouse. Images were reconstructed using FIJI ImageJ software for cell counting. Cells were counted and marked for each image in each channel. DAPI was used to verify cells. Raw counts were recorded in excel. The total number of GFP+ cells was counted and the percent of the GFP+ cells positive for a lineage specific antigen was calculated. For Calb/TH of the OB glomerular layer, images were taken of the entire layer. For total neurons of the OB, images were taken of the entire OB and montage images were reconstructed using FIJI ImageJ.

Dendrite Analysis

GFP/Tomato+ neurons were captured using confocal microscopy. Only neurons that could be followed from the top of apical dendrites to the tips of the basal dendrites were used. Twenty neurons total for each condition from three brains each were analyzed. Neurons were traced using the NeuronJ plugin of FIJI ImageJ, and total dendritic length was calculated using the measure tracings function. These tracings were used to assess dendritic complexity determined by Sholl analysis in FIJI ImageJ.

RNA Isolation and Purification

Mouse brains were put into ice cold 1x Hanks Balanced Salt Solution. Olfactory bulbs were removed using a razor and put into 1mL Qiazol lysis reagent (Qiagen). The tissue was manually homogenized using a pipette. Homogenate incubated in Qiazol for 5 minutes at room temperature. Chloroform was added to each sample, mixed vigorously, and incubated for 3 minutes at room temperature. Phases separated by centrifugation at 12,000g for 15 minutes at 4ºC. The top phase was transferred to a new tube, mixed with 100% isopropanol, and incubated for 10 minutes at room temperature. Samples were centrifuged at 12,000g for 10 minutes at 4ºC. Pellets were saved, washed in 70% ethanol, and centrifuged at 7,500g for 5 minutes at 4ºG. Pellets were briefly air-dried and resuspended in nuclease free H_2O.

RNA DNase Treatment, cDNA Generation, and Real Time PCR

DNA was removed from 200ng of RNA using Turbo DNase (Ambion) following the Manufacturer's protocol. 10ng of DNase-treated RNA was input into a cDNA reaction using the components of Applied Biosystems Taqman Reverse Transcription Reagents Kit. 5x specific primers for hsa-let-7g and snoRNA202 (endogenous control) were generated and provided in the Taqman MicroRNA Assays Kit by Applied Biosystems (PN4427975). cDNA generated using the following thermocycles: 30 minutes at 16ºC, 30 minutes at 42ºC, 5 minutes at 85ºC, and infinite hold at 4ºC. Real time PCR tubes set up containing 20x assay specific for hsa-let-7g and snoRNA202 (Taqman Reverse Transcription Reagents Kit), 2x Taqman Universal PCR Master Mix No AMP Erase UNG (Applied Biosystems), nuclease free H_2O, and 5µL of

cDNA sample. Each sample was done in triplicate. Levels assessed using relative quantification on a 7500 Real Time PCR System (Applied Biosystems). cDNA was generated for mRNA from P19 cells using the Ominscript Reverse Transcription kit (Qiagen) following the manufacturer's protocol. 500ng of DNase-treated RNA was input into each reaction. Real time PCR was performed using Power SYBER green PCR master mix 2x (Applied Biosystems). Each primer was used at a final concentration of 2µM. Relative levels of expression were determined for LIN41, LIN28, and GAPDH (endogenous control). LIN41 3'UTR primers *GTGTGGTAGGCAAAGGGATAG, AGGGTTAGGGAGTGAGGTG*; LIN28 ORF primers *GGTCTGGAATCCATCCGTGTCA, TCCTTGGCATGATGGTCTAGCC*; GAPDH primers *AGGTCGGTGTGAACGGATTTG, TGTAGACCATGTAGTTGAGGTCA*. Each sample was done in triplicate. Levels assessed using relative quantification on a 7500 Real Time PCR System (Applied Biosystems).

Plasmids and Plasmid Construction

LIN28-expressing and the GFP control plasmids were reported previously (Matsuda & Cepko, 2004; Balzer et al., 2010). Renilla (pARG-RL) and luciferase (pARG-FF) cell culture reporter plasmids were provided by Dr. Hristo Houbaviy (Wu et al., 2014). An oligonucleotide for a let-7A target site with *Bam*HI restriction sites (Fig 15B) was cloned into the 3'UTR of the luciferase plasmid. The circRNA-expressing plasmids contained the CAG promoter (lacking the intron), the inverted repeat sequences and splice sites from the pcDNA3-ciRS-7 plasmid of Hansen et al., 2013, and the circle-forming sequence cloned into a *Bam*HI site located between the splice

acceptor and donor. The let-7 sponge sequence was generated by GeneArt (Life Technologies, Carlsbad, CA) to have 36 18-bp sites with complementarity to let-7a, d, f, and g (Table 3). The sponge sequence was cloned into the *Bam*HI site of the circRNA plasmid in both orientations to generate the let-7 sponge and control circRNAs. The *in vivo* Tomato reporter plasmid was generated by amplifying five let-7 target sites from the psiCHECK2-let-7 8x plasmid (Addgene #20931) and inserting them into the 3'UTR of pCAG-tdTomato (Pathania et al., 2012). pCAG-GFP was obtained from Addgene (#11150).

The CRISPR donor plasmid was constructed in a Topo pCR2.1 (Invitrogen) backbone. The *lin41* 5' homologous arm containing sequence from intron three and exon four and the *lin41* 3' homologous arm containing sequence from exon four were both amplified using Phusion High-Fidelity DNA Polymerase (New England Biosystems) with specific restriction sites on either end from mouse genomic DNA (Fig 22). The 5' homologous arm product was cloned into the Topo pCR2.1 vector, first, and then the 3' homologous arm product was cloned in second. GFP was amplified using Phusion High-Fidelity DNA Polymerase with 1) StuI restriction sites on either end, 2) an additional "G" nucleotide before the ATG site in order to keep the sequence in frame with the natural *lin41* sequence of exon four, and 3) a stop codon at the 3' end. The GFP fragment was cloned into the StuI site of the pCR2.1 vector in between the two homologous arms. Oligos designed to target the StuI site were annealed and

cloned into the Precision X Linearized T7 gRNA vector (System Biosciences) following the manufacturer's protocol. Guide RNA oligos: *TGTATGAGACCACCTT-GGGGCTGCAGGAGGCCT, AAACAGGCCTCCTGCAGCCCCAAGGTGGTCTCA*

P19 Cell Culture

Mouse P19 cells were acquired from the ATCC. P19 cells were cultured in αMEM (Sigma-Aldrich) supplemented with 2.5% fetal bovine serum, 7.5% bovine serum, and 50 units/mL penicillin/streptomycin and grown in 37ºC and 5% CO_2. Cell lines were transfected using Xfect Transfection Reagent. Cells were grown for 48 hours then split 1:10 in 10 cm cell culture dishes. Cells were grown for 48 additional hours then integrated cell lines were selected for by 2μg/mL puromycin (Sigma-Aldrich). Individual colonies were selected using trypsin-soaked 3mm cloning discs. Colonies were grown in individual wells. Cell lines were confirmed using the Dual Luciferase Reporter Systems (Promega). Sponge cell lines were harvested and DNA was purified using the Genomic DNA Extraction protocol of the DNAeasy Blood and Tissue Kit (Qiagen). Taq polymerase (Denville Scientific) PCR used to confirm plasmid DNA. LIN28 was confirmed using fluorescence microscopy. Clonal P19 cell line differentiation was induced using $5x10^{-7}$ M retinoic acid (Sigma-Aldrich) and grown on bacterial petri dishes for 5 days. After this time, cell aggregates in suspension were harvested and dissociated. $2x10^6$ cells were plated on tissue culture dishes and grown in αMEM supplemented with N2 supplement (Invitrogen). Cells were fed every other day over the time course. $1x10^6$ cells were harvested at day 0 and 14 for luciferase assays and western blot.

Luciferase Assay

Cell pellets were thawed on ice and resuspended in 300μL 1xPassive lysis buffer. Pellets incubated for 15 minutes at room temperature. Lysis was aliquoted into technical replicates. Firefly and Renilla luciferase assays were completed with the Dual Luciferase Reporter Systems kit (Promega) on a Glomax 20/20 dual injector luminometer (Promega).

Western Blot

Olfactory bulbs were microdissected from the brain, homogenized, and lysed in RIPA buffer (with Halt, 5mM EDTA, and DNASEI) on ice. Cell pellets were thawed and lysed in NP-40 buffer (1% NP-40 Buffer, 50mM Tris HCl pH8.0, 150mM NaCl) on ice for 45 minutes. Lysed cells were centrifuged for 20 minutes at 14,000rpm in 4ºC. The supernate was saved and concentration assessed at 595nm using a spectrophotometer and the Protein Concentration Assay Reagent (Biorad) to generate standards. 20μg of total protein was loaded into a 10% SDS-Page Gel and separated for 1 hour at 200V. PDVF membrane was activated and proteins were transferred at 30V for 1 hour at 4ºC. Membranes were blocked in 10% milk in 1xPBS for 1 hour at room temperature. Primary antibodies incubated overnight at 4ºC and diluted in 5% milk in 1xPBST: mouse GFAP (1:1000, Sigma-Aldrich), mouse TuJ1 (1:1000, Covance), mouse Oct3/4 (1:1000, Santa Cruz), rat LIN28 (1:500), and mouse β-actin (1:1000, Sigma-Aldrich). Bound-primary antibodies detected using HRP-conjugated anti-mouse (1:10,000) and anti-rat (1:12,500) incubated for 1 hour at room temperature and diluted in 5% milk in 1xPBST.

Flow Cytometry

P19 cells were transiently-transfected with GFP (positive control), donor only, or CRISPR/donor plasmids and grown for 24 hours. Cells were trypsinized, washed, and centrifuged at 1500g for 1 minute. The pellet was resuspended in DPBS and the cells were put on ice. Cells were passed through a 25 $^{7/8}$g syringe twice. Cells were incubated in 70% EtOH at 4°C for 16 hours. Cells were centrifuged at 1250g at 4°C for 10 minutes and washed. Cells were passed through a 26 ½g syringe twice. Cells were centrifuged at max speed for 10 minutes, resuspended in DPBS, and put in a glass tube for flow cytometry analysis. Cells sorted on a Coulter EPICS XL-MCL Flow Cytometer and analyzed using EXPO 32 ADC Software. Negative cells were sorted into the "L" gate and positive cells were sorted into the "M" gate.

Statistical Analysis

Student's *t*-test for two samples was used and completed in spreadsheets provided by an online Biological Statistics to calculate significance (McDonald, 2014). Two way ANOVA was used to assess statistical significance for the Sholl analysis using GraphPad Prism 7. Paired *t*-test was used to calculate significance for the luciferase assays using an online calculator, https://www.graphpad.com/quickcalcs/ttest1.cfm.

Chapter 3: LIN28 controls progenitor and neuronal cell fate in postnatal neurogenesis.

Summary:

Although LIN28 is known to regulate both cell fate and tissue growth and at times to promote an undifferentiated state, thus far a unified understanding of LIN28's biological role at the cellular level has not been elucidated. The nervous system is an important setting for understanding developmental timing. The ordered generation of different cell types and the critical switch from stem cells to progenitors requires precise timing and regulation to ensure the proper number and types of differentiated neural cells (McConnell, 1985). LIN28 is expressed in the developing nervous system and evidence supports a role for it in cell fate determination (Balzer et al., 2010).

To explore LIN28's function in post-embryonic development of mammals, I utilized postnatal electroporation to target NSCs in the SVZ (Hartman et al., 2013). Postnatal electroporation is beneficial because it targets this small subset of cells in the SVZ after birth, allowing for wild-type brain development and the ability to follow the cell fate progression for NSCs and their progeny with no gross level interference. This system provides a unique opportunity to study self-renewal, proliferation, differentiation, and cell fate choices in one model. Here I address LIN28's role at the cellular level in postnatal neurogenesis.

Results:

Constitutive LIN28 alters cell fate in the olfactory bulb of the mouse.

I investigated the role of LIN28 in postnatal neurogenesis using neonatal electroporation. Electroporation of P0 to P1 mouse pups targets the NSCs that line the lateral ventricle in the SVZ (Fig 3A, left). Plasmids injected into the lateral ventricle are taken up by NSCs and continue to be expressed in their progeny (Fig 3A, B). NSC daughter cells leave the SVZ and travel through the RMS into the OB where they differentiate into mature neurons (Fig 3A, right). To study LIN28 in this system, I constitutively expressed the open reading frame of LIN28 fused to GFP under the CAG promoter (CMV early enhancer element and chicken beta-actin promoter; Fig 3C; Balzer et al., 2010). CAG-GFP was used as a control.

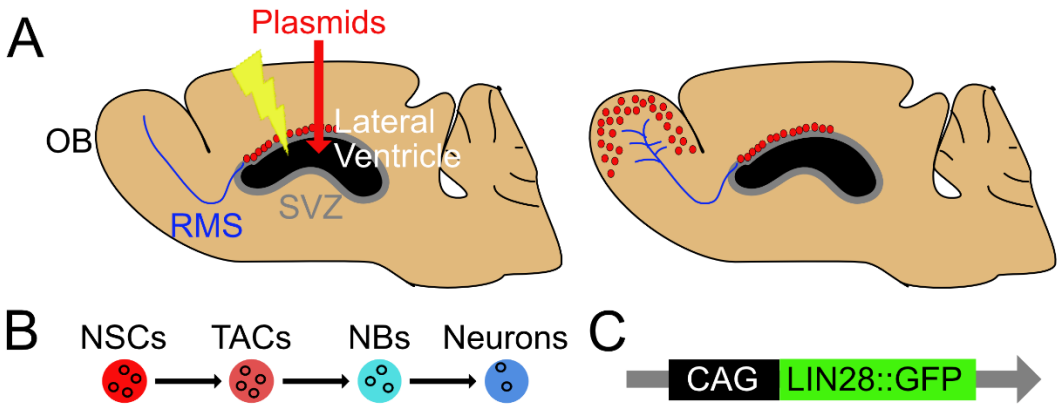

Figure 3. Plasmids can be electroporated directly into NSCs of the SVZ and passed on to NSCs progeny. A) Schematic depicting the electroporation protocol on a sagittal mouse brain section. Left side: At 0 DPE, plasmids are injected into the lateral ventricle, and then electrical impulses are administered so the DNA is incorporated into the NSCs of the SVZ (red dots). Right side: The NSCs of the SVZ produce progeny that migrate through the RMS to the OB at 14 DPE or later. B) Plasmids taken up by NSCs are passed along to their progeny, TACs, NBs, and neurons. Black circles represent plasmid DNA. C) Diagram illustrates the LIN28 plasmid construct. The open reading frame of LIN28 is fused to GFP, and is expressed under the constitutive CAG promoter.

Although we adhered closely to previously established protocols, we sought to confirm the consistency of our procedure (Lacar et al., 2010; Feliciano et al., 2012; Hartman et al., 2013; Mahoney et al., 2016). We used fluorescence to identify cells that either were electroporated or were descended from electroporated cells. Thus, all comparisons between experimental and control regarding marker staining are

normalized to total fluorescent cells. Therefore, relative changes in staining would not be expected to vary due to small differences in electroporation efficiency. Nevertheless, we assessed whether there was variability (1) among the electroporated mice and (2) among all slices from the mice for relative marker staining. We found that the percentage of GFP+ cells also positive for Sox2, for example, was consistent among mice, using 2-4 images per slice, four slices per mouse, and three mice each for control and experimental (Fig 4A, Tables 1 and 2). The variability among three mice, in this case, corresponds to an S.E.M. of ±0.7%. We also found that slices were consistent and representative of each mouse (Fig 4B, Tables 1 and 2). The variation among 12 slices from three mice gave an S.E.M. of ±0.9%. Because only the NSCs in the SVZ are electroporated in any given experiment, we express our results as changes at a cellular level, and not as reflecting whole animal effects. For this reason, our *n* in each case is the number of slices from a minimum of three mice per condition.

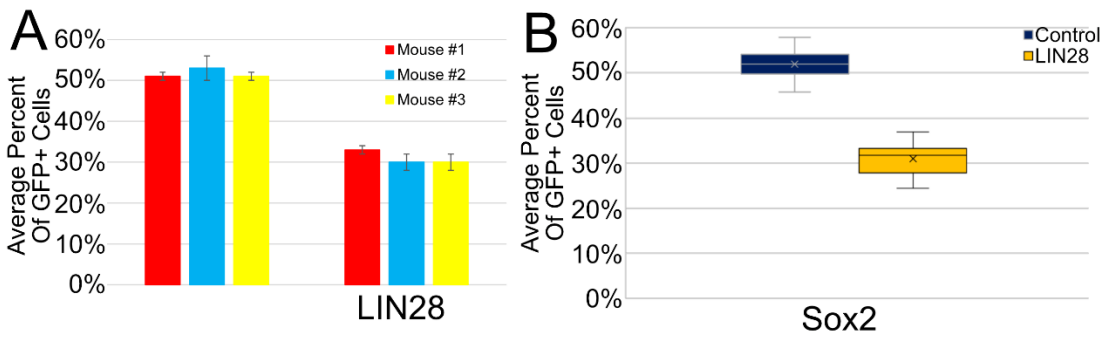

Figure 4. Assessment of variability. A) Bar graph depicting variability from mouse to mouse in both control and LIN28. Average percent of GFP+ cells positive for Sox2 from four slices per mouse, three mice. B) Box and whisker plot showing variability between slices of different mice. n = 12 slices from 3 mice. Average percent of GFP+ cells positive for Sox2.

Table 1. Raw data for Sox2 in the control condition. The raw counts for the total GFP+ cells and the total Sox2+ cells are presented in columns 3 and 4. Counts presented for each image taken per slice. Percentages provided for each image (column 5), per slice (column 6), and per mouse (column 7).

Control	Slice	Total GFP+ Cells	Total GFP/Sox2+ Cells	Percent Positive For Sox2	Percent Positive For Sox2 Per Slice	Percent Positive For Sox2 Per Mouse
Mouse #1	#1	112	55	49%	51%	51%
		76	44	58%		
		153	69	45%		
	#2	111	52	47%	51%	
		131	62	47%		
		32	19	59%		
	#3	125	49	39%	51%	
		175	83	47%		
		65	41	63%		
		82	46	56%		
	#4	149	67	45%	49%	
		147	73	50%		
		141	80	57%		
		139	63	45%		
Mouse #2	#1	115	57	50%	54%	53%
		121	54	45%		
		47	32	68%		
	#2	108	41	38%	46%	
		143	85	59%		
		83	33	40%		
	#3	102	42	41%	54%	
		230	124	54%		
		90	60	67%		
	#4	278	160	58%	58%	
		109	71	65%		
		53	27	51%		
Mouse #3	#1	118	54	46%	49%	51%
		224	118	53%		
		148	74	50%		

	#2	104	55	53%	52%	
		164	90	55%		
		93	46	49%		
	#3	109	53	49%	52%	
		164	85	52%		
		137	78	57%		
	#4	279	145	52%	55%	
		117	67	57%		
		123	68	55%		

Table 2. Raw data for Sox2 in the LIN28 condition. The raw counts for the total GFP+ cells and the total Sox2+ cells are presented in columns 3 and 4. Counts presented for each image taken per slice. Percentages provided for each image (column 5), per slice (column 6), and per mouse (column 7).

LIN28	Slice	Total GFP+ Cells	Total GFP/Sox2+ Cells	Percent Positive For Sox2	Percent Positive For Sox2 Per Slice	Percent Positive For Sox2 Per Mouse
Mouse #1	#1	30	11	37%	33%	33%
		92	29	32%		
		83	25	30%		
	#2	60	21	35%	30%	
		90	21	23%		
		74	24	32%		
	#3	51	20	39%	37%	
		92	30	33%		
		72	28	39%		
	#4	126	40	32%	32%	
		130	46	35%		
		86	26	30%		
Mouse #2	#1	237	80	34%	33%	30%
		75	21	28%		
		104	37	36%		
		25	9	36%		
	#2	188	66	35%	27%	
		55	13	24%		
		23	5	22%		
	#3	159	28	18%	27%	
		55	19	35%		
		55	16	29%		
	#4	139	38	27%	34%	
		57	16	28%		
		53	26	49%		
		10	3	30%		
Mouse #3	#1	85	23	27%	30%	30%
		134	44	33%		
	#2	114	41	36%	31%	

		58	18	31%		
		71	18	25%		
		47	15	32%		
	#3	45	10	22%	24%	
		30	8	27%		
	#4	101	31	31%	33%	
		63	23	37%		

Furthermore, because the LIN28-expressing plasmid is used for the first time here, we assessed whether it was taken up by NSCs as efficiently as the control plasmids. When co-electroporated with tdTomato, if LIN28::GFP electroporates at a lower rate, we would expect to see a higher percentage of tdTomato-only cells, and a lower double-positive population. LIN28::GFP colocalized with tdTomato in 97% and 96% of the total fluorescent cells at 1 and 3 DPE (Fig 5A). This is comparable to the double-positive control GFP+/Tomato+ cells, which were 98% and 97% of the total fluorescent cells at 1 and 3 DPE in the SVZ, respectively (Fig 5A). Therefore, the LIN28::GFP plasmid seemed to electroporate as efficiently as other plasmids. We also asked whether LIN28::GFP expression might cause an increase in apoptosis. Using cleaved Caspase 3 as a marker, we determined less than 1% of the GFP+ cells were apoptotic in both control and LIN28 conditions, and their difference was not statistically significant (Fig 5B).

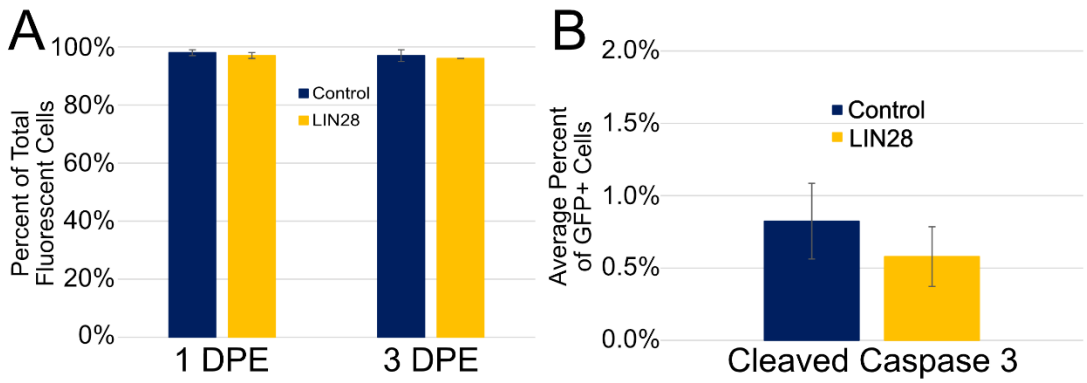

Figure 5. The LIN28::GFP plasmid electroporates at a high rate, and does not cause an increase in apoptosis at 3 DPE. A) Bar graph showing electroporation efficiency at 1 and 3 DPE in the SVZ. Average percent of total fluorescent positive cells positive for both GFP and Tomato. n = 8 slices from 6 mice (control-1 DPE), 10 slices from 6 mice (LIN28::GFP-1 DPE); n = 8 slices from 4 mice (control-3 DPE), 8 slices from 5 mice (LIN28::GFP-3 DPE). B) Average percent of GFP+ cells positive for cleaved caspase 3, a marker for apoptosis, at 3 DPE. In A and B, data presented as mean ± S.E.M. (Student's *t*-test). n = 7 slices from 6 mice.

To begin to understand LIN28's role in postnatal neural development, I first asked whether constitutive LIN28 expression alters neuronal cell fate in the OB at 21 DPE. Two populations of periglomerular neurons were identified using TH and Calb immunostaining. An even distribution of TH+ and Calb+ neurons was seen in the control (Fig 6A top), while a bias towards TH+ neurons was observed in the constitutive LIN28 condition (Fig 6A bottom). In control conditions, Calb+ neurons comprised 18.6% of the GFP+ population in the glomerular layer (Fig 6B). This popula-

tion was significantly reduced to 2.4% in the presence of constitutive LIN28 expression. The TH+ population was dramatically increased; the TH+ neurons more than doubled from 15.4% to 31.7% (Fig 6B). To test whether these changes were the result of mislocalization of migrating cells, I examined the distribution of GFP+ neurons in each of the layers. The vast majority of neurons that migrate into the OB from the SVZ localize to either the GL or GCL. In both control and LIN28, 92% and 91%, respectively, of GFP+ neurons localized to the GCL, and 8% and 9% to the GL, demonstrating that improper tangential migration was not a major factor in the cell fate measurements (Fig 6C). Furthermore, because OB interneuron cell fate is determined in part by region of origin in the SVZ, we assessed whether the cell fates were affected by selective targeting of different SVZ regions. Analysis of GFP fluorescence at 1 DPE, we found that the control and LIN28 plasmids were electroporated throughout both the dorsal and lateral regions of the SVZ (Fig 6D). Therefore, these findings show that expression of LIN28 influences cell fate in the postnatal OB, and can bias developing neurons toward the TH+ periglomerular fate.

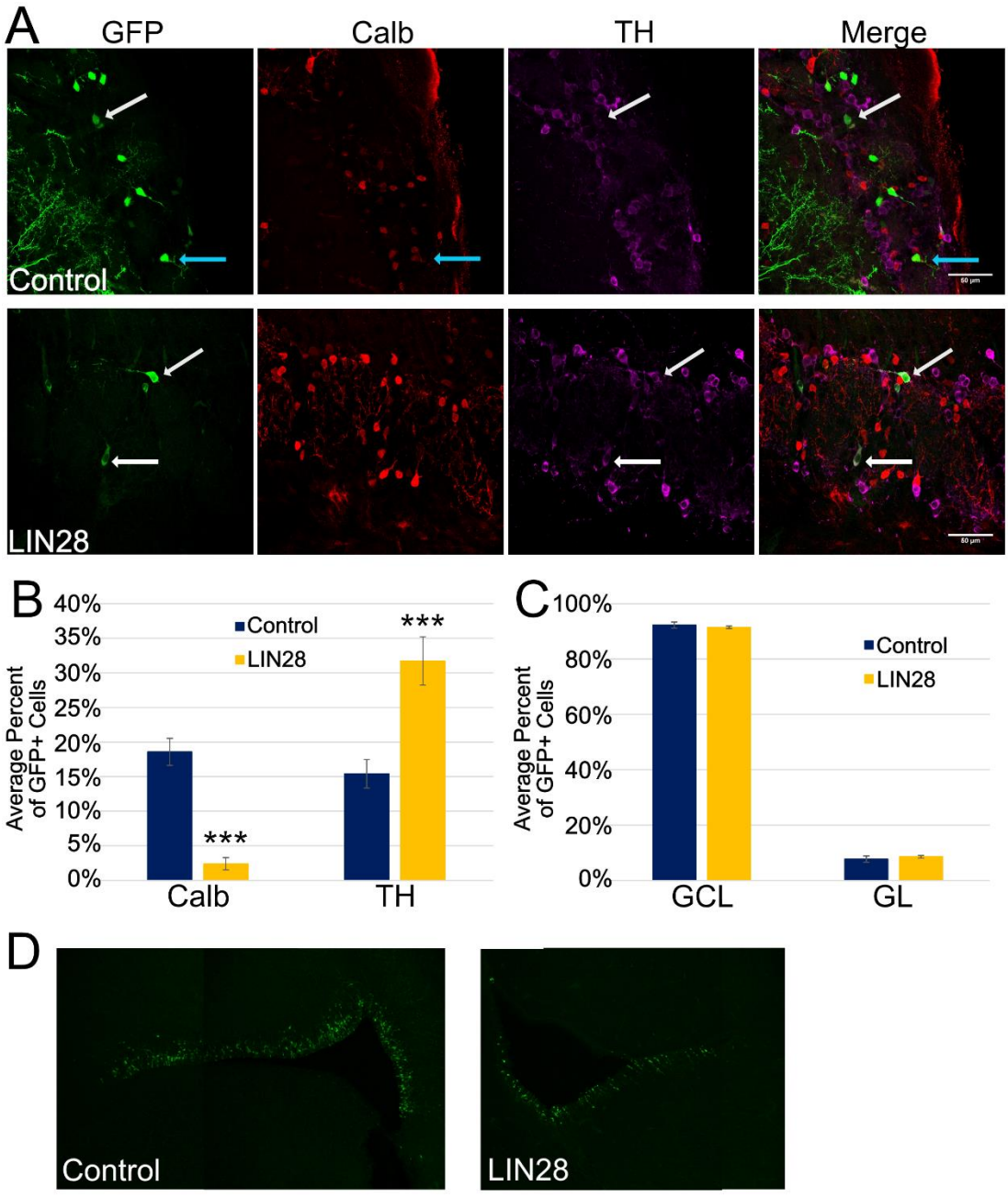

Figure 6. LIN28 alters cell fate in the glomerular layer of the OB at 21 DPE. A) Representative 40x micrographs showing GFP (green), Calb (red), and TH (purple) immunostaining in the glomerular layer. Top: Control. Bottom: LIN28. White arrows, GFP/TH+ neurons; teal arrow, GFP/Calb+ neuron. Scale bars: 50μM. B) Bar

graph depicting the average percent of GFP+ cells positive for Calb or TH at 21 DPE. n = 7 slices from 5 mice (control), n = 10 slices from 5 mice (LIN28::GFP). C) The average percent of GFP+ cells present in either the GCL or GL layers of the OB at 21 DPE. n = 7 slices from 5 mice. In B and C, data presented as mean ± S.E.M. ***, $p \leq 0.005$ versus control (Student's *t*-test).

Constitutive LIN28 reduces the total number of neurons in the olfactory bulb.

During my studies, I observed that while constitutive expression of LIN28 increased TH+ neurons relative to Calb+ neurons, it dramatically reduced overall the amount of newly generated neurons in the OB (Fig 7A). The mean number of neurons at 21 DPE was reduced in the LIN28 condition (393) compared to the control (802) per OB slice, a 50% reduction (Fig 7B). In addition, LIN28 expression reduced the number of neurons per area by 50% compared to control (Fig 7C). Constitutive LIN28 appeared to influence the progress of neurogenesis at an earlier stage.

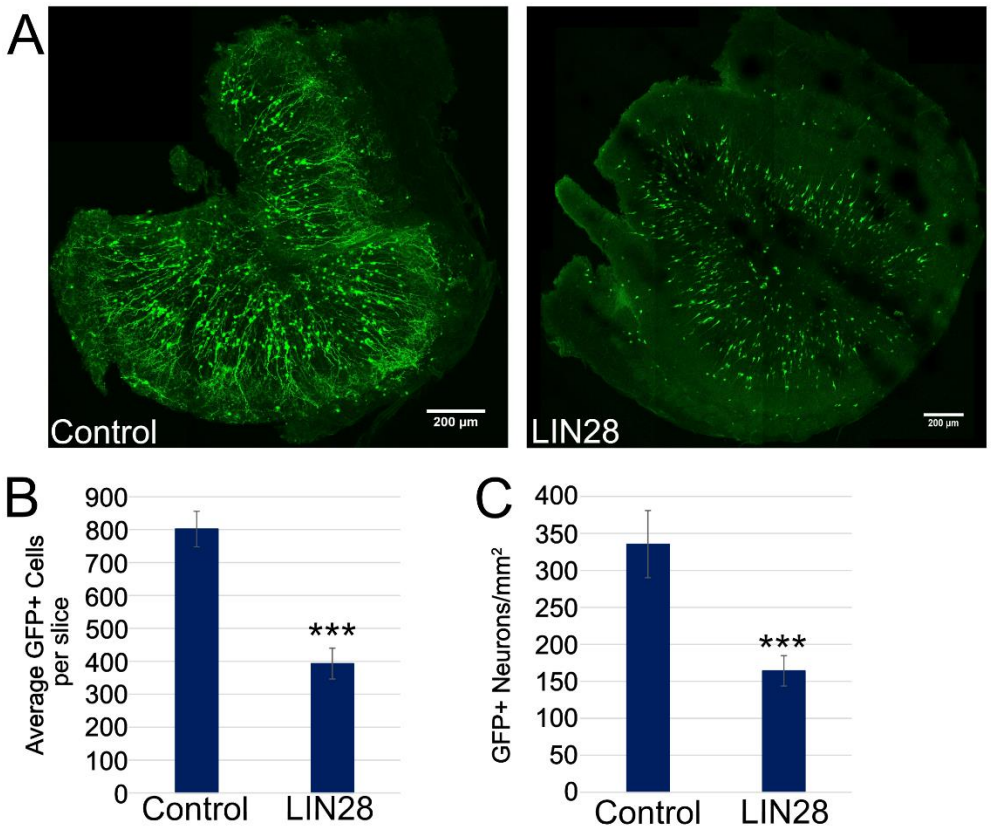

Figure 7. LIN28 reduces the total number of neurons in the OB at 21 DPE. A) Representative 10x micrographs displaying total GFP+ cells in the OB of control (left) and LIN28 (right) at 21 DPE. Scale bars: 200µM. B) Bar graph showing the average number of total GFP+ neurons in each OB slice at 21 DPE. n = 7 slices from 5 mice (control), n = 10 slices from 5 mice (LIN28::GFP). C) The average number of GFP+ neurons per area (mm^2) at 21 DPE. n = 7 slices from 5 mice. In B and C, data presented as mean ± S.E.M. ***, $p \leq 0.005$ versus control (Student's *t*-test).

As seen in Fig. 7A, I observed what appeared to be distinct morphology differences between granule GFP+ neurons in control and LIN28 (Fig 8A). In compari-

son to control, LIN28::GFP expressing granule neurons appeared to lack long branching apical dendrites based on the extent of the fluorescence. To assess whether LIN28 expression altered neuron morphology or simply was restricted in its localization within the cell, I co-electroporated NSCs with CAG promoter driven tdTomato, a red-fluorescing variant of GFP (Shaner et al., 2004). Red fluorescence is seen throughout the neuron, and GFP and Red fluorescence overlapped; however, LIN28::GFP and tdTomato failed to colocalize completely within neurons, with LIN-28::GFP excluded from the apical dendrites (Fig 8B). These co-electroporation experiments revealed that LIN28::GFP was restricted to the soma and basal dendrites.

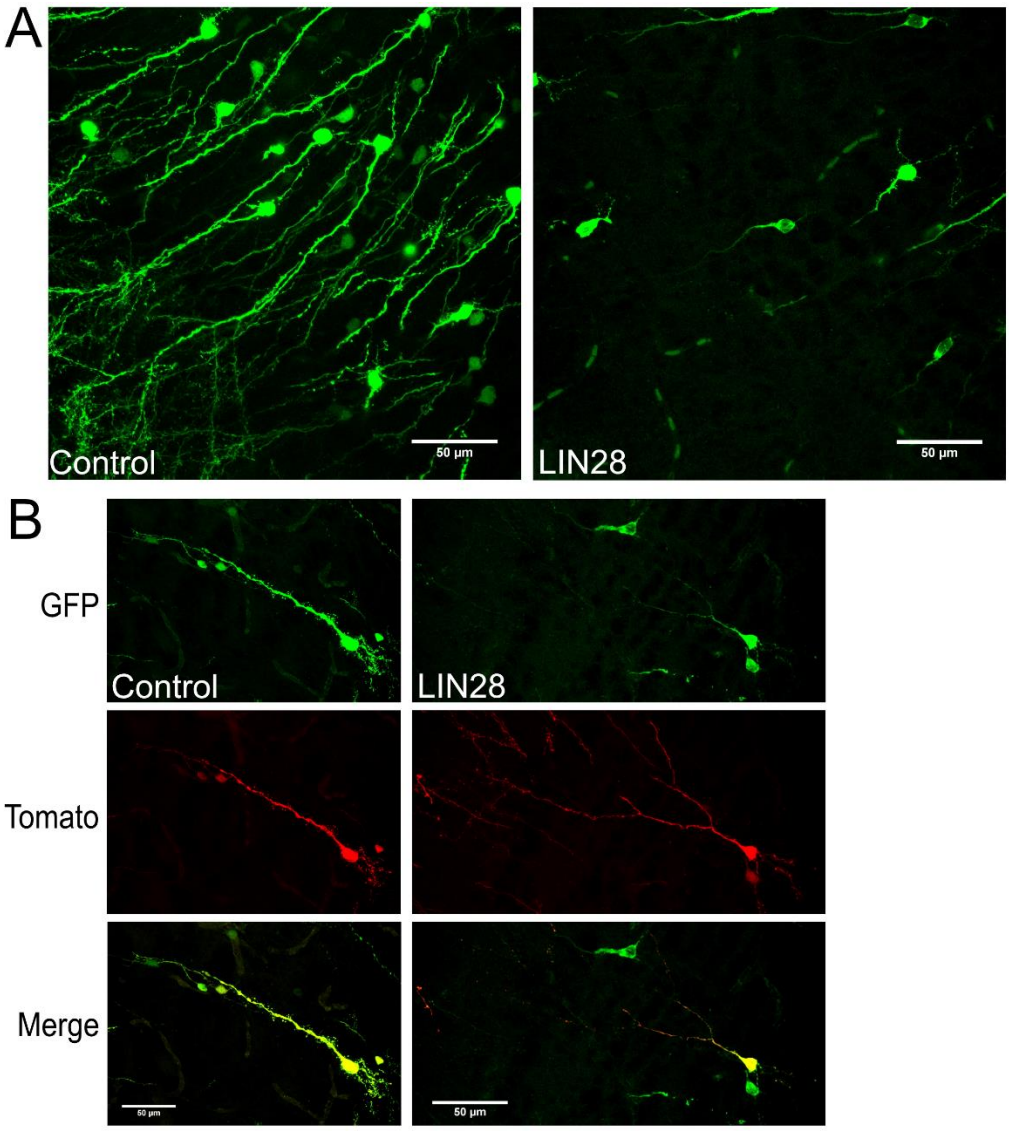

Figure 8. LIN28 does not localize to the apical dendrites of granule neurons in the OB at 21 DPE. A) Representative 40x micrographs depicting GFP+ (green) neurons in control (left) and LIN28 (right) at 21 DPE. Scale bars: 50µM. B) Representative 40x micrographs depicting GFP+ (green), tdTomato+ (red), and the overlap (yellow) of these two fluorescent markers in control (left) and LIN28 (right) neurons at 21 DPE. Scale bars: 50µM.

To specifically assess effects on dendrite formation, I investigated whether constitutive LIN28 expression alters dendritic length and branching complexity. Plasmids expressing tdTomato and either LIN-28::GFP or GFP alone were co-electroporated, and dendrite morphology was examined by red fluorescence. At 21 DPE, average total dendritic length was similar between LIN28-expressing (412 µM) and control neurons (405 µM) (Fig 9A). To analyze changes in complexity and branching, Sholl analysis was used to measure dendrite crossings at 5 µm intervals from the soma, and I found no significant difference between the LIN28 and control conditions (Fig 9B). These data suggest that constitutive LIN28 expression in granule neurons had no observable effect on dendritic growth or complexity.

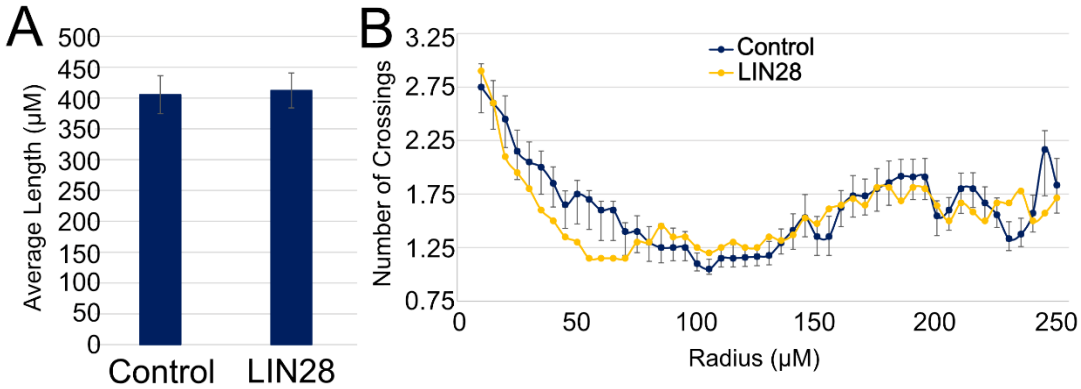

Figure 9. LIN28 does not appear to affect dendritic morphology in the OB at 21 DPE. A) Bar graph depicting the average length of 21 DPE OB neurons. Analysis completed using the NeuronJ function of Fiji Image J. n = 20 neurons per condition. B) Scatter plot of Sholl analysis depicting the average number of crossings from the soma of 21 DPE neurons at 5 micron intervals. Analysis completed using the Sholl Analysis function of Fiji Image J. n = 20 neurons per condition. In A and B, data presented as mean ± S.E.M. A: (Student's *t*-test). B: (Two way anova).

Constitutive LIN28 reduces the neural progenitor population, but does not affect the neural stem cells.

To determine the underlying cause of reduced neuron production, I investigated LIN28 expression during lineage amplification in the SVZ. First, I assessed the expression of endogenous LIN28 in cells derived from the SVZ. Primary NSCs were cultured from P2 SVZ cells and stained for endogenous LIN28, glial fibrillary acidic protein (GFAP), and Nestin. Of the DAPI+ cells, 99% that were positive for either GFAP, a marker for NSCs, or Nestin, a marker for NPCs, were also positive for LIN28 (Fig 10A). Western blot revealed that LIN28 was no longer expressed in neurons of the OB (Fig 10B). To induce differentiation of cultured explanted NSCs, I removed growth factors for 5 days, and found that the resulting cells co-stained with doublecortin (DCX), a marker for NBs and LIN28 (Fig 10C). These findings indicate that endogenous LIN28 is expressed in stem and progenitor cells of the SVZ, as well as cells that differentiated as NBs, but not in neurons of the OB.

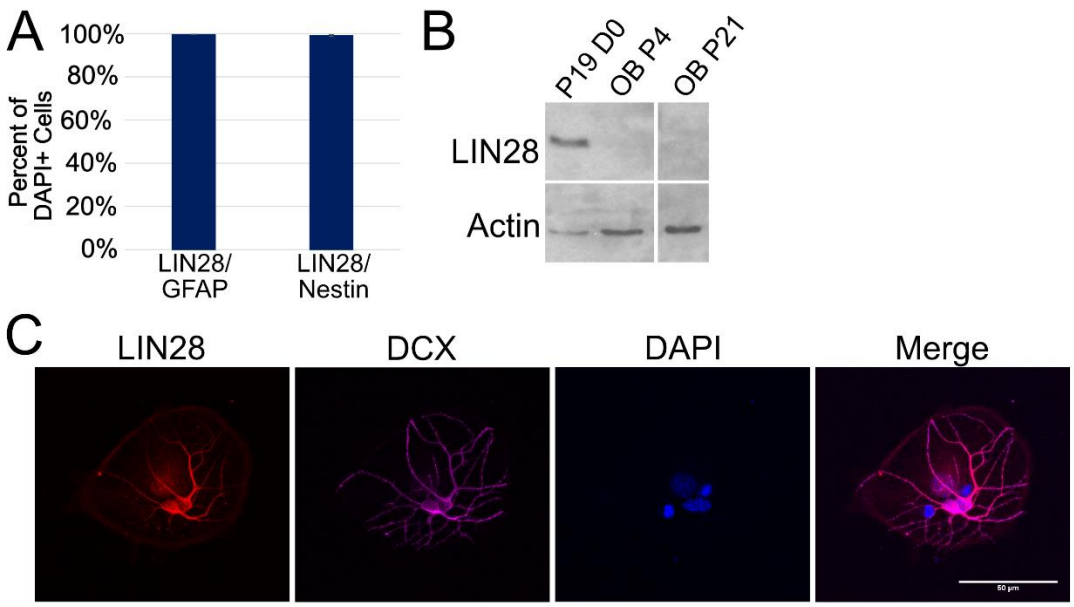

Figure 10. LIN28 is endogenously expressed in explanted primary NSCs derived from the SVZ. A) Percent of explanted primary DAPI+ NSCs positive for GFAP/LIN28 or Nestin/LIN28. B) Representative western blot of LIN28 protein expression in undifferentiated P19 cells and the OB in mice at postnatal days 4 (P4) and 21 (P21). n = 4 mice per day. Actin was used as the loading control. C) 40x micrographs depicting immunostaining of explanted differentiated NSCs derived from the SVZ. LIN28 (red), DCX (purple), and DAPI (blue). Scale bars: 50μM. In A, data presented as mean ± S.E.M. (Student's *t*-test).

I next compared the proportion of two cell populations in the SVZ, NSCs and TACs, under experimental and control conditions. NSCs exhibit radial glial properties, slowly divide, self-renew, and generate all the progeny cell populations of the SVZ. TACs, on the other hand, are fast dividing cells that undergo several rounds of division. At 3 DPE, 22% of the GFP+ cells stained positive for GFAP, which I found

to be similar under both control and LIN28-expressing conditions (Fig 11A,C). By contrast, immunostaining for Sox2, a marker for both NSCs and TACs, revealed a difference between control and LIN28-expressing conditions: 52% of the GFP+ cells were positive for Sox2 in control; however, the Sox2+ population was reduced to 32% of GFP+ cells by constitutive expression of LIN28 (Fig 11A,D).

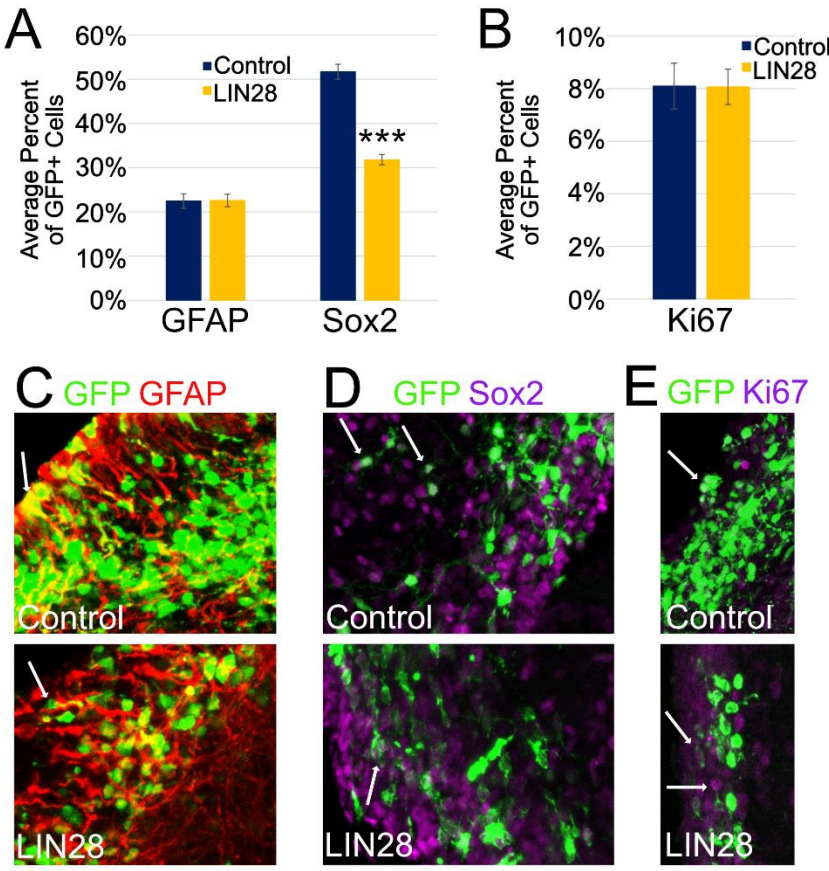

Figure 11. LIN28 affects the cell types of the SVZ differently at 3 DPE. A) Bar graph showing the average percent of GFP+ cells positive for GFAP, a marker for NSCs and Sox2, a marker for NPCs at 3 DPE. n = 8 slices from 5 mice (control-GFAP), n = 7 slices from 5 mice (LIN28::GFP-GFAP) and n = 12 slices from 3 mice (Sox2). B) Bar graph depicting the percent of GFP+ cells positive for Ki67, a marker

for active proliferation at 3 DPE. n = 12 slices from 11 mice (control), n = 9 slices from 11 mice (LIN28::GFP). C-E) Representative 30x micrographs depicting immunostaining of C) NSCs (GFAP-red), D) NPCs (Sox2-purple), and E) actively proliferating cells (Ki67-purple). White arrows depict examples of positive cells in each stain. In A and B, data presented as mean ± S.E.M. ***, $p \leq 0.005$ versus control (Student's *t*-test).

The reduction of the highly proliferative Sox2+ population suggested that constitutive LIN28 expression might have had its first effect in these cells. There are two possible ways to affect proliferation in this situation: 1) the proportion of proliferating cells is reduced, or 2) the proportion of proliferating cells remains the same, but the proliferative stage is shortened, i.e. the number of cell division cycles is reduced by premature differentiation. Using Ki67 as a marker of actively dividing cells, I observed that 8% of the GFP+ cells were actively proliferating in both the control and LIN28 conditions, suggesting no substantial difference in the proportion of proliferating cells (Fig 11B,E).

LIN28 promotes an increase in the neuroblast population.

My observation of endogenous LIN28 in NBs from explanted NSCs (Fig 10C) suggested that LIN28 could have some function in NBs *in vivo*. I examined this population in the SVZ at 3 DPE using DCX as a marker. Immunostaining revealed that constitutive LIN28 promoted a 70% increase compared to control: 11% of the GFP+ cells were positive for DCX in control, which increased to 19% with constitutive

LIN28 expression (Fig 12A). Since NBs are migratory immature neurons, I looked at sagittal sections of the SVZ, RMS, and OB at 7 DPE to see if these cells strayed from the RMS. In both control and constitutive LIN28 conditions, the GFP+ cells remained in the RMS and followed the path from SVZ to OB properly (Fig 12B). Because of the migratory nature of the NBs I questioned whether LIN28's increase in the NB population also meant migration to the OB occurred earlier as well. Since LIN28 reduced the overall number of GFP+ cells as a result of its effects on the Sox2+ population, I could not simply use a difference in the total number of neurons at 7 DPE between the two conditions as a measurement of early migration. I would expect the LIN28 condition to have less neurons as a result of reduced proliferation in the TACs. Instead, I used the total number of neurons at 7 DPE as a proportion of the total neurons in the OB at 21 DPE as a measure of early NB migration. If LIN28 NBs were exiting the SVZ and migrating to the OB at the same time as control, I would expect a similar percentage of neurons comparing 7 to 21 DPE. Control conditions at 7 DPE averaged 467 GFP+ neurons versus 260 in the LIN28 condition (Fig 12C). The control at 7 DPE was 58% of the 21 DPE totals, whereas LIN28 was 66% of the 21 DPE total. This suggested more NBs had migrated to the OB in the presence of constitutive LIN28 compared to control. This may also indicate that LIN28 promoted a more substantial increase in the NB population of the SVZ, but it could not be quantified due to their early exit from the region. Therefore, it appears that LIN28 was not only endogenously expressed in NBs, but it promoted an increase in this population. The increase in this NB population caused increased exit from the SVZ, entry into the RMS, and ultimately migration to the OB.

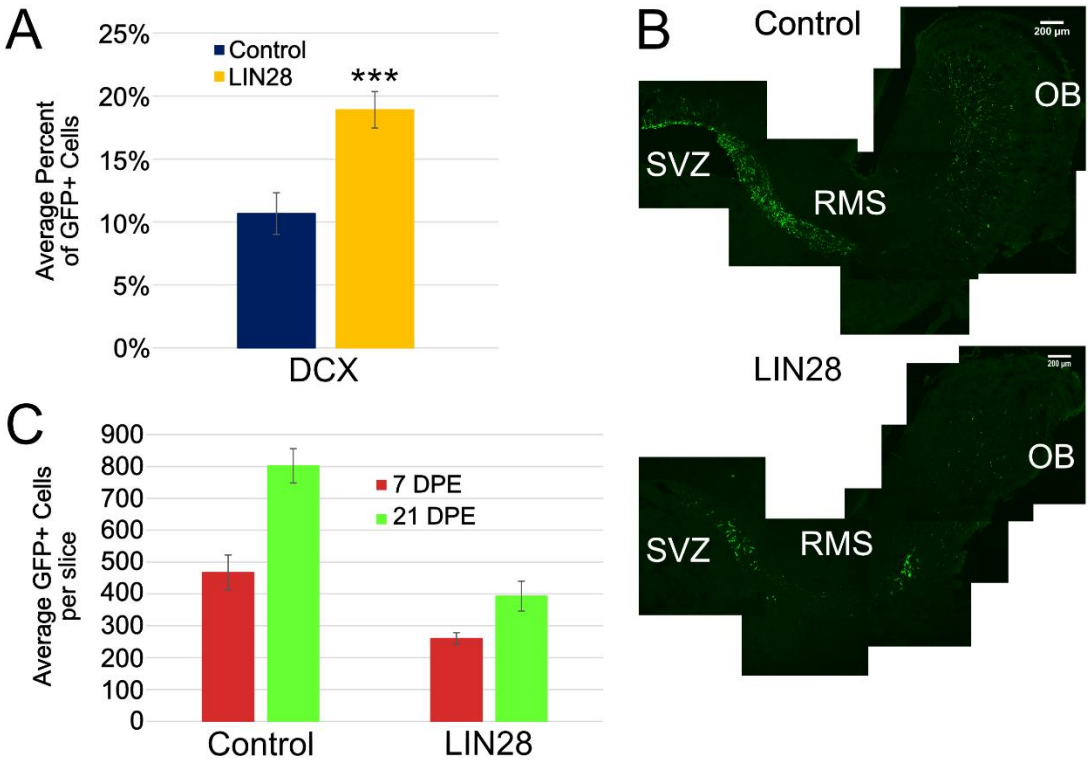

Figure 12. LIN28 increases the neuroblast population in the SVZ at 3 DPE and promotes early exit of neuroblasts. A) Bar graph showing the average percent of GFP+ cells positive for DCX, a marker for NBs, at 3 DPE. n = 7 slices from 6 mice (control), n = 6 slices from 6 mice (LIN28::GFP). B) Representative 10x sagittal micrographs showing the GFP+ cells (green) in the SVZ, RMS, and OB for control (top) and LIN28 (bottom) at 7 DPE. Scale bars: 200µM. C) Bar graph displaying the average total GFP+ cells at 7 and 21 DPE. 21 DPE data presented earlier in Figure 7. n = 11 slices from 4 mice (control), n = 7 slices from 4 mice (LIN28::GFP). In B and D, data presented as mean ± S.E.M. ***, $p \leq 0.005$ versus control (Student's *t*-test).

LIN28 causes early astrogliogenesis, but ultimately a reduction in the total number of astrocytes.

At 3 DPE, I occasionally observed production of GFP+ astrocytes following LIN28 electroporation well before they should normally appear. Although the appearance of these astrocytes was infrequent and difficult to quantify due to low numbers, I saw this with independent electroporations of LIN28 plasmids, and early astrocytes were never present in control conditions at this time point. I further explored the glial population at other time points to determine if LIN28 altered astrogliogenesis. To do this, I looked at GFP+ astrocytes in the striatum at 21 DPE, the time when the population of astrocytes peaks. I found the astrocyte populations were distinctly different between the control and constitutive LIN28 (Fig 13A). I quantified astrocytes in the striatum bordering the SVZ as a percent of the GFP+ cells. LIN28 reduced the number of astrocytes by 49%; 26% in control and 13% in constitutive LIN28 conditions (Fig 13B). Control averaged 22 GFP+ astrocytes in the striatum per slice, whereas constitutive LIN28 averaged 7 GFP+ astrocytes per slice (Fig 13C). In addition, I also quantified the number of astrocytes per area (mm^2) in each condition. Constitutive LIN28 significantly reduced the astrocytes per area by 68% (Fig 13D). These data suggest that constitutive expression of LIN28 occasionally caused early astrocyte production, but by the same token caused a reduction in the total number of astrocytes overall.

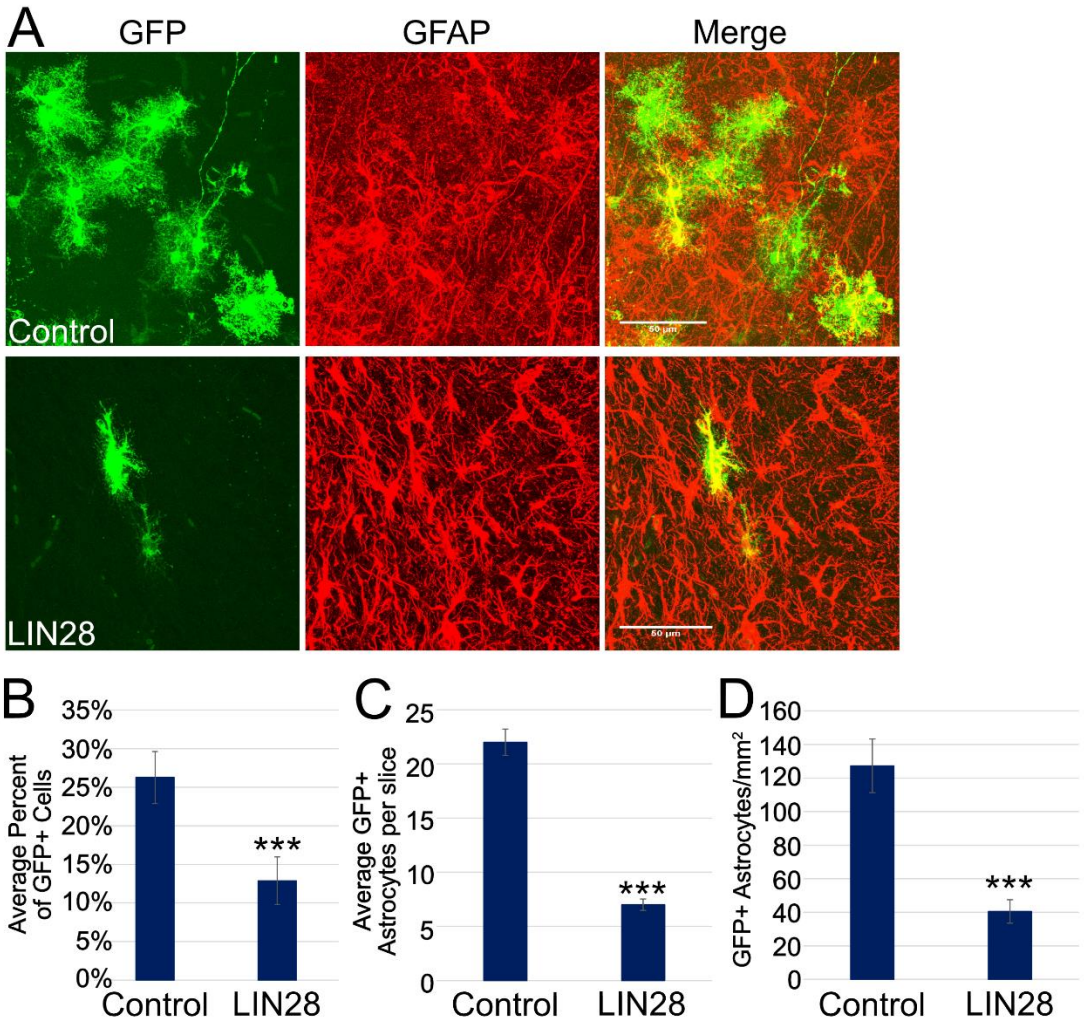

Figure 13. LIN28 reduces the total number of astrocytes at 21 DPE in the striatum. A) Representative 40x micrographs showing GFP(green)/GFAP+(red) astrocytes in the striatum of control (top) and LIN28 (bottom) at 21 DPE. Scale bars: 50μM. B) Bar graph displaying the average percent of GFP+ cells that are positive astrocytes in the striatum bordering the SVZ at 21 DPE. n = 12 slices from 6 mice (control), n = 15 slices from 6 mice (LIN28::GFP). C) The average number of GFP+ astrocytes in the striatum per slice at 21 DPE. n = 7 slices from 6 mice. D) Bar chart depicting the average number of GFP+ astrocytes per area (mm^2) at 21 DPE. n = 7

slices from 6 mice. In B-D, data presented as mean ± S.E.M. ***, $p \leq 0.005$ versus control (Student's *t*-test).

Chapter 4: Let-7 contributes only a subset of LIN28's activity in postnatal neurogenesis determined using a novel circRNA sponge.

Summary:

LIN28 is an RNA-binding protein containing a unique combination of two RNA binding domains, the CSD and CCHC motifs (Moss & Tang, 2003). LIN28's best understood molecular activity is to inhibit the expression of another conserved developmental timing regulator, the miRNA let-7 (Newman et al., 2008; Ryback et al., 2008; Viswanathan et al., 2008). When LIN28 is highly expressed, mature let-7 is absent; as LIN28 is downregulated, mature let-7 accumulates (Newman et al., 2008; Balzer et al., 2010; Vadla et al., 2012). Substantially less understood is LIN28's molecular activity that is independent of let-7 (Balzer et al., 2010; Zhu et al., 2010; Faas et al., 2013). Numerous potential targets have been identified, but a mechanism is not yet clear (Xu et al., 2009; Balzer et al., 2010; Qui et al., 2010; Peng et al., 2011; Yang et al., 2015).

Here I address what fraction, if any, of LIN28's role at the cellular level in postnatal neurogenesis is due to its inhibition of let-7. Because let-7 exists in multiple isoforms expressed from independent genes, I made use of a circular RNA (circRNA) sponge that we demonstrate effectively inhibits let-7 activity in three different systems and produces developmental phenotypes *in vitro* and *in vivo*.

Results:

Let-7 expression increases in the olfactory bulb as the mouse ages.

LIN28 is best known to block the maturation of the miRNA let-7 (Viswanathan et al., 2008). Previous work in our lab demonstrated that LIN28 possesses two separable activities: one to inhibit let-7 accumulation and the other that is independent of this process (Balzer et al., 2010; Vadla et al., 2012). To begin to address whether let-7 has a role in postnatal neurogenesis, I first measured the level of mature let-7 in the OB at different ages—P3, newborn mice; P21, weaned mice; and P56, sexually mature adult mice—compared to undifferentiated (D0) and differentiated (D15) P19 embryonal carcinoma cells (Fig 14). LIN28 is highly expressed at D0 in P19 cells, blocking mature let-7, and as it is down-regulated upon differentiation into neurons and astrocytes, let-7 levels increase about 100 fold. (Fig 14; Balzer et al., 2010). In the OB at P3, let-7 expression was 10 times higher than D15 P19 cells (Fig 14). The level of let-7 further increased about 1.6 fold by P21 and about 4 fold by P56 mice. Thus, let-7 was highly expressed in the OB, consistent with LIN28 being off in neurons (Fig 10B). Furthermore, even though the OB was established before birth and let-7 was already highly expressed in P3 mice, neurons expressed increasing levels of let-7 during the transition to adulthood.

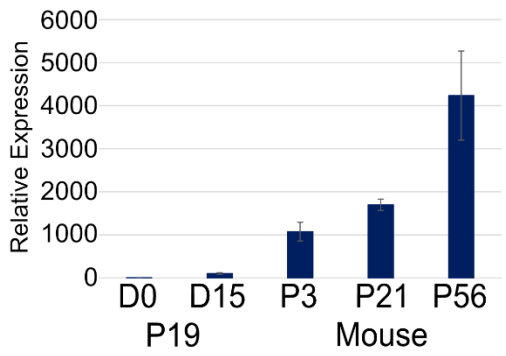

Figure 14. Relative levels of mature let-7 increase over time. Bar graph showing relative levels of let-7g in the OB determined using real time PCR, normalized to the endogenous control snoRNA 202. P19 cells were used as a positive (Day 15) and negative (Day 0) control. "P" means postnatal day. n of 4 mice at each time point. Data presented as mean ± S.E.M.

A circular RNA sponge was used to inhibit let-7 activity.

I next investigated whether some or all of LIN28's effects on postnatal neurogenesis might be due to an inhibition of let-7. To do this, I sought a means to inhibit let-7 in cells developing from the SVZ that is independent of LIN28. Circular RNA sponges have been shown to effectively sequester microRNAs away from their mRNA targets, thereby reducing or eliminating their regulatory effects (Hansen et al., 2013). I therefore endeavored to block let-7 activity directly using such a sponge. To target multiple members of the let-7 family simultaneously, we designed a microRNA sponge containing 36 repeats of randomized let-7 target sites 18 nucleotides apart directed at four members of the family, let-7a, d, f, and g (Balzer et al., 2010; Table 3). In linear splicing, the upstream exon contains a splice donor at the 3' end and the

downstream exon contains a splice acceptor at the 5' end (Fig 15A). These exons are separated by intronic sequence. In the end, the splicing results in the combination of exons and the removal of the intronic sequence. Placing inverted repeats upstream and downstream of the sponge sequence and reversal of the splice acceptor and donor orientation results in stem/loop formation and ultimately circle formation splicing (Fig 15B). Modeled after the work of Hansen et al, constructs were generated to express the let-7 sponge stably as RNA circles. As a control, I generated a version which contained the same 36 repeats but in the opposite orientation resulting in repetitive sequence that cannot bind let-7 microRNAs (Fig 15C).

Table 3. The let-7 target sites in the let-7 circRNA construct.

CTTATACAGACCTACCTC
ACTATACAGATCTACCTC
ACTATACAAATCTACCTC
ACTATGCAGCCCTACCTC
TCTATATAAACCTACCTC
AATATGTAAACCTACCTC
ACTATGTAAACCTACCTC
TCTATACAGATCTACCTC
ACTGTACAAATCTACCTC
ACTATGCAACCCTACCTC
ATTATACAAACCTACCTC
ACTGTACAACTCTACCTC
ACTATACACACCTACCTC
ACTATACAAGTCTACCTC

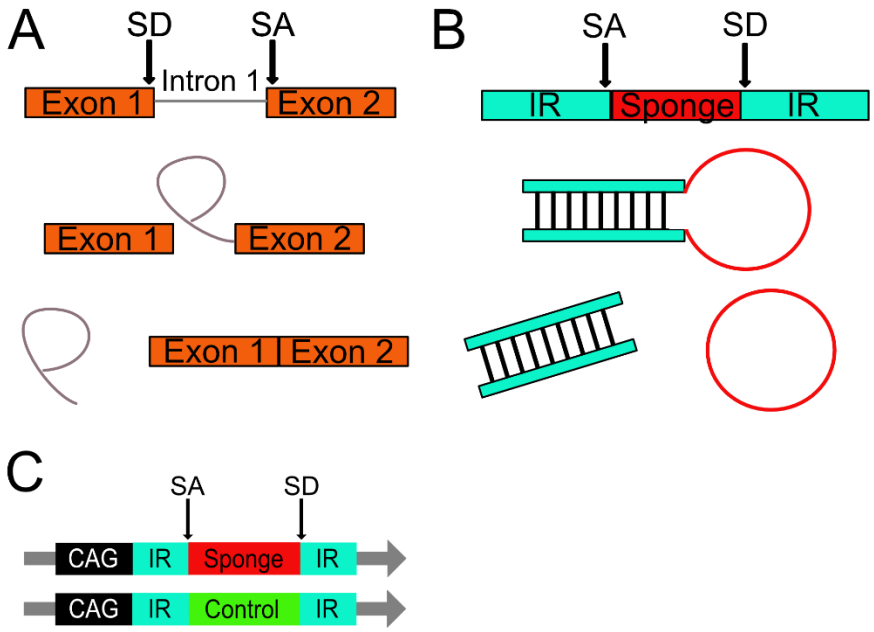

Figure 15. A let-7 circRNA sponge is produced as a result of circle formation splicing. A) Schematic depicting linear splicing. B) Diagram depicting circle formation splicing. C) The circRNA-expressing constructs: let-7 circRNA sponge (top) and the control circRNA (bottom). Inverted repeats are upstream and downstream of the sponge; the construct is expressed under the constitutive CAG promoter. SA, splice acceptor; SD, splice donor, IR, inverted repeats.

To verify the efficacy of the sponge, I tested the let-7 circRNA sponge in mouse P19 cells undergoing neurogenic differentiation *in vitro*. I employed a luciferase reporter assay where the open reading frame of firefly luciferase was constitutively expressed under the CAG promoter, and the 3'UTR contained a let-7a target sequence (Fig 16A,B). Clonal cell lines were generated expressing the luciferase reporter, a Renilla luciferase reporter for normalization, and a test plasmid expressing

the let-7 circRNA sponge, a control circRNA, LIN28::GFP, or the empty vector. The expression of luciferase and renilla was confirmed by a luminometer (Fig 16C). Luciferase and renilla levels, presented as relative light units, vary in each clone. Therefore, the ratio of luciferase to renilla is unique to each clonal cell line and cell lines cannot be compared directly to one another. Instead, comparisons must be made internally, and the pattern of normalized luciferase expression is compared between clonal lines. The third vector was confirmed using pcr of genomic DNA or microscopy. The circRNA (let-7 and control) band was detected using primers directed at the inverted repeat (Fig 16D). The let-7 circRNA and control circRNA plasmids were used as positive controls and the luciferase plasmid as a negative control for the line confirmations (Fig 16E, left). The circRNA band is present in the clonal cell lines, but not in the P19 cells positively confirming the presence of the third vector of interest (Fig 16E, right). LIN28::GFP was visualized using microscopy (Fig 16F).

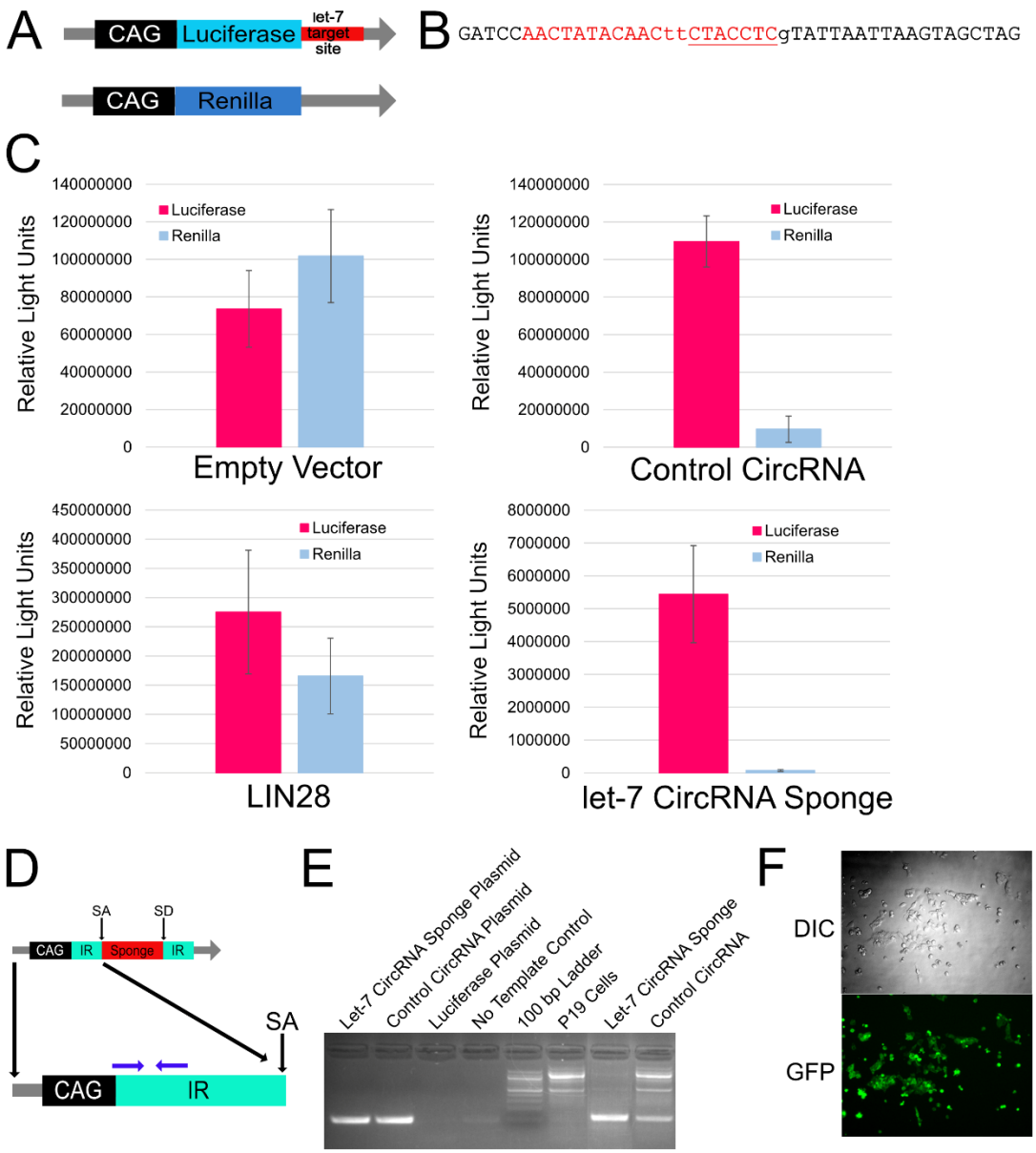

Figure 16. Clonal P19 cells were generated to test the let-7 circRNA sponge efficacy in a luciferase reporter assay. A) Diagram illustrates the luciferase reporter plasmid construct (top) and the renilla plasmid construct (bottom). Both open reading frames are expressed under the CAG promoter. The luciferase reporter contains a let-7A target site in the 3'UTR. B) Let-7 target sight design. Red, microRNA target se-

quence; the seed sequence is underlined. C) Relative expression of luciferase and renilla in the various clonal cell lines. D) Primers directed at a region in the inverted repeats were used to identify the presence of the circRNA control and let-7 circRNA sponge. Blue arrows, primers. E) Agarose gel showing PCR reaction products that are positive bands in the circRNA plasmids, and circRNA cell lines. No bands were present in the luciferase plasmid negative control, no template control, and P19 cells. F) DIC (top) and GFP fluorescence (bottom) of LIN28::GFP expression in the clonal cell line. In C, data presented as mean ± S.E.M.

In undifferentiated cells (day 0), there is no let-7 present, but as the cells differentiate into neurons and astrocytes, let-7 levels increase until the end of the timecourse (day 14). As expected, luciferase was highly expressed at day 0 in all conditions (Fig 17). Upon differentiation, let-7 activity would increase unless blocked, and luciferase expressed from a let-7-regulated reporter would be correspondingly downregulated. With both empty vector and control circRNA, luciferase was downregulated at day 14 by 36% and 63% respectively, (Fig 17, top); however, luciferase expression remained high in the presence of LIN28 and the let-7 circRNA sponge (Fig 17, bottom). Additionally, where luciferase expression only increased 7% at day 14 compared to day 0 in the presence of LIN28, it increased 34% in the presence of the let-7 circRNA sponge suggesting robust inhibition of let-7 activity by the sponge. Thus, the let-7 circRNA sponge was as effective as LIN28 in blocking let-7 during P19 neurogenic differentiation *in vitro*. The effectiveness of the let-7 circRNA sponge

was further validated in *C. elegans.* In this system, the let-7 circRNA sponge phenocopied a *let-7(0)* mutant; 0% of the circRNA sponge animals produced alae and 100% died by bursting (unpublished work, Eric Moss; Reinhart et al., 2000).

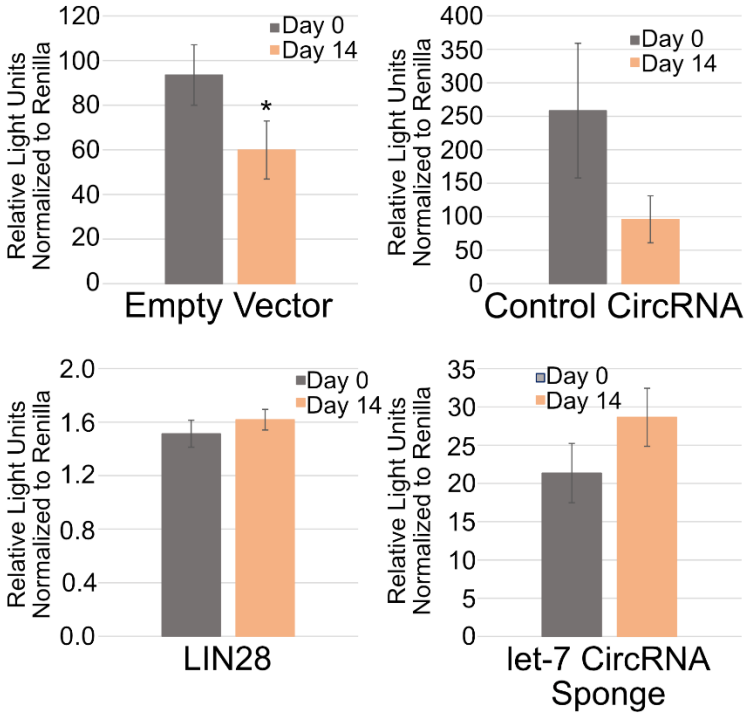

Figure 17. The let-7 circRNA sponge blocks let-7 activity in P19 cells. Bar graphs depicting the luciferase assay. Luciferase levels were normalized to its own internal renilla expression. n = 3-4 differentiations per cell line. Data presented as mean ± S.E.M. *, $p \leq 0.05$ versus control (paired *t*-test)

Previously we showed that constitutive LIN28 inhibited gliogenesis of P19 cells *in vitro,* and so I asked whether direct inhibition of let-7 had the same effect (Balzer et al., 2010). GFAP was detected by immunoblot at day 14 in the control circRNA cell line, but absent in the LIN28 line (Fig 18). When the let-7 circRNA

sponge was expressed, day 14 cells were positive for GFAP, indicating that gliogenesis had occurred. This result suggested LIN28 blocked gliogenesis in differentiating P19 cells independent of let-7.

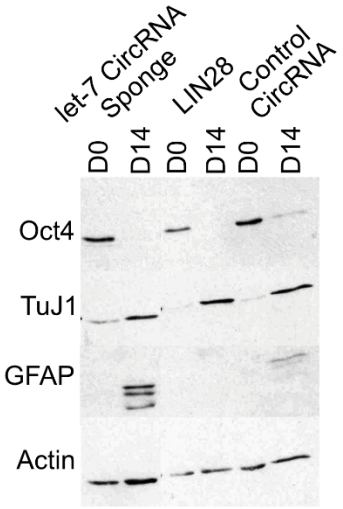

Figure 18. Let-7 does not regulate gliogenesis. Representative western blot showing the results of gliogenesis in the various P19 cell lines. D0, day 0; D14, day 14. Oct4, pluripotency marker; TuJ1, neuron marker. Actin was used as the loading control. n = 3-4 differentiation per cell line.

Direct inhibition of let-7 activity alters neuron fate and abundance in the olfactory bulb.

To block let-7 activity directly in cells developing from the SVZ, I electroporated a sponge-expressing construct into mouse NSCs. To demonstrate the sponge was functional *in vivo,* I electroporated the let-7 circRNA sponge or the control circRNA with CAG-GFP and a repressible CAG-Tomato reporter containing five let-7 target sites in the 3'UTR. If let-7 is expressed and active, I would expect tomato

fluorescence to be downregulated. If the let-7 circRNA sponge is able to effectively inhibit let-7 activity *in vivo*, tomato fluorescence would continue to be expressed. In the SVZ at 21 DPE, 63% of GFP+ cells expressed tomato fluorescence in the control condition, whereas 75% of GFP+ cells expressed tomato in the let-7 circRNA sponge condition (Fig 19). Similarly, more GFP+ granule neurons expressed tomato in the presence of the let-7 circRNA (62%) than in the presence of the control circRNA (55%). Tomato expression was comparable in the control circRNA (43%) and let-7 circRNA sponge (45%) conditions in the periglomerular neurons. The results of the reporter assay suggested the let-7 circRNA sponge could effectively block let-7 activity *in vivo*, consistent with both *C. elegans* and P19 cells.

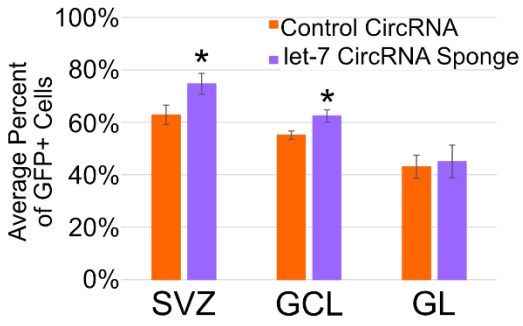

Figure 19. The let-7 circRNA sponge is active and effectively blocks let-7 activity in *in vivo* postnatal neurogenesis. Bar graph depicting the average percent of GFP+ cells expressing Tomato at 21 DPE in the SVZ, and the GCL and GL of the OB. n = 6 slices from 4 mice (control), n = 4 slices from 4 mince (LIN28::GFP). Data presented as mean ± S.E.M. *, $p \leq 0.05$ versus control (Student's *t*-test).

The incorporation of the let-7 circRNA sponge produced a small, statistically insignificant, but quantifiable decrease in GFP+ neurons in the OB at 21 DPE compared to the control circRNA. The control circRNA averaged 797 neurons per slice, consistent with CAG-GFP control, whereas the let-7 circRNA sponge reduced total GFP+ neurons to 649 per slice, a 19% reduction (Fig 20A, B). In addition, the let-7 sponge reduced both populations of periglomerular neurons: Calb+ from 16.3% to 9.8% and TH+ from 16.6% to 12.5% (Figure 20C). Although these populations were reduced compared to their respective control populations, they were both still within the wild-type reported ranges in the literature (Nagayama et al., 2014). Because direct inhibition of let-7 activity in cells developing from the SVZ had only a modest effect on neuron fate and abundance in the OB, a significant fraction of the effects of constitutive LIN28 may be independent of its inhibition of let-7.

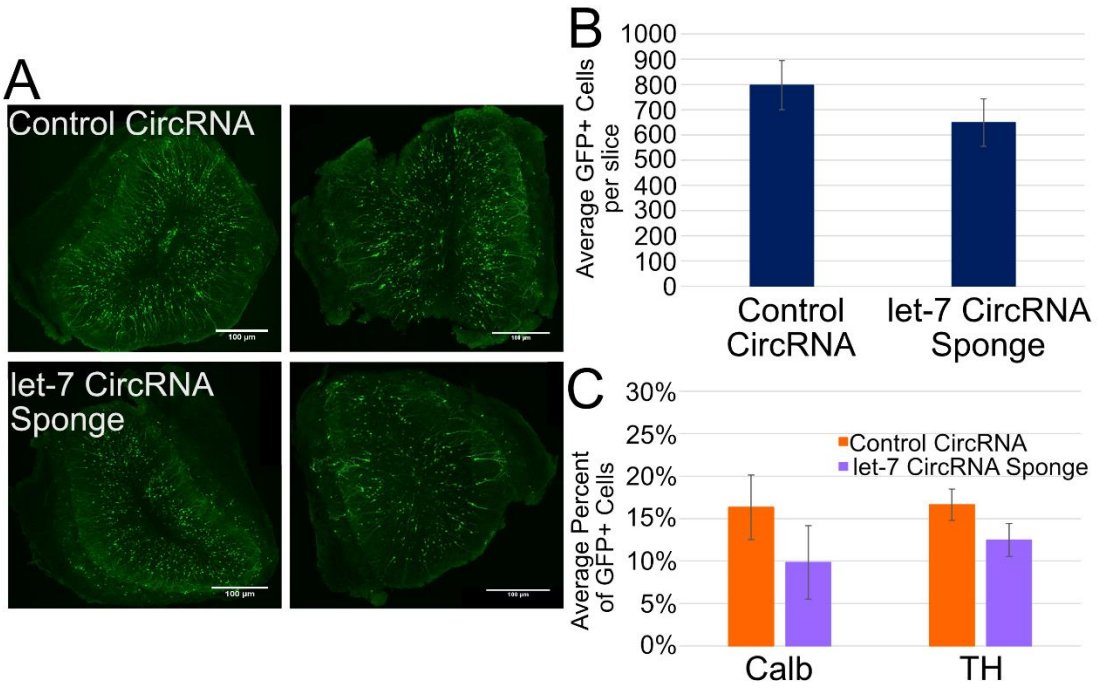

Figure 20. Let-7 has a minor effect on cell fate and total neurons in the OB at 21 DPE. A) Representative 10x micrographs displaying total GFP+ cells (green) in the OB of control circRNA (top left and right) and let-7 circRNA sponge (bottom left and right) at 21 DPE. Scale bars: 100μM. B) Bar graph showing the average total GFP+ neurons in each OB slice at 21 DPE. n = 7 slices from 5 mice (control), n = 7 slices from 6 mice (LIN28::GFP). C) The average percent of GFP+ cells positive for Calb or TH at 21 DPE. n = 7 slices from 5 mice (control), n = 7 slices from 6 mice (LIN28::GFP). In B and C, data presented as mean ± S.E.M.

Chapter 5: LIN41 and its expression in neural differentiation.

Summary:

LIN41 is an E3 ubiquitin ligase protein that is not only expressed in the mammalian developing nervous system and is essential for proper embryonic neural development, but it is also expressed in the terminally differentiated ependymal cells of the SVZ (Maller Schulman et al., 2008; Chen et al., 2012; Cuevas et al., 2015; Mitschka et al., 2015). This has two implications. First, LIN41 may play an important role in developmental timing and cell fate specification in postnatal neurogenesis just as LIN28 does. Second, as LIN41's expression and requirement in mammalian embryonic neural development is similar to LIN28's, this could suggest that the *C. elegans* LIN28/let-7/LIN41 pathway is intact in mammals. Though LIN28, let-7, and LIN41 are all conserved in mammals, and many have shown the recapitulation of the let-7 regulation of LIN41, we still do not know if this pathway is fully intact in mammals (Reinhart et al., 2000; Slack et al., 2000; Kloosterman et al., 2004; Vella et al., 2004; Kanamoto et al., 2006; Lin et al., 2007; O'Farrell et al., 2008). To better understand LIN41 during *in vitro* neurogenesis, I examined LIN41 at the RNA level. I then developed a method that utilizes the genomic editing system, CRISPR/Cas9, to insert GFP into the genomic sequence of LIN41 in P19 cells, in the hopes of providing a fluorescent marker to follow LIN41 expression and to study the effects of LIN41 null in the future.

Results:

In *C. elegans*, LIN41 is highly expressed early in larval development, but is downregulated as development progresses (Vadla et al., 2012). To better understand LIN41 in P19 neural differentiation, I first attempted to identify LIN41's expression over the course of a differentiation. Using primers directed at the 3'UTR of LIN41, I assessed relative levels of LIN41 mRNA in P19 and P19 (GFP) cells (Fig 21A). LIN41 is highly expressed from days 0-3 and is steadily downregulated with very little expression by day 7 and the remainder of the timecourse. In *C. elegans*, there is a distinct delay in the downregulation of LIN41 in respect to LIN28, so I asked whether this was true here as well (Vadla et al., 2012). Primers directed at the open reading frame of LIN28 revealed similar downregulation patterns of LIN28 and LIN41 and no apparent delay (Fig 21B). Since LIN28 indirectly regulates the expression of LIN41 by blocking the maturation of let-7 in *C. elegans*, I asked whether constitutive LIN28 expression would result in constitutive LIN41 mRNA expression. Constitutive LIN28 mRNA remains high over the differentiation time course (Fig 21B). However, it is unable to maintain continuous high expression of LIN41; LIN41 is downregulated normally (Fig 21A). This result makes sense considering retinoic acid-induced differentiation also forces the downregulation of endogenous LIN28 protein, even in the presence of constitutive LIN28 (Balzer et al., 2010).

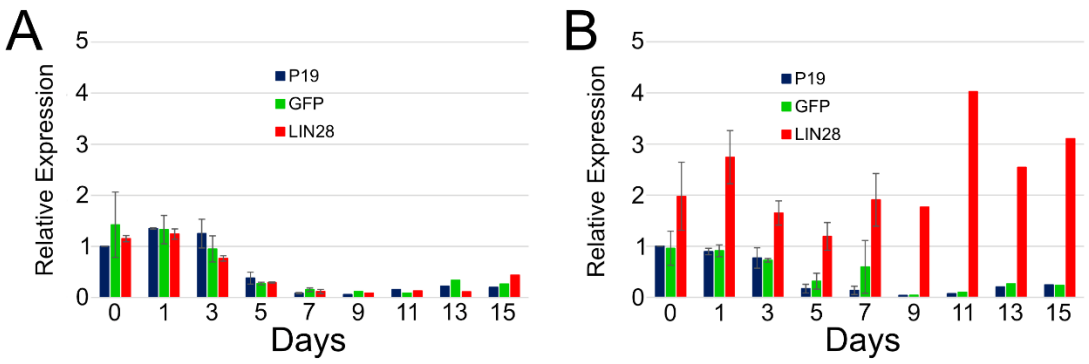

Figure 21. LIN41 and LIN28 mRNA are highly expressed early, and downregulated as neural differentiation progresses. Relative levels of mRNA assessed using Real time PCR in three different cell lines: P19 cells, GFP+ P19 cells, and constitutive LIN28 P19 cells. LIN41 and LIN28 mRNA normalized to internal GAPDH. A) LIN41. B) LIN28. n = 3 differentiations per cell line.

The expression pattern of LIN41 mRNA provided only a limited view into LIN41 in mammals. I next questioned when LIN41 protein was expressed in P19 cells. After trialing numerous LIN41 antibodies, I was unable to detect LIN41 protein by immunoblot. In an attempt to circumvent the antibody issue, I used CRISPR technology to generate chromosomal changes to endogenous *lin41*. Bacteria rely on the CRISPR system, or clustered regularly interspaced short palindromic repeats, as an endogenous defense against invading plasmid and viral DNA (Cong et al., 2013; Mali et al., 2013b). The CAS9 protein cleaves DNA and introduces a double-stranded break in the DNA three basepairs upstream of a predicted protospacer-adjacent motif (PAM) NGG (Cong et al., 2013; Mali et al., 2013a). CAS9 is directed to the cleavage region of interest by the guide RNA which includes the PAM at the 3' end (Mali et

al., 2013b). Mouse genomic *lin41* consists of four exons (Fig 22). A predicted cleavage site was located close to a StuI restriction site in the fourth exon. I designed a donor plasmid containing GFP with a stop codon surrounded by homologous arms upstream and downstream of the StuI site (Fig 22). This cell line would provide two benefits: 1) I would be able to follow the protein expression of LIN41 under its natural promoter by following GFP fluorescence; 2) I would be able to study the role of LIN41 by generating a null cell line.

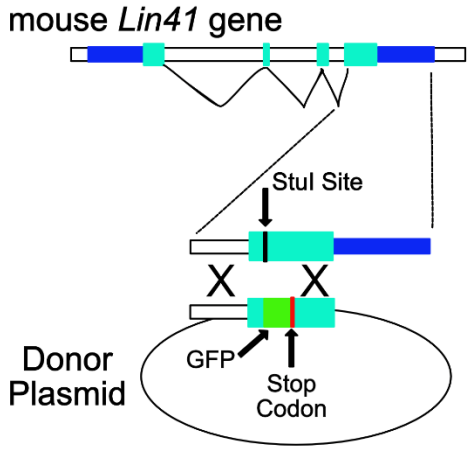

Figure 22. CRISPR schematic to insert GFP into chromosomal LIN41. Top: diagram of genomic mouse *Lin41*. Blue boxes represent 5' and 3'UTR regions. Mint boxes represent *Lin41* exons. Bottom: zoom in on intron three, exon four, and the 3'UTR. The StuI site is highlighted where CAS9 is targeted. The donor plasmid contains homologous sequence to the third intron upstream of GFP and a stop codon and the end of the fourth exon downstream.

If the CAS9 protein properly cleaved at the targeted region and homologous recombination occurred, GFP would be inserted in the start of the fourth exon and

convert the remaining sequence into additional 3'UTR (Fig 23A). The CRISPR target site removes the NHL domains rendering the LIN41 protein nonfunctional (Chang et al., 2012; Loedige et al., 2013). I built the donor plasmid without any mammalian antibiotic resistance in order to prevent any non-specific integration; however, the drawback to this method is very fast proliferation. I successfully identified GFP+ cells in culture using a fluorescent microscope, but the event was rare and hard to capture due to the rapid proliferation. I split a possible GFP+ clone into an individual well and attempted to identify whether GFP had inserted. GFP was no longer expressed, but it was possible the loss of LIN41 caused some differentiation to occur therefore GFP was downregulated. Because of this possibility, I designed a PCR scheme to identify if GFP was inserted. CAS9 and homologous recombination could occur in one or both alleles, so I generated primers that would capture both the endogenous LIN41 allele and the GFP+ insert (Fig 23B). Since the wildtype allele was much smaller than the GFP-insert allele, I performed a test PCR on the donor plasmid, a plasmid that expresses the ORF of LIN41, and a mixture of the two to ensure the primers could detect each allele individually and in a heterogeneous mixture. The wildtype and GFP-insert alleles could both be detected individually and together (Fig 23C). When I completed the PCR on my cells of interest, my possible positive clone was negative and only the endogenous LIN41 band was detected the same as control (Fig 23D).

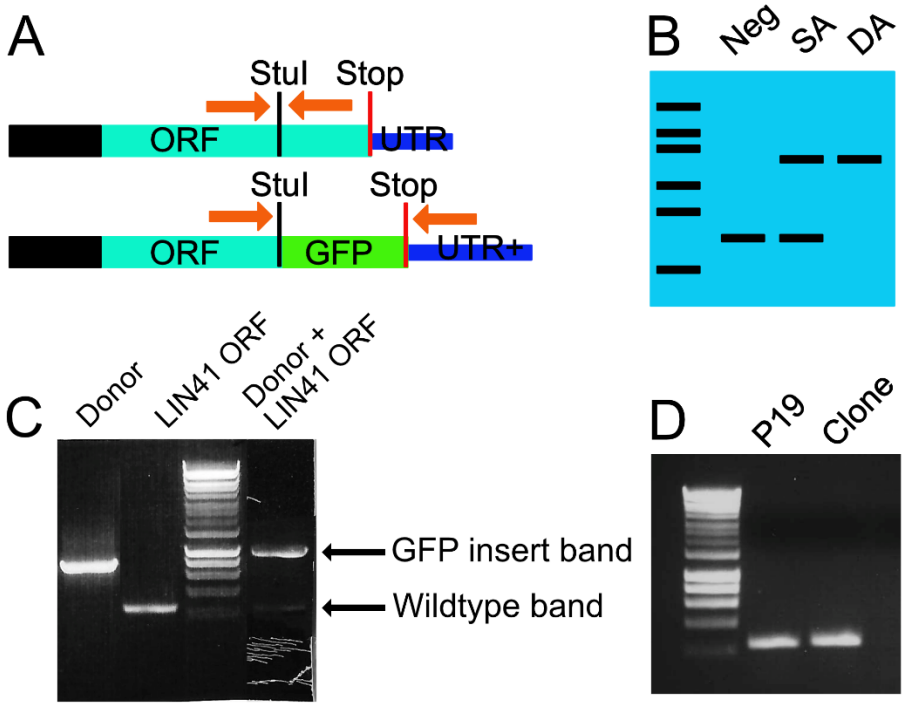

Figure 23. PCR scheme to detect GFP insertion into the chromosome. A) Primers designed around the StuI site that would capture the endogenous *Lin41* sequence, and *Lin41::GFP*. B) CAS9 could target one or both alleles; the primers could detect all three possible outcomes: Negative integration (left), single allele (middle), and double allele (right). Neg, negative; SA, single allele; DA, double allele. C). Agarose gel depicting PCR test demonstrating that the primer set can detect each band individually (Donor, left; LIN41 ORF, middle) and in a heterogenous mixture (Donor + LIN41 ORF, right). D) Agarose gel depicting Lin41 PCR product from P19 cells and a CRISPR/Donor clone.

Since I had visualized a few GFP+ cells but was unable to physically isolate said cells, I looked for another way to confirm that I was having successful integration and expression of GFP. I used flow cytometry to sort GFP+ and GFP- cells.

GFP+ and GFP- cells could be clearly detected and sorted; as demonstrated by the P19 (negative) and GFP+ (positive) controls (Fig 24 top). To verify the donor plasmid could not integrate on its own, I assessed the cells in a donor only transfection, and confirmed all cells were GFP- and the donor could only integrate in the presence of the CRISPR plasmid (Fig 24 middle). Following three independent transfections of the donor and CRISPR plasmids together, I found successful expression of GFP in two out of the three experiments (Fig 24 middle/bottom). Although I successfully demonstrated the viability of this method, I did not physically generate the cell line. The next step of this project requires cell sorting to generate the actual cell line.

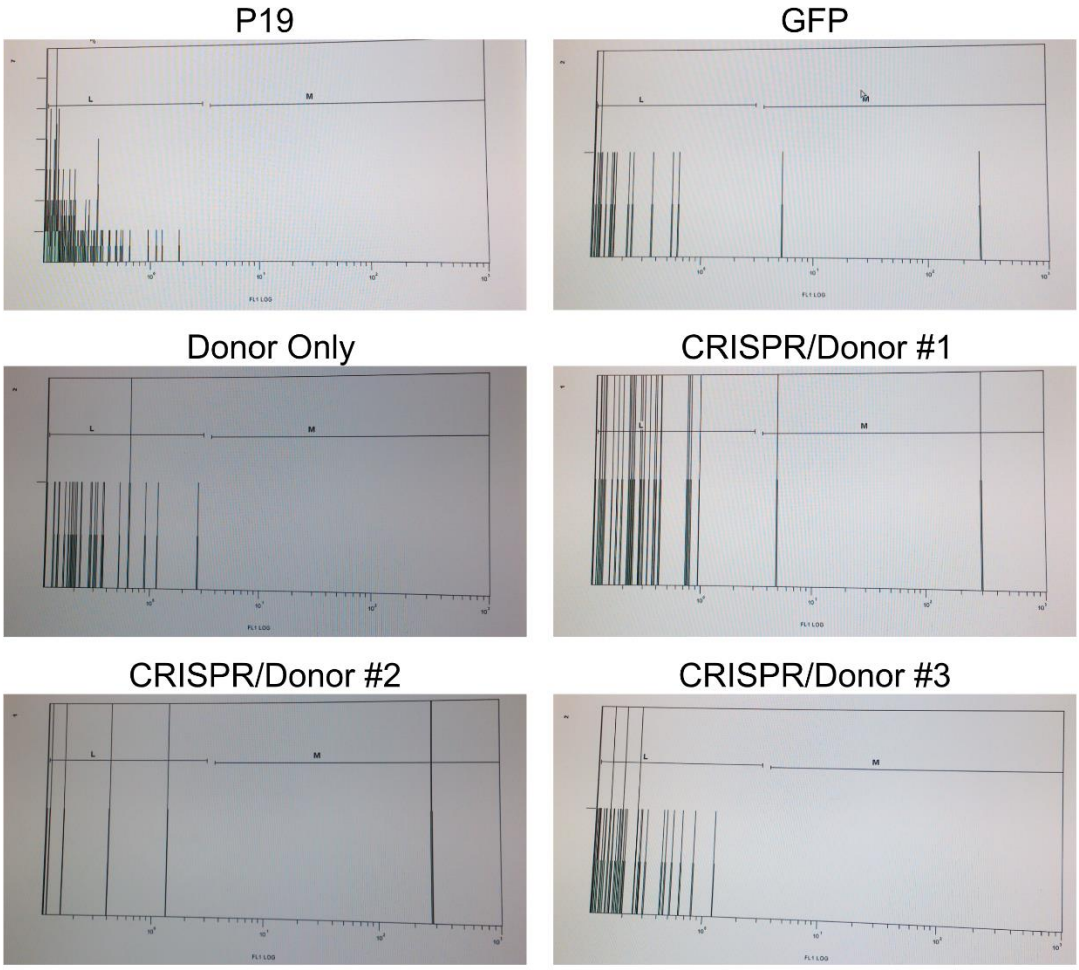

Figure 24. GFP+ cells can be detected in CRISPR/Donor transfections and separated from the GFP- population by flow cytometry. Histograms depicting GFP+ and – populations in various cell lines. GFP- cells are sorted in the "L" portion of the histogram; GFP+ cells in the "M" portion of the histogram. P19 cells were used as a negative control. GFP+ P19 cells were used as a positive control.

Chapter 6: Discussion (Summary and Conclusions)

The conservation of *C. elegans* heterochronic regulators LIN28, let-7, and LIN41 in mammals inspired the question whether the function of these molecules was preserved as well, that is do they regulate developmental transitions in mammals as they do in *C. elegans.* Furthermore, these three genes have a complex genetic relationship in regards to one another and whether that relationship is intact in mammals remains unanswered. I utilized neurogenesis as a model to answer 1) what role LIN28 plays in development and cell fate choices at the cellular level in mammals, 2) is it dependent or independent of let-7, and 3) what contribution LIN41 may have to the overall process as both a downstream target or a separate entity.

Constitutive expression of LIN28 in cells derived from the SVZ caused several distinct effects on postnatal neurogenesis in the mouse: it dramatically reduced the number of differentiated neurons, it altered the relative abundance of two neuronal subtypes, it reduced the population of proliferating neural progenitors in the SVZ while increasing the proportion of NBs, it promoted exit of NBs from the SVZ, and it reduced the number of astrocytes while occasionally causing them to appear early. Direct inhibition of let-7, one of LIN28's targets, caused a small change in differentiated neurons consistent with its involvement in a subset of LIN28's phenotypes.

LIN28 is often described as a pluripotency factor that promotes proliferation. Based on our previous knowledge of LIN28's activity in embryonic neural development and, more broadly, other systems such as *C. elegans*, I expected LIN28 might

cause an increase in the NSC population as a result of continual reiteration, and consequently block terminal differentiation, yet it did not. Although LIN28 is endogenously expressed in the NSCs, it does not have a clear function in this population. In *C. elegans*, LIN28 is expressed in both the L1 and L2 stages, but it functions only in the L2 stage while LIN-14 regulates the L1 (Ambros & Horvitz, 1987; Ambros, 1989; Euling & Ambros, 1996). Disruption in LIN28's normal expression, either loss or gain, directly effects the L2 stage resulting in a precocious or reiterative phenotype, respectively (Ambros & Horvitz, 1984; Moss et al., 1997; Vadla et al., 2012). However, in either case, L1 is unaffected. This observation can be paralleled to what I am seeing in this system. LIN28 is expressed in NSCs, but its apparent lack of purpose in regards to this cell type results in no effect on the NSC population dynamics. Even though the NSCs were unaffected, I might still expect the highly proliferative TACs to be altered by constitutive LIN28, likely expanding and extending the proliferative stage. In fact, the opposite occurred, and the TAC population was significantly reduced. I observed that the proportion of actively proliferating cells was unchanged by constitutive LIN28. Furthermore, neither electroporation efficiency nor an increase in apopotosis were factors in the TAC reduction.

An explanation for the reduction in proliferating TACs may be connected to the fact that constitutive LIN28 promotes an increase in the NB population. Over the course of normal postnatal neurogenesis in the SVZ, NSCs slowly divide, self-renew, and ultimately form daughter cells (the TACs) that divide rapidly, in comparison. The TACs undergo several rounds of division then further differentiate to NBs (Costa et

al., 2011; Ponti et al., 2013a; Ponti et al., 2013b). I propose that when LIN28 is constitutively expressed, the TACs exit the proliferation stage early, thus promoting the NB population (Figure 25). This would also explain the premature appearance of astrocytes, where the cell fate switch to astrogliogenesis is also moved up in time. Importantly, the shortening of the TAC's proliferation stage ultimately reduces the overall number of their descendants. Therefore, although LIN28 promotes a proportional increase in the NB population, the total number of all cell types (NPCs, NBs, astrocytes, and neurons) is reduced.

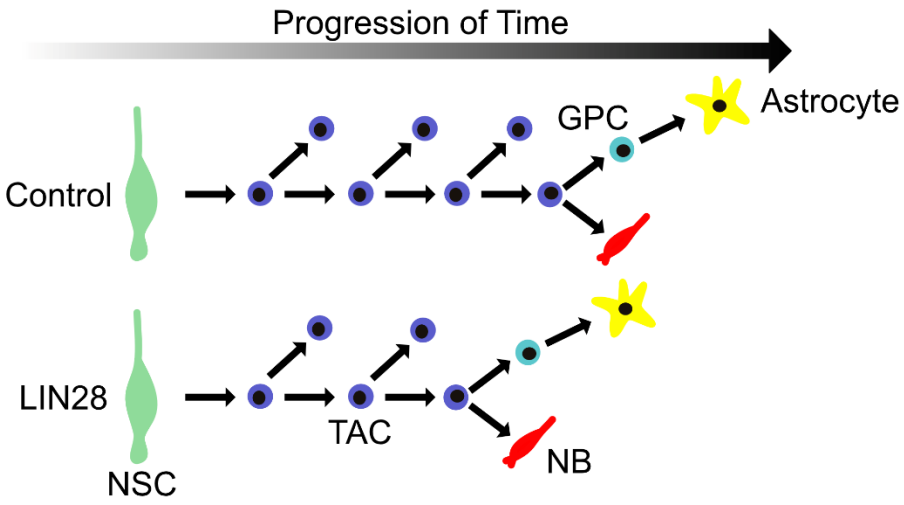

Figure 25. LIN28 causes transit-amplifying cells to prematurely differentiate to neuroblasts, and cause early astrogliogenesis. Control (top), LIN28 (bottom). NSC, neural stem cell (green); TAC, transit-amplifying cell (blue); NB, neuroblast (red); GPC, glial progenitor cell (light blue).

To directly answer the question whether LIN28 causes early cell cycle exit towards differentiation and reduces the length of time in the proliferation stage, I propose two different experiments, one *in vitro* and one *in vivo*. The first experiment would be an *in vitro* clonal differentiation assay. This assay allows for individual NSCs to form colonies, where the progeny and number of divisions can be ascertained. Following electroporation of control and LIN28 plasmids into the lateral ventricles, the NSCs of the SVZ are microdissected at 1 DPE and plated at low densities. The low density of NSCs allows for single cells on the dish. Cells are fixed and observed four days later. GFP+ colonies are accessed for the total number of cells per colony and the different cell types of each colony, in other words, GFAP+, Mash1+, or DCX+. Comparing the control and LIN28 colony dynamics would provide a method for viewing whether LIN28 reduces the rounds of division for the TACs and promotes early differentiation of the NBs. The work in this thesis strongly supports that LIN28 is promoting differentiation to NBs at the expense of continued TAC proliferation, so I suspect this experiment would show early differentiation to NBs in culture. If I wished to follow the lineage of specific cells, this experiment could be taken to the next level, and live imaging could be used to follow individual cells, how and when they divide, and what progeny they produce.

Another approach to understanding LIN28's function here would be an *in vivo* cell cycle exit assay (Das et al., 2009; Farhy et al., 2013). Proliferating Cell Nuclear Antigen (PCNA) is associated with DNA polymerase δ and is highly expressed in proliferating cells but not detected in non-proliferating cells; it can be used as an endogenous marker for proliferation (Coltrera & Gown, 1991; Muskhelishvili et al.,

2003). Control and LIN28 plasmids would be injected and electroporated following the normal protocol. 5-ethynyl-2′-deoxyuridine (EdU) would be injected two hours before mice were sacrificed; in order to study different populations, I would sacrifice mice at 1 and 3 DPE. The extent of cell cycle exit would be determined by the number of cells positive for EdU but negative for PCNA. Edu+/PCNA- would be expressed as a percent of the total Edu+ cells (Das et al., 2009; Farhy et al., 2013). Actively dividing cells would incorporate Edu; if they continued to proliferate, PCNA would be expressed, in other words, the cells would be identified as Edu+/PCNA+. However, if the cells exited the cell cycle, then PCNA would be negative. As I suspect LIN28 reduces proliferation, I would expect a higher percentage of Edu+/PCNA- cells (increased cell cycle exit) compared to control.

The question arises whether the effects of constitutive LIN28 on the cell fate changes in the OB relate to the premature switch from proliferation to differentiation in the SVZ. Loss of Pax6, which is normally highly expressed in TACs of the SVZ, resulted in the reduction of the TH+ population, demonstrating that periglomerular cell fate choices were determined quite early during neurogenesis (Kohwi et al., 2005). Therefore, while promoting a switch from the proliferating TAC stage to the NB stage, constitutive LIN28 may have also affected a contemporaneous switch concerning cell fate decisions in the periglomerular layer. The periglomerular subtypes are generated in a specific order, TH+ first and Calb+ second, during embryonic development (Batista-Brito et al., 2008). If this relationship is also true in postnatal neurogenesis, LIN28's preferential generation of TH+ neurons, an earlier fate, occurred at the expense of Calb+ neurons, a later fate. Alternatively, the distinct localization of

the two types of PGCs is suggestive of unique physiological roles; for example, TH+ cells, but not Calb+ cells, are able to receive direct inputs from olfactory nerves (Lledo et al., 2008). For this reason, it is possible LIN28 promoted TH+ cells over Calb+ cells for a functional purpose. Why LIN28 might regulate cells based on their function is unclear, and likely would not have a connection to developmental timing such as its role in glucose metabolism.

My experiments with cultured primary NSCs revealed endogenous LIN28 was expressed in both neural progenitors and NBs. I have not been able to achieve sensitive staining of histological sections using our anti-LIN28 antibodies, so I do not know the levels of LIN28 in each of these populations *in vivo.* Nevertheless, I must consider how exogenous expression of LIN28 can alter the behavior of TACs and NBs in which LIN28 is already endogenously expressed. From investigations into muscle development it was found that different levels of constitutive LIN28 caused different outcomes (Polesskaya et al., 2007). This is not unique to LIN28: It has been shown for another pluripotency factor Oct 3/4 that different levels of the factor cause different outcomes: an increase in expression caused differentiation while loss of expression resulted in loss of pluripotency (Niwa et al., 2000). I speculate that the absolute level—not merely presence or absence—of LIN28 in a developing cell plays a role in its cell-type specific proliferation or differentiation choices. Although LIN28 may be endogenously expressed in TACs, higher levels may promote a switch from proliferation to differentiation into the NB stage.

The possibility that concentration is an important factor in LIN28's effects introduces an interesting question about LIN28's expression in postnatal neurogenesis.

Is LIN28 highly (or higher) expressed in NSCs and NBs, but lower in TACs? It would provide a better understanding of LIN28 in this system if I knew LIN28's expression patterns at the protein level. At this time, I feel that trying to determine the absolute level of protein either *in vitro* or *in vivo* is extremely difficult. To determine the actual levels in a given population of cells would require a pure population. This can be achieved with an undifferentiated pool of NSCs, but beyond this stage and cell type it would be difficult to distinguish the populations. NSCs are heterogeneous in nature; even if the culture was synchronized, I do not believe you could achieve pure populations of TACs and NBs and in the number of cells required. Therefore, you could never be sure the levels of LIN28 specifically represented a certain population. The challenge to achieve this in culture is difficult at best, and likely impossible in tissue. However, if I could procure pure populations of NSCs, TACs, and NBs, then I would assess the absolute levels of LIN28 protein using an ELISA assay. This could then provide an answer whether concentration is indeed an important factor in LIN28's effects.

My findings run counter to prevailing narratives about LIN28. First, constitutive expression of LIN28 in *C. elegans* and some mammalian systems is generally thought to promote proliferation and tissue growth over differentiation. However, in my *in vivo* experiments, constitutive LIN28 appears to reduce proliferation at one developmental stage (TACs) and cause precocious development of one cell type (astrocytes). Detailed studies in *C. elegans* show that LIN28 acts primarily in a developmental timing mechanism where cells of different lineages use that timing information in different ways: in some cases to proliferate if appropriate and in other cases

to stay quiescent (Ambros & Horvitz, 1984; Rougvie & Moss, 2013). I should not be surprised to find as I learn more about LIN28's activity in different developmental contexts that its up- or down-regulation causes cell behaviors particular to a given tissue and developmental time point. LIN28 is not simply a promoter of proliferation and an undifferentiated state (Faas et al., 2013). Furthermore, LIN28's expression in NBs was surprising only because that cell type is already committed to a neuronal lineage. LIN28 is also expressed in regenerating muscle and erythroblasts, which are also committed lineages (Polesskaya et al., 2007; de Vasconcellos et al., 2014).

As a developmental timing regulator, gain- and loss-of function mutations result in opposite phenotypes (Ambros & Horvitz, 1984; Moss et al., 1997). Therefore, I must ask what happens in postnatal neurogenesis when LIN28 is null. I have access to a floxed LIN28 mouse; electroporation of a constitutive CRE plasmid would remove LIN28 (LIN28 knock down) from the SVZ NSCs. I would assess changes to postnatal neurogenesis and cell fate as done in this thesis with constitutive LIN28.

First, I might expect LIN28 knock down to increase the length of time in the proliferative stage allowing for more divisions than control. The extent of this delay could vary greatly. It could simply result in a minor one or two additional rounds of division. On the other hand, it could have a major effect and completely block the progression to differentiation to NBs. Although the experiment is the only way to measure the extent of this effect, I suspect LIN28 will have some in-between outcome. Since constitutive LIN28 is not able to fully skip the proliferation stage altogether, I doubt it is potent enough to completely block differentiation on the other

end. I propose no change on the NSCs, an increase in the TACs, and ultimately a decrease in the proportion of NBs.

The early appearance and overall reduction in astrocytes is a direct result of LIN28 moving developmental events up in time (precocious phenotype). In the loss of function, I suspect there would be a delay in the initial appearance of astrocytes with an increase in the overall astrocyte population. The extent of this increase, again, would rely heavily on the impact LIN28 knock down had on the proliferation stage and TAC population. Like the astrocyte population, I feel the total neurons in the OB will increase compared to control. Although, many of these phenotypes would be classified as retarded, I think the neurogenesis process will be more of a "delayed retarded" not a traditional retarded where later fates are never achieved. With this in mind, I believe LIN28 knock down will have no effect on neuron maturation. My theory that constitutive LIN28 results in preferential development of TH+ GL neurons over Calb+ simply as a preference for an earlier fate over a later fate, would suggest that loss of LIN28 would cause a reduction in the TH+ population and an increase in the Calb+ population. I demonstrate dramatic changes in the distribution of these different populations; I would expect LIN28 knock down to produce equally significant changes in the opposite direction.

Although LIN28's most well-known molecular activity is to inhibit the maturation of the let-7 miRNA, in several different systems LIN28 has been shown to operate by other mechanisms in the cell (Newman et al., 2008; Rybak et al., 2008; Viswanathan et al., 2008; Balzer et al., 2010; Vadla et al., 2012; Faas et al., 2013;

Tsialikas & Romer-Seibert, 2015). Since the secondary mechanism is not well defined, I are unable to determine what fraction of LIN28's biological roles are attributable to either mechanism. In *C. elegans*, the majority of LIN28's activity is let-7 independent (Vadla et al., 2012). Therefore, I attempted to shed some light on whether constitutive LIN28's effects in postnatal development were due to its inhibition of let-7. To do this, I developed a circRNA sponge specific for let-7 based on the work of the Kjems lab (Hansen et al., 2013). Although other sponge methods have been validated, the circular form of the RNA enhances its stability within the cell, and simultaneously targets multiple family members at one time. Our let-7 circRNA contains 36 repeats of target sites 18 nucleotides apart that were optimized to four different let-7 variants observed in neurogenesis. This circRNA sponge is effective in three systems: *C. elegans, in vitro* neurogenesis, and in postnatal neurogenesis. Despite its measured effectiveness at inhibiting let-7 activity, my observations suggest that let-7 makes a minor contribution to the effects I observed and that LIN28's other activities may account for the majority of the phenotypes.

Petri et al. recently demonstrated a decline in radial migration of NBs in the OB following knockdown of let-7 using a different kind of sponge (Petri et al., 2017). It is difficult to compare the results directly. I note that they introduced their lentiviral vectors at 10 weeks into the RMS, whereas I introduced our sponge at P0-1 into the SVZ and assessed at 3 weeks. I showed there is a dramatic rise in let-7 levels in the OB over time. It is difficult to know, given the state of our knowledge, when relevant let-7 targets are acting and being repressed to control proper postnatal neurogenesis. Furthermore, let-7 is highly expressed in the OB as a whole, but the precise level of

let-7 in each individual neuron is still unknown. At this time, I cannot say whether concentration of let-7 is a factor in its activity.

While LIN28's let-7 dependent pathway has been extensively studied, less is known about LIN28's let-7 independent activity or the downstream targets of this pathway. let-7 seems to play only a minor part in LIN28's effects on postnatal neurogenesis of the SVZ, so what other downstream target(s) account for the remainder of LIN28's effects? This question is not easily answered, or even embarked upon. Several genome-wide studies have attempted to unveil alternative targets for LIN28 (Peng et al., 2011; Cho et al., 2012; Wilbert et al., 2012; Hafner et al., 2013). While uncovering thousands of potential targets, the consensus between each study is not 100%, most likely due to the use of different techniques. Knowing that LIN28 functions differently depending on the system as well as the developmental time point, it is likely its targets will vary from one system to another and between different developmental time points. This characteristic of LIN28 makes predicting viable targets for one system based on the results of another difficult.

LIN28 promoted an increase in the proportion of NBs at the expense of TAC proliferation suggesting possible targets in two areas, 1) cell cycle proteins or 2) proteins essential for NB differentiation. It seems unlikely that cell cycle proteins would be a viable target for LIN28 in this system. The majority of the research demonstrates that LIN28 regulates alternative targets through "translational stimulation" and binding of mRNA (Xu & Hang, 2009; Xu et al., 2009; Qui et al., 2010; Feng et al., 2012; Lei et al., 2012; Li et al., 2012; Hafner et al., 2013). In mammalian embryonic stem

cells, LIN28 promoted the expression of cell cycle proteins, and by extension, proliferation (Xu et al., 2009). Since LIN28 shortens the proliferative stage, the only way it could be regulating the same proteins would be through some means of translational repression, causing cells to exit the cycle. It seems more likely that LIN28 might positively regulate proteins required for proper differentiation to NBs. What these proteins may be is unclear at this time.

One possible target could be a member of the PI3K-Akt-mTOR signaling pathway. S6 and 4E-BP are downstream targets of the mTOR pathway and are commonly used as a measure of mTOR's activity indirectly (Hartman et al., 2013; Yang et al., 2015). When mTOR is active, S6 and 4E-BP are phosphorylated. 4E-BP^{P} is unable to interact with eIF4E and therefore cap-dependent translation can occur (Peter et al., 2015). Yang et al. demonstrated a connection between LIN28 and the mTOR pathway during embryonic nervous development, where loss and gain of LIN28 resulted in a decrease or increase, respectively, of phosphorylated S6 (Yang et al., 2015). This could suggest it is a possible target for LIN28, especially since the mTOR pathway is important in postnatal neurogenesis of the SVZ (Hartman et al., 2013). mTOR appears to regulate NSCs' decision to self-renew or to differentiate to TACs and, at first glance, this would not suggest a connection with LIN28's function. However, 4E-BP^{P} is expressed in ~80% of NBs in the SVZ (Hartman et al., 2013). This is indicative of active mTOR and cap-dependent translation. Since LIN28 is both expressed in NBs and promotes this population of cells, this could be a possible intersection of these two pathways. Additionally, LIN28 has been shown to both co-pu-

rifiy with eIF3β and eIF4E in mRNPs and to be associated with polyribosomes suggesting a possible role in translation (Balzer & Moss, 2007; Polesskaya et al., 2007). Furthermore, loss of LIN28 resulted in a shift of target mRNAs from the polysomal to the nonpolysomal fraction (Peng et al., 2011). If these two pathways converged, what might LIN28's target be? It is possible LIN28 may directly bind and promote expression of mTOR itself. The putative consensus sequence for LIN28 to bind target mRNA "GGAGA" is present one time in the 3'UTR of mTOR (Wilbert et al., 2012). Using software to predict secondary structure I also identified that this sequence is predicted to end in an "A" bulge site also proposed to be important to LIN28's mRNA binding (Fig 26; Lei et al., 2012). While this evidence could point to mTOR as a possible non-let-7 target in postnatal neurogenesis, significant experimentation would be required to prove this theory. Furthermore, whether a connection between mTOR and LIN28 truly exists in this system, it also does not rule out the possibility that LIN28 directly regulates other non-mTOR targets that are essential to NB generation.

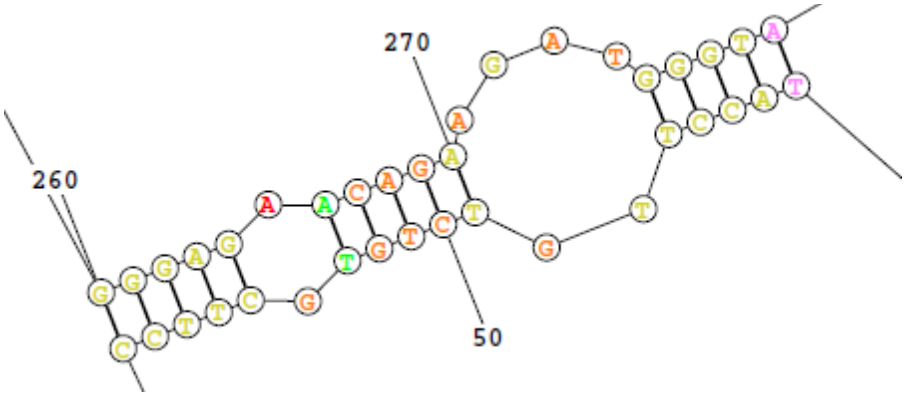

Figure 26. mTOR contains a predicted LIN28 mRNA binding site in its 3'UTR. Basepairs 261-265 represent the conserved GGAGA binding site. Basepair 265 ends in a predicted "A" bulge site suggested to be important in mRNA binding for LIN28. RNAstructure (https://rna.urmc.rochester.edu/RNAstructureWeb/Servers/Predict1/Predict1.html) used to predict the secondary structure using the 3'UTR mRNA sequence NM_020009.2 for mus musculus mTOR.

In *C. elegans*, LIN41 acts downstream of LIN28 and carries out a subset of its developmental functions. I examined whether the same might be true in neurogenesis. I successfully demonstrated 1) the RNA expression pattern of LIN41 in P19 cells during neural differentiation and 2) that I could use CRISPR technology and homologous recombination to generate a LIN41null-GFP expressing cell line. However, I was unable to study LIN41 protein *in vitro*. Since moving on from the LIN41 project, Chang et al. demonstrated that LIN41 protein is expressed in undifferentiated P19 cells (Chang et al., 2012). However, they only show a LIN41 mRNA timecourse similar to my own, not what happens to the protein, leaving this question still to be answered and formally confirmed. It is clear that the LIN28/let-7 portion of the heterochronic

pathway is conserved in mammals and there is some evidence that suggests the let-7/LIN41 pathway is conserved as well (Kanamoto et al., 2006; Maller Schulman et al., 2008). It is not a far leap to assume these three molecules still function as one axis in mammals. Knowing that LIN41 protein is expressed in undifferentiated P19 cells and its RNA is downregulated, the protein is likely downregulated too. As LIN41 is expressed in the developing nervous system and is a downstream effector of LIN28 in *C. elegans* this could suggest it plays some role in P19 neural differentiation (Maller Schulman et al., 2008; Chen et al., 2012).

Constitutive LIN28 has two distinct effects in P19 neural differentiation: 1) blocks gliogenesis and 2) increases neurogenesis (Balzer et al., 2010). My work with the let-7 circRNA sponge clearly demonstrates LIN28's effects on gliogenesis are independent of let-7 and are the result of LIN28's other activity. This would suggest it is unlikely LIN41 plays any part in this role, but to be thorough, I would constitutively express LIN41 in P19 cells and assess any changes to neurogenesis and gliogenesis using western blot and immunofluorescence. Furthermore, how LIN28 causes reiteration of neurogenesis remains unanswered. I would differentiate the let-7 circRNA sponge cell line and assess any changes to neurogenesis using immunofluorescence. Comparing population changes identified by immunostaining (if any) of constitutive LIN28, constitutive LIN41, and the let-7 circRNA sponge (let-7 null) during neurogenesis, I could determine whether LIN28 regulates this process through its independent pathway, let-7, or through let-7/LIN41.

LIN41 plays an important role in embryonic neural development like LIN28 (Chen et al., 2012). What role might LIN41 play in postnatal neurogenesis? It was

surprising to see LIN41 expressed in the terminally differentiated ependymal cells of the SVZ (Cuevas et al., 2015). This discovery inspires several possibilities. First, the upregulation of LIN41 in a differentiated cell type, like LIN28 in NBs, could suggest LIN41 promotes this cell fate. I would electroporate constitutive LIN41, and assess any changes to the ependymal population at 3 DPE. For our general understanding of LIN28 and LIN41 in mammals, I would also assess the other populations, NSCs, TACs, and NBs, to determine if the changes to these populations by LIN28 have some connection to LIN41. Since the LIN28 phenotypes in postnatal neurogenesis are mostly independent of let-7, it is likely they are LIN41-independent as well. However, it is possible that LIN41 has its own unique impact on one or more of these populations. Likewise, since I did not initially look at the ependymal population it is possible LIN28 has some unforeseen purpose here as well.

I expect that further use of postnatal electroporation can be used to dissect the mechanism regulating sequential cell behaviors during postnatal neurogenesis in which LIN28 plays a crucial part. Other factors may be studied and other manipulations may be made to provide a clearer understanding of the nature of its role in developmental timing, tissue growth, and differentiation at a cellular level. I have already seen that its function is not simply in pluripotency and proliferation, but may be tied in with the specific needs of a developing tissue in its particular context.

Chapter 7: References

Abbott AL, Alvarez-Saavedra E, Miska EA, Lau NC, Bartel DP, Horvitz HR, Ambros V (2005) The let-7 MicroRNA family members mir-48, mir-84, and mir-241 function together to regulate developmental timing in Caenorhabditis elegans. Dev Cell. 9:403-14.

Aeschimann F, Kumari P, Bartake H, Gaidatzis D, Xu L, Ciosk R, Großhans H (2017) LIN41 Post-transcriptionally Silences mRNAs by Two Distinct and Position-Dependent Mechanisms. Mol Cell. 65:476-489.e4.

Agoston Z, Heine P, Brill MS, Grebbin BM, Hau AC, Kallenborn-Gerhardt W, Schramm J, Götz M, Schulte D (2014) Meis2 is a Pax6 co-factor in neurogenesis and dopaminergic periglomerular fate specification in the adult olfactory bulb. Development. 141:28-38.

Alvarez-Buylla A, Garcia-Verdugo JM (2002) Neurogenesis in adult subventricular zone. J Neurosci. 22:629-34.

Ambros V (1989) A hierarchy of regulatory genes controls a larva-to-adult developmental switch in C. elegans. Cell. 57:49-57.

Ambros V, Horvitz HR (1984) Heterochronic mutants of the nematode Caenorhabditis elegans. Science. 226:409-16.

Ambros V, Horvitz HR (1987) The lin-14 locus of Caenorhabditis elegans controls the time of expression of specific postembryonic developmental events. Genes Dev. 4:398-414.

Aravin AA, Lagos-Quintana M, Yalcin A, Zavolan M, Marks D, Snyder B, Gaasterland T, Meyer J, Tuschl T (2003) The small RNA profile during Drosophila melanogaster development. Dev Cell. 5:337-50.

Balzer E, Heine C, Jiang Q, Lee VM, Moss EG (2010) LIN28 alters cell fate succession and acts independently of the let-7 microRNA during neurogliogenesis in vitro. Development. 37:891-900.

Balzer E, Moss EG (2007) Localization of the developmental timing regulator Lin28 to mRNP complexes, P-bodies and stress granules. RNA Biol. 4:16-25.

Bartel DP (2004) MicroRNAs: genomics, biogenesis, mechanism, and function. Cell. 116:281-97.

Batista-Brito R, Close J, Machold R, Fishell G (2008) The distinct temporal origins of olfactory bulb interneuron subtypes. J Neurosci. 28:3966-75.

Bhuiyan MI, Lee JH, Kim SY, Cho KO (2013) Expression of exogenous LIN28 contributes to proliferation and survival of mouse primary cortical neurons in vitro. Neuroscience. 248:448-58.

Calzolari F, Michel J, Baumgart EV, Theis F, Götz M, Ninkovic J (2015) Fast clonal expansion and limited neural stem cell self-renewal in the adult subependymal zone. Nat Neurosci. 18:490-2.

Caygill EE, Johnston LA (2008) Temporal regulation of metamorphic processes in Drosophila by the let-7 and miR-125 heterochronic microRNAs. Curr Biol. 18:943-50.

Cayouette M, Barres BA, Raff M (2003) Importance of intrinsic mechanisms in cell fate decisions in the developing rat retina. Neuron. 40:897-904.

Cevec M, Thibaudeau C, Plavec J (2008) Solution structure of a let-7 miRNA:lin-41 mRNA complex from C. elegans. Nucleic Acids Res. 36:2330-7.

Cevec M, Thibaudeau C, Plavec J (2010) NMR structure of the let-7 miRNA interacting with the site LCS1 of lin-41 mRNA from Caenorhabditis elegans. Nucleic Acids Res. 38:7814-21.

Chang HM, Martinez NJ, Thornton JE, Hagan JP, Nguyen KD, Gregory RI (2012) Trim71 cooperates with microRNAs to repress Cdkn1a expression and promote embryonic stem cell proliferation. Nat Commun. 3:923.

Chen J, Lai F, Niswander L (2012) The ubiquitin ligase mLin41 temporally promotes neural progenitor cell maintenance through FGF signaling. Genes Dev. 26:803-15.

Cho J, Chang H, Kwon SC, Kim B, Kim Y, Choe J, Ha M, Kim YK, Kim VN (2012) LIN28A is a suppressor of ER-associated translation in embryonic stem cells. Cell. 151:765-77.

Cimadamore F, Amador-Arjona A, Chen C, Huang CT, Terskikh AV (2013) SOX2-LIN28/let-7 pathway regulates proliferation and neurogenesis in neural precursors. Proc Natl Acad Sci U S A. 110:E3017-26.

Coltrera MD, Gown AM (1991) PCNA/cyclin expression and BrdU uptake define different subpopulations in different cell lines. J Histochem Cytochem. 39:23-30.

Cong L, Ran FA, Cox D, Lin S, Barretto R, Habib N, Hsu PD, Wu X, Jiang W, Marraffini LA, Zhang F (2013) Multiplex genome engineering using CRISPR/Cas systems. Science. 339:819-23.

Copley MR, Babovic S, Benz C, Knapp DJ, Beer PA, Kent DG, Wohrer S, Treloar DQ, Day C, Rowe K, Mader H, Kuchenbauer F, Humphries RK, Eaves CJ (2013) The Lin28b-let-7-Hmga2 axis determines the higher self-renewal potential of fetal haematopoietic stem cells. Nat Cell Biol. 15:916-25.

Coppola A, Romito A, Borel C, Gehrig C, Gagnebin M, Falconnet E, Izzo A, Altucci L, Banfi S, Antonarakis SE, Minchiotti G, Cobellis G. Cardiomyogenesis is controlled by the miR-99a/let-7c cluster and epigenetic modifications (2014) Stem Cell Res. 12:323-37.

Corre C, Shinoda G, Zhu H, Cousminer DL, Crossman C, Bellissimo C, Goldenberg A, Daley GQ, Palmert MR (2016) Sex-specific regulation of weight and puberty by the Lin28/let-7 axis. J Endocrinol. 228:179-91.

Costa, MR, Ortega F, Brill MS, Beckervordersandforth R, Petrone C, Schroeder T, Götz M, Berninger B (2011) Continuous live imaging of adult neural stem cell division and lineage progression in vitro. Development. 138:1057-68.

Cuevas E, Rybak-Wolf A, Rohde AM, Nguyen DT, Wulczyn FG (2015) Lin41/Trim71 is essential for mouse development and specifically expressed in postnatal ependymal cells of the brain. Front Cell Dev Biol. 3:20.

Darr H, Benvenisty N (2009) Genetic analysis of the role of the reprogramming gene LIN-28 in human embryonic stem cells. Stem Cells. 27:352-62.

Das G, Choi Y, Sicinski P, Levine EM (2009) Cyclin D1 fine-tunes the neurogenic output of embryonic retinal progenitor cells. Neural Dev. 4:15.

Del Rio-Albrechtsen T, Kiontke K, Chiou SY, Fitch DH (2006) Novel gain-of-function alleles demonstrate a role for the heterochronic gene lin-41 in C. elegans male tail tip morphogenesis. Dev Biol. 297:74-86.

de Vasconcellos JF, Fasano RM, Lee YT, Kaushal M, Byrnes C, Meier ER, Anderson M, Rabel A, Braylan R, Stroncek DF, Miller JL (2014) LIN28A expression reduces sickling of cultured human erythrocytes. PLoS One. 9:e106924.

Docherty CK, Salt IP, Mercer JR (2016) Lin28A induces energetic switching to glycolytic metabolism in human embryonic kidney cells. Stem Cell Res Ther. 7:78.

Doetsch F, Caillé I, Lim DA, García-Verdugo JM, Alvarez-Buylla A (1999) Subventricular zone astrocytes are neural stem cells in the adult mammalian brain. Cell. 97:703-16.

Ecsedi M, Rausch M, Großhans H (2015) The let-7 microRNA directs vulval development through a single target. Dev Cell. 32:335-44.

Elliott J, Jolicoeur C, Ramamurthy V, Cayouette M (2008) Ikaros confers early temporal competence to mouse retinal progenitor cells. Neuron. 60:26-39.

Euling S, Ambros V (1996) Heterochronic genes control cell cycle progress and developmental competence of C. elegans vulva precursor cells. Cell. 84:667-76.

Faas L, Warrander FC, Maguire R, Ramsbottom SA, Quinn D, Genever P, Isaacs HV (2013) Lin28 proteins are required for germ layer specification in Xenopus. Development. 140:976-86.

Farhy C, Elgart M, Shapira Z, Oron-Karni V, Yaron O, Menuchin Y, Rechavi G, Ashery-Padan R (2013) Pax6 is required for normal cell-cycle exit and the differentiation kinetics of retinal progenitor cells. PLoS One. 8:e76489.

Faunes F, Gundermann DG, Muñoz R, Bruno R, Larraín J (2017) The heterochronic gene Lin28 regulates amphibian metamorphosis through disturbance of thyroid hormone function. Dev Biol. 425:142-151.

Feliciano DM, Quon JL, Su T, Taylor MM, Bordey A (2012)Postnatal neurogenesis generates heterotopias, olfactory micronodules and cortical infiltration following single-cell Tsc1 deletion. Hum Mol Genet. 21:799-810.

Feliciano DM, Lafourcade CA, Bordey A (2013)Neonatal subventricular zone electroporation. J Vis Exp 50197

Feng C, Neumeister V, Ma W, Xu J, Lu L, Bordeaux J, Maihle NJ, Rimm DL, Huang Y (2012) Lin28 regulates HER2 and promotes malignancy through multiple mechanisms. Cell Cycle. 11:2486-94.

Fuentealba LC, Rompani SB, Parraguez JI, Obernier K, Romero R, Cepko CL, Alvarez-Buylla A (2015) Embryonic Origin of Postnatal Neural Stem Cells. Cell. 161:1644-55.

Gao FB, Durand B, Raff M (1997) Oligodendrocyte precursor cells count time but not cell divisions before differentiation. Curr Biol. 7:152-5.

Grebbin BM, Hau AC, Groß A, Anders-Maurer M, Schramm J, Koss M, Wille C, Mittelbronn M, Selleri L, Schulte D (2016) Pbx1 is required for adult subventricular zone neurogenesis. Development. 143:2281-91.

Hack MA, Saghatelyan A, de Chevigny A, Pfeifer A, Ashery-Padan R, Lledo PM, Götz M (2005) Neuronal fate determinants of adult olfactory bulb neurogenesis. Nat Neurosci. 8:865-72.

Hafner M, Max KE, Bandaru P, Morozov P, Gerstberger S, Brown M, Molina H, Tuschl T (2013) Identification of mRNAs bound and regulated by human LIN28 proteins and molecular requirements for RNA recognition. RNA. 19:613-26.

Hagan JP, Piskounova E, Gregory RI (2009) Lin28 recruits the TUTase Zcchc11 to inhibit let-7 maturation in mouse embryonic stem cells. Nat Struct Mol Biol. 16:1021-5.

Hanna J, Saha K, Pando B, van Zon J, Lengner CJ, Creyghton MP, van Oudenaarden A, Jaenisch R (2009) Direct cell reprogramming is a stochastic process amenable to acceleration. Nature. 3:595-601.

Hansen TB, Jensen TI, Clausen BH, Bramsen JB, Finsen B, Damgaard CK, Kjems J (2013) Natural RNA circles function as efficient microRNA sponges. Nature. 495:384-8.

Harandi OF, Ambros VR (2015) Control of stem cell self-renewal and differentiation by the heterochronic genes and the cellular asymmetry machinery in Caenorhabditis elegans. Proc Natl Acad Sci U S A. 112:E287-96.

Hartman NW, Lin TV, Zhang L, Paquelet GE, Feliciano DM, Bordey A (2013) mTORC1 targets the translational repressor 4E-BP2, but not S6 kinase 1/2, to regulate neural stem cell self-renewal in vivo. Cell Rep. 5:433-44.

Heo I, Joo C, Cho J, Ha M, Han J, Kim VN (2008) Lin28 mediates the terminal uridylation of let-7 precursor MicroRNA. Mol Cell. 32:276-84.

Heo I, Joo C, Kim YK, Ha M, Yoon MJ, Cho J, Yeom KH, Han J, Kim VN (2009) TUT4 in concert with Lin28 suppresses microRNA biogenesis through pre-microRNA uridylation. Cell. 138:696-708.

Homem CC, Knoblich JA (2012) Drosophila neuroblasts: a model for stem cell biology. Development. 139:4297-310.

Isshiki T, Pearson B, Holbrook S, Doe CQ (2001) Drosophila neuroblasts sequentially express transcription factors which specify the temporal identity of their neuronal progeny. Cell. 106:511-21.

Jackson PK, Eldridge AG, Freed E, Furstenthal L, Hsu JY, Kaiser BK, Reimann JD (2000) The lore of the RINGs: substrate recognition and catalysis by ubiquitin ligases. Trends Cell Biol. 10:429-39.

Jang ES, Goldman JE (2011) Pax6 expression is sufficient to induce a neurogenic fate in glial progenitors of the neonatal subventricular zone. PLoS One. 6:e20894.

Johnson SM, Lin SY, Slack FJ (2003) The time of appearance of the C. elegans let-7 microRNA is transcriptionally controlled utilizing a temporal regulatory element in its promoter. Dev Biol. 259:364-79.

Kanamoto T, Terada K, Yoshikawa H, Furukawa T (2006) Cloning and regulation of the vertebrate homologue of lin-41 that functions as a heterochronic gene in Caenorhabditis elegans. Dev Dyn. 235:1142-9.

Kawahara H, Okada Y, Imai T, Iwanami A, Mischel PS, Okano H (2011) Musashi1 cooperates in abnormal cell lineage protein 28 (Lin28)-mediated let-7 family microRNA biogenesis in early neural differentiation. J Biol Chem. 286:16121-30.

Kloosterman WP, Wienholds E, Ketting RF, Plasterk RH (2004) Substrate requirements for let-7 function in the developing zebrafish embryo. Nucleic Acids Res. 32:6284-91.

Kohwi M, Doe CQ (2013) Temporal fate specification and neural progenitor competence during development. Nat Rev Neurosci. 14:823-38.

Kohwi M, Osumi N, Rubenstein JL, Alvarez-Buylla A (2005) Pax6 is required for making specific subpopulations of granule and periglomerular neurons in the olfactory bulb. J Neurosci. 25:6997-7003.

Kosaka K, Kosaka T (2007) Chemical properties of type 1 and type 2 periglomerular cells in the mouse olfactory bulb are different from those in the rat olfactory bulb. Brain Res. 1167:42-55.

Kriegstein A, Alvarez-Buylla A (2009) The glial nature of embryonic and adult neural stem cells. Annu Rev Neurosci. 32:149-84.

Kwon SC, Yi H, Eichelbaum K, Föhr S, Fischer B, You KT, Castello A, Krijgsveld J, Hentze MW, Kim VN (2013) The RNA-binding protein repertoire of embryonic stem cells. Nat Struct Mol Biol. 20:1122-30.

Lacar B, Young SZ, Platel JC, Bordey A (2010) Imaging and recording subventricular zone progenitor cells in live tissue of postnatal mice. Front Neurosci. 4

Lagos-Quintana M, Rauhut R, Meyer J, Borkhardt A, Tuschl T (2003) New microRNAs from mouse and human. RNA. 9:175-9.

Lai EC, Tomancak P, Williams RW, Rubin GM (2003) Computational identification of Drosophila microRNA genes. Genome Biol. 4:R42.

Lancman JJ, Caruccio NC, Harfe BD, Pasquinelli AE, Schageman JJ, Pertsemlidis A, Fallon JF (2005) Analysis of the regulation of lin-41 during chick and mouse limb development. Dev Dyn. 234:948-60.

Lee H, Han S, Kwon CS, Lee D (2016) Biogenesis and regulation of the let-7 miRNAs and their functional implications. Protein Cell. 7:100-13.

Lee RC, Feinbaum RL, Ambros V (1993) The C. elegans heterochronic gene lin-4 encodes small RNAs with antisense complementarity to lin-14. Cell. 75:843-54.

Lei XX, Xu J, Ma W, Qiao C, Newman MA, Hammond SM, Huang Y (2012) Determinants of mRNA recognition and translation regulation by Lin28. Nucleic Acids Res. 40:3574-84.

Li N, Zhong X, Lin X, Guo J, Zou L, Tanyi JL, Shao Z, Liang S, Wang LP, Hwang WT, Katsaros D, Montone K, Zhao X, Zhang L (2012) Lin-28 homologue A (LIN28A) promotes cell cycle progression via regulation of cyclin-dependent kinase 2 (CDK2), cyclin D1 (CCND1), and cell division cycle 25 homolog A (CDC25A) expression in cancer. J Biol Chem. 287:17386-97.

Lightfoot HL, Bugaut A, Armisen J, Lehrbach NJ, Miska EA, Balasubramanian S (2011) A LIN28-dependent structural change in pre-let-7g directly inhibits dicer processing. Biochemistry. 50:7514-21.

Lim LP, Lau NC, Weinstein EG, Abdelhakim A, Yekta S, Rhoades MW, Burge CB, Bartel DP (2003) The microRNAs of Caenorhabditis elegans. Genes Dev. 17:991-1008.

Lin YC, Hsieh LC, Kuo MW, Yu J, Kuo HH, Lo WL, Lin RJ, Yu AL, Li WH (2007) Human TRIM71 and its nematode homologue are targets of let-7 microRNA and its zebrafish orthologue is essential for development. Mol Biol Evol. 24:2525-34.

Lledo PM, Merkle FT, Alvarez-Buylla A (2008) Origin and function of olfactory bulb interneuron diversity. Trends Neurosci. 31:392-400.

Lledo PM, Saghatelyan A (2005) Integrating new neurons into the adult olfactory bulb: joining the network, life-death decisions, and the effects of sensory experience. Trends Neurosci. 8:248-54.

Loedige I, Gaidatzis D, Sack R, Meister G, Filipowicz W (2013) The mammalian TRIM-NHL protein TRIM71/LIN-41 is a repressor of mRNA function. Nucleic Acids Res. 41:518-32.

Lois C, Alvarez-Buylla A (1994) Long-distance neuronal migration in the adult mammalian brain. Science.264:1145-8.

Lois C, García-Verdugo JM, Alvarez-Buylla A (1996) Chain migration of neuronal precursors. Science. 271:978-81.

Loughlin FE, Gebert LF, Towbin H, Brunschweiger A, Hall J, Allain FH (2011) Structural basis of pre-let-7 miRNA recognition by the zinc knuckles of pluripotency factor Lin28. Nat Struct Mol Biol. 19:84-9.

Mahoney C, Feliciano DM, Bordey A, Hartman NW (2016) Switching on mTORC1 induces neurogenesis but not proliferation in neural stem cells of young mice. Neurosci Lett. 614:112-8.

Mali P, Aach J, Stranges PB, Esvelt KM, Moosburner M, Kosuri S, Yang L, Church GM (2013)a CAS9 transcriptional activators for target specificity screening and paired nickases for cooperative genome engineering. Nat Biotechnol. 31:833-8.

Mali P, Yang L, Esvelt KM, Aach J, Guell M, DiCarlo JE, Norville JE, Church GM (2013)b RNA-guided human genome engineering via Cas9. Science. 339:823-6.

Maller Schulman BR, Liang X, Stahlhut C, DelConte C, Stefani G, Slack FJ (2008) The let-7 microRNA target gene, Mlin41/Trim71 is required for mouse embryonic survival and neural tube closure. Cell Cycle. 7:3935-42.

Matsuda T, Cepko CL (2004) Electroporation and RNA interference in the rodent retina in vivo and in vitro. Proc Natl Acad Sci U S A. 101:16-22.

Maurange C, Cheng L, Gould AP (2008) Temporal transcription factors and their targets schedule the end of neural proliferation in Drosophila. Cell. 133:891-902.

Mayr F, Schütz A, Döge N, Heinemann U (2012) The Lin28 cold-shock domain remodels pre-let-7 microRNA. Nucleic Acids Res. 40:7492-506.

McConnell SK (1985) Migration and differentiation of cerebral cortical neurons after transplantation into the brains of ferrets. Science. 229:1268-71.

McDonald, JH (2014) Handbook of Biological Statistics (3rd ed.). Sparky House Publishing, Baltimore, Maryland.

Meares GP, Rajbhandari R, Gerigk M, Tien CL, Chang C, Fehling SC, Rowse A, Mulhern KC, Nair S, Gray GK, Berbari NF, Bredel M, Benveniste EN, Nozell SE (2018) MicroRNA-31 is required for astrocyte specification. Glia. 66:987-998.

Menn B, Garcia-Verdugo JM, Yaschine C, Gonzalez-Perez O, Rowitch D, Alvarez-Buylla A (2006) Origin of oligodendrocytes in the subventricular zone of the adult brain. J Neurosci. 26:7907-18.

Merkle FT, Mirzadeh Z, Alvarez-Buylla A (2007) Mosaic organization of neural stem cells in the adult brain. Science. 317:381-4.

Mitschka S, Ulas T, Goller T, Schneider K, Egert A, Mertens J, Brüstle O, Schorle H, Beyer M, Klee K, Xue J, Günther P, Bassler K, Schultze JL, Kolanus W (2015) Co-existence of intact stemness and priming of neural differentiation programs in mES cells lacking Trim71. Sci Rep. 5:11126.

Morton MC, Neckles VN, Seluzicki CM, Holmberg JC, Feliciano DM (2018) Neonatal Subventricular Zone Neural Stem Cells Release Extracellular Vesicles that Act as a Microglial Morphogen. Cell Rep.23:78-89.

Moss EG (2007) Heterochronic genes and the nature of developmental time. Curr Biol. 17:R425-34.

Moss EG, Lee RC, Ambros V (1997) The cold shock domain protein LIN-28 controls developmental timing in C. elegans and is regulated by the lin-4 RNA. Cell. 88:637-46.

Moss EG, Romer-Seibert J (2014) Cell-intrinsic timing in animal development. Wiley Interdiscip Rev Dev Biol. 3:365-77.

Moss EG, Tang L (2003) Conservation of the heterochronic regulator Lin-28, its developmental expression and microRNA complementary sites. Dev Biol. 58:432-42.

Muskhelishvili L, Latendresse JR, Kodell RL, Henderson EB (2003) Evaluation of cell proliferation in rat tissues with BrdU, PCNA, Ki-67(MIB-5) immunohistochemistry and in situ hybridization for histone mRNA. J Histochem Cytochem. 51:1681-8.

Nagayama S, Homma R, Imamura F (2014) Neuronal organization of olfactory bulb circuits. Front Neural Circuits. 8:98.

Nam Y, Chen C, Gregory RI, Chou JJ, Sliz P (2011) Molecular basis for interaction of let-7 microRNAs with Lin28. Cell. 147:1080-91.

Newman MA, Thomson JM, Hammond SM (2008) Lin-28 interaction with the Let-7 precursor loop mediates regulated microRNA processing. RNA. 14:1539-49.

Nguyen DTT, Richter D, Michel G, Mitschka S, Kolanus W, Cuevas E, Wulczyn FG (2017) The ubiquitin ligase LIN41/TRIM71 targets p53 to antagonize cell death and differentiation pathways during stem cell differentiation. Cell Death Differ. 24:1063-1078.

Niwa H, Miyazaki J, Smith AG (2000) Quantitative expression of Oct-3/4 defines differentiation, dedifferentiation or self-renewal of ES cells. Nat Genet. 24:372-6.

O'Farrell F, Esfahani SS, Engström Y, Kylsten P (2008) Regulation of the Drosophila lin-41 homologue dappled by let-7 reveals conservation of a regulatory mechanism within the LIN-41 subclade. Dev Dyn. 237:196-208.

Ouchi Y, Yamamoto J, Iwamoto T (2014) The heterochronic genes lin-28a and lin-28b play an essential and evolutionarily conserved role in early zebrafish development. PLoS One. 9:e88086.

Papaioannou G, Inloes JB, Nakamura Y, Paltrinieri E, Kobayashi T (2013) let-7 and miR-140 microRNAs coordinately regulate skeletal development. Proc Natl Acad Sci U S A. 110:E3291-300.

Pasquinelli AE, Reinhart BJ, Slack F, Martindale MQ, Kuroda MI, Maller B, Hayward DC, Ball EE, Degnan B, Müller P, Spring J, Srinivasan A, Fishman M, Finnerty J, Corbo J, Levine M, Leahy P, Davidson E, Ruvkun G (2000) Conservation of the sequence and temporal expression of let-7 heterochronic regulatory RNA. Nature. 408:86-9.

Pathania M, Torres-Reveron J, Yan L, Kimura T, Lin TV, Gordon V, Teng ZQ, Zhao X, Fulga TA, Van Vactor D, Bordey A. (2012) miR-132 enhances dendritic morphogenesis, spine density, synaptic integration, and survival of newborn olfactory bulb neurons. PLoS One. 7:e38174.

Peng S, Chen LL, Lei XX, Yang L, Lin H, Carmichael GG, Huang Y (2011) Genome-wide studies reveal that Lin28 enhances the translation of genes important for growth and survival of human embryonic stem cells. Stem Cells. 29:496-504.

Pepper AS, McCane JE, Kemper K, Yeung DA, Lee RC, Ambros V, Moss EG (2004) The C. elegans heterochronic gene lin-46 affects developmental timing at two larval stages and encodes a relative of the scaffolding protein gephyrin. Development. 131:2049-59.

Pérez LM, Bernal A, San Martín N, Lorenzo M, Fernández-Veledo S, Gálvez BG (2013) Metabolic rescue of obese adipose-derived stem cells by Lin28/Let7 pathway. Diabetes. 62:2368-79.

Peter D, Igreja C, Weber R, Wohlbold L, Weiler C, Ebertsch L, Weichenrieder O, Izaurralde E (2015) Molecular architecture of 4E-BP translational inhibitors bound to eIF4E. Mol Cell. 57:1074-1087.

Petri R, Pircs K, Jönsson ME, Åkerblom M, Brattås PL, Klussendorf T, Jakobsson J (2017) let-7 regulates radial migration of new-born neurons through positive regulation of autophagy. EMBO J. 36:1379-1391.

Piskounova E, Polytarchou C, Thornton JE, LaPierre RJ, Pothoulakis C, Hagan JP, Iliopoulos D, Gregory RI (2011) Lin28A and Lin28B inhibit let-7 microRNA biogenesis by distinct mechanisms. Cell. 147:1066-79.

Platel JC, Dave KA, Gordon V, Lacar B, Rubio ME, Bordey A (2010) NMDA receptors activated by subventricular zone astrocytic glutamate are critical for neuroblast survival prior to entering a synaptic network. Neuron. 65:859-72.

Polesskaya A, Cuvellier S, Naguibneva I, Duquet A, Moss EG, Harel-Bellan A (2007) Lin-28 binds IGF-2 mRNA and participates in skeletal myogenesis by increasing translation efficiency. Genes Dev. 21:1125-38.

Ponti G, Obernier K, Alvarez-Buylla A (2013)a Lineage progression from stem cells to new neurons in the adult brain ventricular-subventricular zone. Cell Cycle. 12:1649-50.

Ponti G, Obernier K, Guinto C, Jose L, Bonfanti L, Alvarez-Buylla A (2013)b Cell cycle and lineage progression of neural progenitors in the ventricular-subventricular zones of adult mice. Proc Natl Acad Sci U S A. 110:E1045-54.

Qian X, Goderie SK, Shen Q, Stern JH, Temple S (1998) Intrinsic programs of patterned cell lineages in isolated vertebrate CNS ventricular zone cells. Development. 125:3143-52.

Qiu C, Ma Y, Wang J, Peng S, Huang Y (2010) Lin28-mediated post-transcriptional regulation of Oct4 expression in human embryonic stem cells. Nucleic Acids Res. 38:1240-8.

Raff M (2007) Intracellular developmental timers. Cold Spring Harb Symp Quant Biol. 72:431-5.

Raff MC, Lillien LE (1988) Differentiation of a bipotential glial progenitor cell: what controls the timing and the choice of developmental pathway? J Cell Sci Suppl. 10:77-83.

Reinhart BJ, Slack FJ, Basson M, Pasquinelli AE, Bettinger JC, Rougvie AE, Horvitz HR, Ruvkun G (2000) The 21-nucleotide let-7 RNA regulates developmental timing in Caenorhabditis elegans. Nature. 403:901-6.

Rougvie AE, Moss EG (2013) Developmental transitions in C. elegans larval stages. Curr Top Dev Biol. 105:153-80.

Roush S, Slack FJ (2008) The let-7 family of microRNAs. Trends Cell Biol. 18:505-16.

Rybak A, Fuchs H, Hadian K, Smirnova L, Wulczyn EA, Michel G, Nitsch R, Krappmann D, Wulczyn FG (2009) The let-7 target gene mouse lin-41 is a stem cell specific E3 ubiquitin ligase for the miRNA pathway protein Ago2. Nat Cell Biol. 11:1411-20.

Rybak A, Fuchs H, Smirnova L, Brandt C, Pohl EE, Nitsch R, Wulczyn FG (2008) A feedback loop comprising lin-28 and let-7 controls pre-let-7 maturation during neural stem-cell commitment. Nat Cell Biol. 10:987-93.

Sauvageot CM, Stiles CD (2002) Molecular mechanisms controlling cortical gliogenesis. Curr Opin Neurobiol. 12:244-9.

Schulman BR, Esquela-Kerscher A, Slack FJ (2005) Reciprocal expression of lin-41 and the microRNAs let-7 and mir-125 during mouse embryogenesis. Dev Dyn. 234:1046-54.

Shaner NC, Campbell RE, Steinbach PA, Giepmans BN, Palmer AE, Tsien RY (2004) Improved monomeric red, orange and yellow fluorescent proteins derived from Discosoma sp. red fluorescent protein. Nat Biotechnol. 22:1567-72.

Shen Q, Wang Y, Dimos JT, Fasano CA, Phoenix TN, Lemischka IR, Ivanova NB, Stifani S, Morrisey EE, Temple S (2006) The timing of cortical neurogenesis is encoded within lineages of individual progenitor cells. Nat Neurosci. 9:743-51.

Shinoda G, Shyh-Chang N, Soysa TY, Zhu H, Seligson MT, Shah SP, Abo-Sido N, Yabuuchi A, Hagan JP, Gregory RI, Asara JM, Cantley LC, Moss EG, Daley GQ (2013) Fetal deficiency of lin28 programs life-long aberrations in growth and glucose metabolism. Stem Cells. 31:1563-73.

Shyh-Chang N, Zhu H, Yvanka de Soysa T, Shinoda G, Seligson MT, Tsanov KM, Nguyen L, Asara JM, Cantley LC, Daley GQ (2013) Lin28 enhances tissue repair by reprogramming cellular metabolism. Cell. 155:778-92.

Slack FJ, Basson M, Liu Z, Ambros V, Horvitz HR, Ruvkun G (2000) The lin-41 RBCC gene acts in the C. elegans heterochronic pathway between the let-7 regulatory RNA and the LIN-29 transcription factor. Mol Cell. 5:659-69.

Slack F, Ruvkun G (1998) Heterochronic genes in development and evolution. Biol Bull. 195:375-6.

Temple S (2001) The development of neural stem cells. Nature. 414:112-7.

Temple S, Raff MC (1986) Clonal analysis of oligodendrocyte development in culture: evidence for a developmental clock that counts cell divisions. Cell. 44:773-9.

Tocchini C, Keusch JJ, Miller SB, Finger S, Gut H, Stadler MB, Ciosk R (2014) The TRIM-NHL protein LIN-41 controls the onset of developmental plasticity in Caenorhabditis elegans. PLoS Genet. 10:e1004533.

Tong MH, Mitchell D, Evanoff R, Griswold MD (2011) Expression of Mirlet7 family microRNAs in response to retinoic acid-induced spermatogonial differentiation in mice. Biol Reprod. 85:189-97.

Torok M, Etkin LD (2001) Two B or not two B? Overview of the rapidly expanding B-box family of proteins. Differentiation. 67:63-71.

Tsialikas J, Romens MA, Abbott A, Moss EG (2017) Stage-Specific Timing of the microRNA Regulation of lin-28 by the Heterochronic Gene lin-14 in Caenorhabditis elegans. Genetics. 205:251-262.

Tsialikas J, Romer-Seibert J (2015) LIN28: roles and regulation in development and beyond. Development. 142:2397-404.

Tsukamoto T, Gearhart MD, Spike CA, Huelgas-Morales G, Mews M, Boag PR, Beilharz TH, Greenstein D (2017) LIN-41 and OMA Ribonucleoprotein Complexes Mediate a Translational Repression-to-Activation Switch Controlling Oocyte Meiotic Maturation and the Oocyte-to-Embryo Transition in Caenorhabditis elegans. Genetics. 206:2007-2039.

Vadla B, Kemper K, Alaimo J, Heine C, Moss EG (2012) lin-28 controls the succession of cell fate choices via two distinct activities. PLoS Genet. 8:e1002588.

Van Wynsberghe PM, Kai ZS, Massirer KB, Burton VH, Yeo GW, Pasquinelli AE (2011) LIN-28 co-transcriptionally binds primary let-7 to regulate miRNA maturation in Caenorhabditis elegans. Nat Struct Mol Biol. 18:302-8.

Vella MC, Choi EY, Lin SY, Reinert K, Slack FJ (2004) The C. elegans microRNA let-7 binds to imperfect let-7 complementary sites from the lin-41 3'UTR. Genes Dev. 18:132-7.

Viswanathan SR, Daley GQ, Gregory RI (2008) Selective blockade of microRNA processing by Lin28. Science. 320:97-100.

Vogt EJ, Meglicki M, Hartung KI, Borsuk E, Behr R (2012) Importance of the pluripotency factor LIN28 in the mammalian nucleolus during early embryonic development. Development. 139:4514-23.

Wang L, Nam Y, Lee AK, Yu C, Roth K, Chen C, Ransey EM, Sliz P (2017) LIN28 Zinc Knuckle Domain Is Required and Sufficient to Induce let-7 Oligouridylation. Cell Rep. 18:2664-2675.

Wilbert ML, Huelga SC, Kapeli K, Stark TJ, Liang TY, Chen SX, Yan BY, Nathanson JL, Hutt KR, Lovci MT, Kazan H, Vu AQ, Massirer KB, Morris Q, Hoon S, Yeo GW (2012) LIN28 binds messenger RNAs at GGAGA motifs and regulates splicing factor abundance. Mol Cell. 48:195-206.

Winner B, Cooper-Kuhn CM, Aigner R, Winkler J, Kuhn HG (2002) Long-term survival and cell death of newly generated neurons in the adult rat olfactory bulb. Eur J Neurosci. 16:1681-9.

Worringer KA, Rand TA, Hayashi Y, Sami S, Takahashi K, Tanabe K, Narita M, Srivastava D, Yamanaka S (2014) The let-7/LIN-41 pathway regulates reprogramming to human induced pluripotent stem cells by controlling expression of prodifferentiation genes. Cell Stem Cell. 14:40-52.

Wu L, Belasco JG (2005) Micro-RNA regulation of the mammalian lin-28 gene during neuronal differentiation of embryonal carcinoma cells. Mol Cell Biol. 25:9198-208.

Wu S, Aksoy M, Shi J, Houbaviy HB (2014) Evolution of the miR-290–295/miR-371–373 cluster Family Seed Repertoire. PLoS ONE. 9(9):e108519.

Wu YC, Chen CH, Mercer A, Sokol NS (2012) Let-7-complex microRNAs regulate the temporal identity of Drosophila mushroom body neurons via chinmo. Dev Cell. 23:202-9.

Xia X, Ahmad I (2016) let-7 microRNA regulates neurogliogenesis in the mammalian retina through Hmga2. Dev Biol. 410:70-85.

Xu B, Huang Y (2009) Histone H2a mRNA interacts with Lin28 and contains a Lin28-dependent posttranscriptional regulatory element. Nucleic Acids Res. 37:4256-63.

Xu B, Zhang K, Huang Y (2009) Lin28 modulates cell growth and associates with a subset of cell cycle regulator mRNAs in mouse embryonic stem cells. RNA. 15:357-61.

Yang DH, Moss EG (2003) Temporally regulated expression of Lin-28 in diverse tissues of the developing mouse. Gene Expr Patterns. 3:719-26.

Yang M, Yang SL, Herrlinger S, Liang C, Dzieciatkowska M, Hansen KC, Desai R, Nagy A, Niswander L, Moss EG, Chen JF (2015) Lin28 promotes the proliferative capacity of neural progenitor cells in brain development. Development. 142:1616-27.

Yokoyama S, Hashimoto M, Shimizu H, Ueno-Kudoh H, Uchibe K, Kimura I, Asahara H (2008) Dynamic gene expression of Lin-28 during embryonic development in mouse and chicken. Gene Expr Patterns. 8:155-60.

Yu G, Yang Y, Tian G (2010) Expressing and characterization of mLIN-41 in mouse early embryos and adult muscle tissues. J Mol Histol. 41:295-305.

Yu J, Vodyanik MA, Smuga-Otto K, Antosiewicz-Bourget J, Frane JL, Tian S, Nie J, Jonsdottir GA, Ruotti V, Stewart R, Slukvin II, Thomson JA (2007) Induced pluripotent stem cell lines derived from human somatic cells. Science. 318:1917-20.

Zhao C, Sun G, Li S, Lang MF, Yang S, Li W, Shi Y (2010) MicroRNA let-7b regulates neural stem cell proliferation and differentiation by targeting nuclear receptor TLX signaling. Proc Natl Acad Sci U S A. 107:1876-81.

Zheng K, Wu X, Kaestner KH, Wang PJ (2009) The pluripotency factor LIN28 marks undifferentiated spermatogonia in mouse. BMC Dev Biol. 9:38.

Zhu H, Shah S, Shyh-Chang N, Shinoda G, Einhorn WS, Viswanathan SR, Takeuchi A, Grasemann C, Rinn JL, Lopez MF, Hirschhorn JN, Palmert MR, Daley GQ (2010) Lin28a transgenic mice manifest size and puberty phenotypes identified in human genetic association studies. Nat Genet. 42:626-30.

Zhu H, Shyh-Chang N, Segrè AV, Shinoda G, Shah SP, Einhorn WS, Takeuchi A, Engreitz JM, Hagan JP, Kharas MG, Urbach A, Thornton JE, Triboulet R,

Gregory RI; DIAGRAM Consortium; MAGIC Investigators, Altshuler D, Daley GQ (2011) The Lin28/let-7 axis regulates glucose metabolism. Cell. 147:81-94.

Abbreviations List:

4E-BP = eIF4E-binding proteins

C. elegans = Caenorhabiditis elegans

CAG = constitutive chicken beta actin promoter

Calb = calbindin

CCHC = cysteine cysteine histidine cysteine

circRNA = circular RNA

CRISPR = clustered regularly interspaced short palindromic repeats

CSD = cold shock domain

DPE = days post electroporation

DCX = doublecortin

EDU = 5-ethynyl-2′-deoxyuridine

eIF4E = eukaryotic translation initiation factor 4E

ESCs = embryonic stem cells

GCL = granule cell layer

GFAP = glial fibrillary acidic protein

GFP = green fluorescent protein

GL = glomerular layer

iPSCs = induced pluripotent stem cells

mRNPs = ribonucleoprotein complexes

mTOR = mechanistic target of rapamycin kinase

NBs = neuroblasts

NPCs = neural progenitor cells

NSCs = neural stem cells

O.C.T. = optimal cutting temperature

OB = olfactory bulb

P19 cells = mouse embryonal carcinoma cells

PAM = protospacer adjacent motif

PCNA = proliferating cell nuclear antigen

PGCs = periglomerular cells

Pre-miRNA = precursor microRNA

Pri-miRNA = primary microRNA

RISC = RNA-induced silencing complex

RMS = rostral migratory stream

SVZ = subventricular zone

TACs = transit-amplifying cells

TH = tyrosine hydroxalase

Attributions:

Figure 1:

- Diagram and figure created by Jennifer Romer-Seibert

Figure 2:

- Diagram created by Jennifer Tsialikas (Tsialikas & Romer-Seibert, 2015)

Figure 3:

- Diagrams and figure created by Jennifer Romer-Seibert

Figure 4:

- Electroporation by Jennifer Romer-Seibert
- Experiments, data analysis, and statistical analysis by Jennifer Romer-Seibert
- Figure created by Jennifer Romer-Seibert

Figure 5:

- Electroporation, experiments, data analysis, and statistical analysis by Jennifer Romer-Seibert
- Figure created by Jennifer Romer-Seibert

Figure 6:

- Electroporation by Nathaniel Hartman
- Experiments, data analysis, and statistical analysis by Jennifer Romer-Seibert
- Figure created by Jennifer Romer-Seibert

Figure 7:

- Electroporation by Nathaniel Hartman
- Experiments, data analysis, and statistical analysis by Jennifer Romer-Seibert

- Figure created by Jennifer Romer-Seibert

Figure 8:

- A-Electroporation by Nathaniel Hartman
- B-Electroporation, experiments by Jennifer Romer-Seibert
- Figure created by Jennifer Romer-Seibert

Figure 9:

- Electroporation, experiments, data analysis, and statistical analysis by Jennifer Romer-Seibert
- Figure created by Jennifer Romer-Seibert

Figure 10:

- Cell culture, experiments, western blot, data analysis, and statistical analysis by Jennifer Romer-Seibert
- Figure created by Jennifer Romer-Seibert

Figure 11:

- Electroporation, experiments, data analysis, and statistical analysis by Jennifer Romer-Seibert
- Figure created by Jennifer Romer-Seibert

Figure 12:

- Electroporations, experiments, data analysis, and statistical analysis by Jennifer Romer-Seibert
- Figure created by Jennifer Romer-Seibert

Figure 13:

- Electroporation by Nathaniel Hartman
- Experiments, data analysis, and statistical analysis by Jennifer Romer-Seibert
- Figure created by Jennifer Romer-Seibert

Figure 14:

- Experiment, data analysis, and statistical analysis by Jennifer Romer-Seibert
- Figure created by Jennifer Romer-Seibert

Figure 15:

- Diagrams and figure created by Jennifer Romer-Seibert

Figure 16:

- Cell culture, experiments, data analysis, and statistical analysis by Jennifer Romer-Seibert
- Figure created by Jennifer Romer-Seibert

Figure 17:

- Cell culture, experiments, data analysis, and statistical analysis by Jennifer Romer-Seibert
- Figure created by Jennifer Romer-Seibert

Figure 18:

- Experiments and data analysis by Jennifer Romer-Seibert
- Figure created by Jennifer Romer-Seibert

Figure 19:

- Electroporation, experiments, data analysis, and statistical analysis by Jennifer Romer-Seibert
- Figure created by Jennifer Romer-Seibert

Figure 20:

- Electroporation, experiments, data analysis, and statistical analysis by Jennifer Romer-Seibert
- Figure created by Jennifer Romer-Seibert

Figure 21:

- Cell culture, experiments, data analysis, and statistical analysis by Jennifer Romer-Seibert
- Figure created by Jennifer Romer-Seibert

Figure 22:

- CRISPR scheme, diagram and figure created by Jennifer Romer-Seibert

Figure 23:

- Experiment and data analysis by Jennifer Romer-Seibert
- Diagram and figure created by Jennifer Romer-Seibert

Figure 24:

- Cell culture, experiments, and data analysis by Jennifer Romer-Seibert
- Figure created by Jennifer Romer-Seibert

Figure 25:

- Diagram and figure created by Jennifer Romer-Seibert

Figure 26:

- Figure created by Jennifer Romer-Seibert
- RNA prediction by Jennifer Romer-Seibert

Table 1:

- Data analysis by Jennifer Romer-Seibert
- Table created by Jennifer Romer-Seibert

Table 2:

- Data analysis by Jennifer Romer-Seibert
- Table created by Jennifer Romer-Seibert

Table 3:

- Designed by Eric Moss
- Table created by Eric Moss